Stationary Properties of High Critical Temperature Proximity Effect Josephson Junctions

K.A. Delin[a]

Conductus, Inc.
969 W. Maude Ave., Sunnyvale, CA 94086

A.W. Kleinsasser[a]

IBM Research Division, T. J. Watson Research Center
P. O. Box218, Yorktown Heights, New York 10598

Abstract

The discovery of superconductors with high critical temperatures (T_c) has led to a considerable effort to fabricate Josephson junctions operating at temperatures approaching, or even exceeding, 77 K for both scientific investigations and potential applications. Superconductor-normal-superconductor (SNS) devices, with noble or oxide metals as normal interlayers, are perhaps the most widely explored high-T_c junction type at present. Although demonstrations of individual high-~ SNS devices exhibiting excellent current-voltage characteristics, high critical current-resistance products, and low noise behavior have been made, reproducible devices suitable for electronic applications are elusive. It is therefore important to ask how well these nominally SNS high-T_c junctions are understood. We review the available data, with emphasis on junction critical currents, and conclude that there is little evidence supporting a conventional proximity effect interpretation in the majority of reported high-T_c devices. The strongest candidates for SNS behavior are junctions in which N is a superconductor above its transition temperature. We discuss the present experimental and theoretical understanding of SNS junctions with emphasis on the implications for future research and development of these devices.

(a) Present address: Center for Space Microelectronic Technology, Jet Propulsion Laboratory, California Institute of Technology, 4800 Oak Grove Drive, Pasadena, CA 91109-8099.

1. INTRODUCTION

The Josephson effect can be envisioned as a small overlap of quantum-mechanical wavefunctions between two weakly-coupled superconductors [1]-[5]. The primary manifestation of the effect is the flow of a lossless supercurrent $I_s = I_c \sin\phi$ across the junction, where ϕ is the difference in the phases of the wavefunctions across the junction and I_c is the maximum, or critical, supercurrent. The critical current reflects the strength of the electrode coupling. In this paper we will examine stationary junction properties (time-independent ϕ), primarily in devices having high critical temperature (T_c) superconducting electrodes.

Although the original Josephson devices were tunnel junctions, the general concept of overlapping wavefunctions applies equally well to other weakly-coupled superconducting structures [6]. Most Josephson applications such as superconducting quantum interference devices (SQUIDS) [7] and single flux quantum logic [8] require a single-valued (non-hysteretic) current-voltage (I – V) characteristic. This behavior is natural in non-tunneling weak links. In contrast, tunnel junctions offer such characteristics only when their intrinsically high capacitance is externally shunted by a resistor, at some cost to performance [9]. Tunnel junctions have prevailed as the low-T_c technology of choice because robust, reproducible devices with high electrical performance can be fabricated with acceptable margins. Research on alternative low-T_c junction types was largely abandoned when Nb-based tunnel junction technology with good control of critical currents (roughly ±10% of the target value) became routinely available in the early 1980's [1 O].

Following the discovery of the high-T_c superconductors in 1986, efforts began immediately to produce electronic devices based on them. Recent attempts to develop high-T_c Josephson technology are reminiscent of the similar drives to develop low-T_c junctions in the 1960's and 1970's [1 1]. Attempts to fabricate tunnel junctions with high-T_c electrodes have not yet been particularly successful. The present need is to find a reliable high-T_c Josephson technology that is as generally applicable as tunnel junction technology has proven to be for low-T_c applications.

Demonstrations of the Josephson effect in high-T_c materials were made almost immediately following the discovery of the materials themselves, and a variety of functional Josephson weak links have been fabricated [12]. Significant initial successes were achieved with junctions based on clean grain boundaries in high-T_c films, an approach that is not known to be possible with traditional metallic superconductors but is natural in oxide superconductors [1 3]. However, the search for a *manufacturable* technology has led to a significant effort aimed at developing superconductor-normal-

superconductor (SNS) junctions. Such devices were fairly successful with low-T_c materials prior to the perfection of tunnel junctions.

The physical basis for SNS junctions is the proximity effect, the leakage of Cooper pairs out of the superconductor and into the normal metal near an SN interface. In contrast to tunnel junctions, in which Cooper pairs are forbidden from the insulating region between the superconducting banks, Cooper pairs move through the N region of an SAW junction by ordinary metallic transport. Conventional proximity effect theory has not been tested to any great extent on either high-7 materials or at high (>1 O K) temperatures. On the other hand, despite possible evidence for an unconventional pairing mechanism and order parameter symmetry in high-T_c materials [14], there is no a *priori* reason to believe that the conventional proximity effect should not be observable in high-~ SNS junctions. At present, we cannot yet tell if the basic physics of high-T_c junctions is radically different from or essentially the same as that of low-T_c ones.

Examples abound in the literature of individual high-T_c weak links exhibiting nominally SNS behavior by virtue of their current-voltage characteristics. Although these structures have acceptable electrical properties, there is significant reason to doubt that the vast majority of them can be understood in terms of conventional proximity effect theory [15]. In other words, many nominally SNS high-~ junctions are probably not SNS devices at all. Of course, this statement in itself does not directly impact the usefulness of the devices fabricated. However, if conventional proximity effect theory is to be used to guide the development of these devices into a practical technology, it is essential to apply the correct description.

One distinguishing characteristic of many high-T_c weak links, including nominally SNS devices, is an approximately linear temperature dependence of junction critical current:

$$I_c = I_{co}\left(1 - \frac{T}{T_c}\right), \tag{1}$$

over the *entire* range below T_c, the transition temperature of the superconducting electrodes. Indeed, Eqn. (1) approximately describes data from grain boundary junctions, which are the best-characterized high- T_c Josephson junctions to date. In contrast, the quasi-linear $I_c(T)$ behavior is not typical of low-T_c Josephson junctions and is inconsistent with conventional proximity effect theory. The most obvious conclusion is that Eqn. (1) describes the various types of high-T_c junction structures because the underlying mechanisms for the Josephson behavior in these high-T_c devices is the same. For example, many nominally SNS junctions may actually be arrays of grain-boundary-like pinholes. In other words, the temperature dependence of I_c provides at

least circumstantial evidence that the majority of high-T_c Josephson junctions designated as " *SNS*" in the literature are probably not governed by the proximity effect at all.

The term "*SNS*" by convention identifies a junction in which Josephson current is the result of weak coupling of the superconducting electrodes through a normal layer via the proximity effect. Although we will show that most claimed " *SNS*" junctions do not meet this definition, we will follow the existing literature in referring to any junction in which electrode coupling is *intended* to occur via the proximity effect as an *SNS* device. In addition, applying the term "barrier" to the *N* layer of an *SNS* device implies tunneling, which is not the intended mode of current transport. Therefore, this term is not appropriate in discussing SNS devices, unless it refers to actual barriers at the SN interfaces. We will instead refer to the normal region as the "interlayer."

Barriers can and do occur at some SN interfaces. We designate such junctions as *SINIS*, where *I* denotes an insulator. This idea is easily generalized to other non-ideal *SN* interfaces. We will treat *SINIS* junctions as a subset of the general case of SNS devices because the underlying physics is the same. The behavior of an *SNS* junction is influenced by both what happens to the superconducting order parameter in crossing the *SN* interfaces, which primarily affects the magnitude of I_c, and by loss of coherence in *N* itself, which affects the length and temperature dependence of I_c. In general, conventional *SNS* proximity effect theory provides an adequate description of low-T_c device behavior [16].

In superconductor-semiconductor-superconductor (*SSmS*) junctions, an *SNS* description focusing on the behavior of the order parameter in the interlayer is also fairly successful in describing, for example, the temperature dependence of the critical current. However, the *SINIS* nature of these *SSmS* devices was largely ignored for years, even though the interfaces turned out to be important in understanding basic device properties such as the *magnitude* of I_c [17]. With high-T_c *SNS* devices, the situation is reversed: It is well-accepted that interface resistance dominates device resistance in most cases [18] and that the devices are therefore *SINIS* ones. However, in high-T_c devices little attention has been given to the effect of the loss of coherence in N, as reflected in the temperature dependence of the critical current.

In this paper, we will attempt to establish that conventional proximity effect theory, based on the Bardeen-Cooper-Schrieffer (BCS) theory of superconductivity [19], provides an adequate description of experimental results in only a few reported high-T_c devices. This will enable us to argue that most alleged " SNS" high-T_c devices are likely not truly SNS in nature. It is important to thoroughly understand this issue because

much present research focuses on developing a high-T, device technology based on *SNS* devices. If many useful junctions are actually non-*SNS* in nature, the future directions of materials-related research should be impacted. If the existence of *any* high-T_c *SNS* junctions obeying conventional proximity effect theory can be firmly established, and we believe that such cases exist [20], then the theory can provide a useful tool for evaluating further device development. Such a successful test of the theory would provide strong motivation to reject claims of *SNS* behavior that obviously violates the theory. We emphasize that the present discussion is aimed at understanding device physics and guiding future research. That a particular device conforms to conventional *SNS* theory does not, in itself, make it useful from the point of view of applications.

The organization of this paper is as follows. In Section II we review the basic properties of various types of high-T_c weak links. Proximity effect theory, as applied to *SNS* junctions is discussed in Section III, with low-T: experimental results briefly examined in Section IV. Section V presents a comparative study of high-~ *SNS* junctions. Finally, Section VI discusses the implications of our analysis for future device development.

II. SURVEY OF HIGH-T_c WEAK LINKS

In this section, we briefly review the basic theoretical descriptions of weak links and survey the various types of high-T_c devices demonstrated to date. This overview of experimental results is intended to be representative of the literature, not exhaustive. Our survey will focus on the temperature dependence of the experimentally-measured device critical current, I_c. In particular, we will be interested in the *shape* of normalized $I_c(T)$ data over the *entire* temperature range below T_c. As we shall see, this measurement provides a clear insight into the nature of the junction in question, allowing us to distinguish *SNS* devices from other junction types. Although the temperature dependence of I_c close to T_c is often studied in detail, its theoretical interpretation is ambiguous, as we will discuss in Section III, Finally, the *magnitude* of the critical current is also important but its interpretation is more complex.

Before we begin our survey, several other points should be emphasized. At low temperatures, critical currents can increase to values so large that the Josephson penetration depth [21] becomes smaller than the junction size, which affects the interpretation of experimental data. In other cases, devices which are acceptable Josephson junctions near T_c change character at low temperatures, becoming simple superconducting filaments. Such junctions can often be eliminated from consideration because their characteristics change from “junction-like,” characterized by a sharp onset

of the voltage state with $V \propto (I^2 - I_c^2)^{1/2}$ (upward concavity) to "flux-f low-like," characterized by a rounded $I - V$ curve with downward concavity just above I_c. The latter curves may resemble noise-rounded characteristics [22], but the deviation from the ideal (non-noise-rounded) case increases with decreasing temperature rather than decreasing.

Finally, we note that analysis in terms of reduced temperature, T/T_c, requires specification of T_c. We will use as our definition of T_c the extrapolated temperature at which I_c apparently goes to zero, which is reasonable when the overall form of the data resembles the linear relationship of Eqn. (1). This definition may not be appropriate when $I_c(T)$ data from long *SNS* devices are compared to theory. In such cases, T_c must be determined independently because I_c can be immeasurably small over a considerable range below T_c. In many situations, the apparent T_c of the device is considerably lower than the value characteristic of the electrode films. As will be discussed in Section III, the proximity effect cannot account for any significant reduction of T_c in these devices, and the reduction is presumably due to degradation of the films in processing. One likely criterion for a well-fabricated device is a T_c very close to that of the bulk electrode material.

A. Basic Classifications of Weak Links

Tunnel Junctions

Tunnel junctions are by far the best-understood Josephson devices. The Ambegaokar-Baratoff [23] prediction for the critical current, z,, of a tunnel junction at a temperature, T is:

$$I_c = \frac{\pi\, \mathrm{A(T)}}{2\, eR_n} \tanh\left[\frac{\mathrm{A}(T))}{2kT}\right], \qquad (2)$$

where R_n is the normal state zero-bias resistance of the junction and 2A is the energy gap of the (identical) superconducting electrodes. For the standard BCS prediction 2A(0) = $3.53k\ T_c$ [24], the $I_c(T)$ dependence is illustrated in Fig. 1a. Eqn. (2) is well-established experimentally for low- T_c materials *[3]*.

Point Contacts

The weak coupling required for the Josephson effect can also be provided by connecting two massive superconducting banks by a tiny bridge of superconductor material. Kulik and Omel'yanchuk derived expressions for the supercurrent in a point

contact by considering two superconducting electrodes separated by a tiny orifice of radius a in an otherwise opaque interface, with $a<<\xi_s$, the coherence length in the superconducting electrodes. For a dirty ($\ell_s<<a$) 'contact [25]:

$$I_s = \frac{4A(T)}{eR_n}\sum_{n=0}^{\infty}\frac{\pi kT\cos\frac{\phi}{2}}{\left(\omega_n^2 + \Delta^2(T)\cos^2\frac{\phi}{2}\right)^{1/2}}\tan^{-1}\left[\frac{\Delta(T)\sin\frac{\phi}{2}}{\left(\omega_n^2 + \Delta^2(T)\cos^2\frac{\phi}{2}\right)^{1/2}}\right] \quad (3)$$

where ℓ_s is the mean free path in the superconducting electrodes, $\omega_n = (2n+1)\pi kT$ are the Matsubara frequencies in the Fourier sum of the Fermi-Dirac distribution, and ϕ is the difference in the phases of the quantum-mechanical wavefunctions characterizing the two superconducting electrodes. For a clean ($\ell_s>>a$) contact [26].

$$I_s = \frac{\pi\Delta(T)}{eR_n}\sin\left(\frac{\phi}{2}\right)\tanh\left(\frac{\Delta(T)\cos\frac{\phi}{2}}{2kT}\right). \quad (4)$$

In Eqns. (3) and (4), the relationship between supercurrent and phase is non-sinusoidal, deviating from the ideal Josephson relationship, $I_s = I_c\sin\phi$. However, these deviations from ideality are not extreme except at low temperatures. In fact, Eqns. (3) and (4) are equivalent to Eqn. (2) with $I_s = I_c\sin\phi$ for $\Delta(T)<<kT$. Although non-ideal behavior may affect device function, we will not concern ourselves here with the implications of non-sinusoidal current-phase relations, as these are of importance primarily in the voltage (non-stationary) state. (Note that in the present context "clean" and "dirty" refer to the ratio of the mean free path, ℓ_s, to the contact dimensions. In all subsequent discussions, these terms will be used in their proximity effect context, referring to the ratio of the mean free path, ℓ_n, to the coherence length in the normal interlayer of an *SNS* junction.)

Point contacts have larger predicted I_cR_n products than tunnel junctions. Eqns. (2) - (4) predict that eI_cR_n / A(0) = $\pi/2, 0.66\pi$, and π for tunnel junctions, dirty point contacts, and clean point contacts, respectively. The dependence of I_c predicted by Eqns. (2) - (4), normalized to zero-temperature values, are illustrated in Fig. 1, for the case $2A(0) = 3.53kT_c$. Note that the normalized tunnel junction and dirty point contact curves (Figs, 1a and b, respectively) have similar shapes, while the clean point contact curve (Fig. 1c) is quasi-linear, roughly approximating the linear dependence of Eqn. (1) (Fig. Id).

The value of $\Delta(0)/kT_c$ has a major influence on the shape of $I_c(T)$ within these theories. We illustrate this point in Fig. 2, which shows normalized $I_c(T)$ curves for tunnel junctions and point contacts with reduced values for $2\Delta(0)/kT_c$. The values were chosen to result in quasi-linear behavior in the tunnel junction (Fig. 2a) and dirty point contact (Fig, 2b) cases and nearly-linear behavior in the clean point contact case (Fig. 2c). The relevance of this exercise will be apparent as we examine actual experimental data.

SNS Junctions

The critical current and conductance of a tunnel junction decrease exponentially with barrier thickness, and typical useful barriers are on the order of $1nm$ thick. *SNS* devices are attractive because they can circumvent the ultra-thin barrier requirement. The conventional theoretical description of *SNS* junctions will be discussed in detail in Section Ill. For now, we need only note that the critical current I_c of an *SNS* junction decays exponentially with increasing electrode separation, L, as:

$$I_c = I_{co}e^{-L/L_o} \qquad (L>> LO). \tag{5a}$$

We shall see that the characteristic decay length L_0 is typically ξ_n (T), the coherence length in N. This exponential dependence on L results from the spatial decay of the superconducting order parameter on the normal side of an *SN* interface over a distance of order ξ_n. Generally, ξ_n is much longer than typical tunnel barrier thicknesses. Locally, the junction critical current *density*, J_c, obeys

$$J_c = J_{co}e^{-L/L_o} \qquad (L >> L_o) \tag{5b}$$

In the simplest cases, $I_c = J_c\mathcal{A}$, where $\mathcal{A}$ is the cross-sectional area of the junction.

The prefactors I_{co} and J_{co} in Eqns. *(5)* are somewhat temperature dependent, but the exponential factor $\exp[-L/L_o(T)]$ dominates the temperature dependence of I_c, resulting in a dramatic increase in I_c as temperature decreases below T_c. This upward concavity in $I_c(T)$ is opposite to that of the curves in Fig. 1. More importantly, the exponential dependence implies major deviations from the linear behavior of Eqn. (1) and the quasi-linear behavior of Fig. lc. These ideas will be fundamental to our discussion of SNS devices.

Because the normal coherence length ξ_n plays such a central role in the discussions that follow, it is worthwhile to develop an intuitive idea of its significance. As in the case of ξ_s,, its counterpart in the superconducting materials, ξ_n reflects the mean size of a

Cooper pair [27] in the N material. A straightforward estimate of the coherence length is obtained from the uncertainty principle. Consider a clean N material with transition temperature T_{cn} = O and mean free path ℓ_n large compared with other relevant length scales. The uncertainty principle states that the product of the position and momentum uncertainties of a Cooper pair exceeds $\hbar$. The position uncertainty is the mean size of the Cooper pair itself, ξ_{nc}. The. momentum uncertainty, δp, can be estimated as $v_n \delta p \approx \delta E$, where v_n is the Fermi velocity in N and δE is the uncertainty in the energy around the Fermi surface, about kT in a normal material (or about A in a superconductor). Thus, ξ_{nc} is approximately $\hbar v_n / kT$. It is therefore not surprising to find that, in the clean limit $(\ell_n >> \xi_{nc})$, ξ_{nc} is given by [28]:

$$\xi_{nc} = \tau_T v_n, \tag{6}$$

where $\tau_T = \hbar/(2\pi kT)$ = 1.22/ T $ps - K$.

In the dirty limit $(\ell_n << \xi_n)$, the usual random walk argument leads to an expression for ξ_{nd}:

$$\xi_{nd} \cdot (\xi_{nc} \ell_n / d)^{1/2} = (\tau_T D_n)^{1/2}, \tag{7}$$

where D_n is the carrier diffusion constant in N ($D_n = v_n \ell_n / d$, where d is the dimensionality). Throughout the remainder of this work, we will use the subscripts "n", "c", and "d" to denote the N layer and the clean and dirty limits, respectively. Note that "clean" and "dirty" refer here to the ratio ℓ_n / ξ_{nc}, and not to the ratio of ℓ_n to contact dimensions.

For arbitrary ℓ_n, Eqns. (6) and (7) represent upper limits to the value of ξ_n. For typical noble metals, V_n=1-2x $106\ m/s$, so ξ_{nc} =300-600 nm at $4.2\ K$ and 15-30 nm at 77 K. For thin noble metal N films, ℓ_n is typically limited by the film thickness. So, if ℓ_n < 100 nm, ξ_{nd}<100-140 nm at 4.2 K and 20-30 nm at $77\ K$. Thus, at low enough temperatures, the dirty limit prevails, while the clean limit can hold at relatively high temperatures ($\approx 77\ K$). For oxide N layers, v_n is an order of magnitude or more smaller, reducing ξ_n proportionally.

Classes of devices labeled "*SNS*" include SN'S devices, where N' denotes a superconductor above its transition temperature T_{cn}, and *SINIS* junctions, where "*I*" refers to an interface region with significant scattering created by, for example, grain boundaries, poor material stoichiometry, or tunnel barriers.

Unconventional Superconducting Order Parameter

In contrast to conventional superconductors, experimental evidence suggests that Cooper pairs in high-T_c cuprate superconductors do not exhibit spherically-symmetric (s-wave) pairing. In particular, the case for d-wave pairing is presently rather strong [14]. The impact of unconventional pairing on the critical. current of Josephson tunnel junctions has been examined theoretically using the tunneling Hamiltonian formalism [29]. It was found that the shape of $I_c(T)$ deviates from that predicted by Eqn. (2) for s-wave superconductors. In the case of $s + id$ symmetry, $I_c(0)$ is reduced by a factor of 0.67 and the shape of $I_c(T)$ lies between curves b and c in Fig. 1, In the case of d-wave pairing, the shape of $I_c(T)$ is very close to the linear dependence of Eqn. (1).

Unconventional pairing symmetry should also affect the shape of $I_c(T)$ in the case of other, non-tunneling, types of Josephson junctions. In fact, it is possible that the symmetry of the order parameter in the superconducting electrodes is the origin of the seemingly ubiquitous quasi-linear dependence of $I_c(T)$ in a wide variety of high-T_c junctions. Nevertheless, the detailed implications of unconventional pairing symmetry for the theory of SNS junctions are unknown at present, One might therefore argue that it is futile to examine experimental high-T_c data in terms of conventional theory. However, we will be interested primarily in long SNS junctions, whose behavior is dominated by the exponentially-decaying superconducting wavefunction in the normal interlayer. The symmetry of the superconducting order parameter should have little, if any, effect on the temperature-dependent decay length. Consequently, the exponential dependence of $I_c(T;L)$, given by Eqns. (5), should be unaffected by the symmetry of the order parameter in the electrodes. Variations in the shape of $I_c(T)$ are to be expected, but only the temperature-dependent prefactor in Eqns. (5) is affected. Thus, although the precise magnitude and the fine details of the temperature dependence of the critical current of an SNS junction will undoubtedly depend on the order parameter symmetry in S, the basic signatures associated with the conventional proximity effect should hold in all cases.

B. High-T_c Grain Boundary and Tunnel Junctions

The Josephson effect was originally understood as a manifestation of tunneling between superconductors and demonstrated in low-T_c tunnel junctions. It was quickly recognized, however, that the concept of overlapping wavefunctions also readily applies to other weakly-coupled superconducting systems [2]-[5]. Since well-behaved high-T_c tunnel junctions have remained elusive, it is fortunate that typical grain boundaries in oxide superconducting materials act as natural Josephson weak links. This allowed demonstrations of the Josephson effect in high-T_c materials soon after their discovery,

and was the basis for early explorations of high-~. electronics [30].

Grain Boundary Junctions

The presence of grain boundaries in oxide superconductors alters the electrical properties to a much greater extent than unconventional superconductors. In ordinary materials, grain boundaries typically *enhance* critical currents by acting as flux pinning centers. In contrast, grain boundaries in oxide superconductors act as weak links [31], providing a natural means for fabricating Josephson junctions. Fig. 3a is a schematic diagram of a grain boundary junction, which may be fabricated using the naturally-occurring grain boundaries in a polycrystalline film [32], by growing a high-T_c film on a bicrystal substrate [33], or with a bi-epitaxial process [34] -[36] in which grain boundaries are produced by the selective use of seed layers. The hi-crystal technique has the advantage of controlling the relative angle between the grain boundaries. The bi-epitaxial process gives only a 45° disorientation between adjacent $YBa_2Cu_3O_{7-\delta}$ grains for an underlying yttria stabilized zirconia (YSZ) [34],[36] or MgO [35] seed layer but has the advantage of placing junctions at arbitrary locations on a substrate. Finally, grain boundaries can be induced by growing a high-~ superconductor film over a steep step deliberately introduced into the substrate [37], [38], as illustrated schematically in Fig. 3b. Well-behaved Josephson junctions have been produced by many groups by each of these methods. Figures 4- 6 show data for the temperature dependence of I_c for several representative grain boundary junctions.

Models of grain boundary junctions [41] include near-ideal Josephson elements in series with superconducting filaments (which add kinetic inductance) and non-superconducting shunt paths. Both tunnel and point contact models have been used for the Josephson elements. In Figs. 4-6, the data are scaled to $I_c(0)$. Fitting such data implicitly introduces an arbitrary prefactor, a practice consistent with the idea of shunt paths which do not carry significant supercurrent. In natural grain boundary junctions $I_c(T)$ is fairly linear, as shown in Fig. 4a, although it rises noticeably above the linear dependence at low temperatures. This dependence is also characteristic of hi-crystal grain boundary junctions, as shown in Figs. 4b and 4c. Low-angle grain boundaries exhibit more nearly linear $I_c(T)$ dependence *[40]*. Bi-epitaxial and step edge junctions have similar temperature dependence, as shown in Figs. 5 and 6.

None of the data shown in Figs. 4-6 resemble the theoretical curves of Fig. 1. However, it has been noted [31] that some grain boundary junction data can be fit by Eqn. (2) if a gap $2\mathrm{A}(0)$ in the range kT_c to $1.5\,kT_c$, smaller than the usual BCS value of 3.53 kT_c [24], is assumed, The fact that the curves of Fig. 2 resemble the data in Figs. 4-6 shows that this idea works for point contact, as well as tunnel junction, models. In Section Ill, we

will see that curves of this general quasi-linear shape can also be obtained from *SNS* models for particular values of interlayer thickness. That data can be fit to Eqns. (2)-(4) by adjusting $\Delta(0)/kT_c$ underscores the idea that, even for tunneling between identical superconductors, there is no single universal theoretical $I_c(T)$ curve,

A reduced gap in the active region of the junction is at least plausible because of the anisotropy in A. In $YBa_2Cu_3O_{7-\delta}$, a small gap may occur even in the ah-planes [42]. As we shall see in Section III, gap reduction near high-~. superconductor interfaces with non-superconducting materials is expected. However, fitting data with curves such as those shown in Fig. 2 represents only a naive and *ad* hoc comparison with standard theories. It does not constitute a strong argument for tunneling or point contact descriptions of grain boundaries. For example, Eqns. (2)-(4) do not allow fits to all available data on grain boundary junctions. By demonstrating that several basic models can fit experimental data of the type shown in Figs. 4-6, we illustrate the dangers of drawing sweeping conclusions from I_c (7') data alone.

Tunnel Junctions

The fabrication of tunnel junctions with conventional metallic superconducting electrodes has become straightforward [43]. The electrode films are typically polycrystalline and can be deposited at room temperature. Tunnel barriers are formed by oxidation of metal films, either the metallic base electrode itself or a very thin metal film deposited on the base electrode. Junction properties are sensitive to those properties of the electrode films within a coherence length ξ_s (typically 10-100 nm) of the barrier, This distance is sufficiently large in many low-~. materials to allow the superconducting electrode films to be characterized by their bulk properties.

In the case of some conventional compound superconductors, such as the binary $A-15$ materials, the need for epitaxial film growth leads to high processing temperatures, resulting in problems with barrier integrity during counterelectrode deposition. The short superconducting coherence length in these materials makes it difficult to achieve bulk properties in the counterelectrode adjacent to the interface. The net result is that no viable tunnel junctions with two $A-15$ electrodes have yet been produced. These problems are present in the case of high-T_c oxide superconductors as well. It is difficult to fabricate tunnel junctions in which the bulk properties of high-T_c electrodes are maintained to within ξ_s (roughly 2 nm) of the barrier. The superconductors' complex chemical structures and large anisotropies lead to additional processing problems. Nevertheless, attempts to fabricate high-T_c tunnel junction have been made, and the results offer insights that will prove valuable in our later examination of *SNS* devices. We cite here examples of devices intended as tunnel junctions which exhibited

Josephson currents.

Robertazzi *et al.* [44] demonstrated $YBa_2Cu_3O_{7-\delta}$-MgO-$YBa_2Cu_3O_{7-\delta}$ *edge* junctions with excellent Josephson weak link properties. The MgO layers were rather thick for tunnel barriers; for a 3.2 rim-thick barrier, the device critical current density was as large as $J_c = 0.3\ mA/\mu m^2$. In addition, the $I-V$ characteristics were non-hysteretic, an unexpected result given the intended SIS device structure. Consequently, the authors were led to conclude that the junctions were actually arrays of superconducting microconstrictions in an insulating MgO matrix. Subsequently, this work was extended to $SrTiO_3$ *[45]* and $NdGaO_3$ [46] barriers with similar results. Fig. 7 shows $I_c(T)$ for a representative nominally SIS junction after different processing steps.

The general resemblance of these curves to those obtained for grain boundary junctions, shown in Figs. 4-6, suggests that a similar transport mechanism is involved in these device structures [44]. Indeed, it is natural to suppose that an array of pinholes or microconstrictions should behave in a manner similar to a grain boundary junction, which is modeled in much the same way. We do not argue that these nominally SIS junctions are literally equivalent to grain boundaries, only that the underlying origin of their weak-link nature is similar.

Although attempts to fabricate artificially-layered structures in the form of high-T_c tunnel junctions have not been particularly successful, it has been recognized that tunneling may play a natural role in transport along the c-axis direction in layered cuprate superconductors, particularly materials such as $Bi_2Sr_2CaCu_2O_8$ and $Tl_2Ba_2Ca_2Cu_3O_{10}$ which are significantly more anisotropic than even $YBa_2Cu_3O_{7-\delta}$. Critical currents in the c-axis direction of single crystals of several cuprates have been studied [47] -[49]. The results for $Bi_2Sr_2CaCu_2O_8$, $(Pb,Bi)_2Sr_2CaCu_2O_8$, and $Tl_2Ba_2Ca_2Cu_3O_{10}$ are very similar, and strongly suggest viewing the crystals as stacks of tunnel junctions. In contrast, critical currents in single crystals of $YBa_2Cu_3O_{7-\delta}$ behave like an ordinary anisotropic superconductors [48]. Figure 8 shows $I_c(T)$ for $(Pb,Bi)_2Sr_2CaCu_2O_8$ *[49]* and $Tl_2Ba_2Ca_2Cu_3O_{10}$ [48] single crystals. Also shown is the Ambegaokar-Baratoff theoretical prediction **[23]** for tunnel junctions, Eqn. (2), assuming the standard BCS value for the gap, $2\Delta(0) = 3.53kT_c$. This agreement between experiment and theory strongly suggests that conventional tunnel junctions are possible in high-~. materials, and that the notion of relating the critical current to the BCS prediction for the energy gap, is plausible in at least some circumstances.

C. High-T_c SNS Junctions

Co-planar and Sandwich SNS Junctions

The simplest SNS structures are coplanar bridges and thin film sandwiches [6], schematically illustrated in Fig. 9a and 9b. Both require submicrometer lithography in order to be useful for device applications. For bridges, the device length (electrode separation), L, must be less than a few times ξ_n in order to achieve useful critical currents. For sandwiches, the device area must be extremely small in order to achieve practical critical currents and resistances (assuming that the resistance is dominated by the normal metal and not parasitic interracial effects). As a result, sandwich and lithographically-defined co-planar geometries have received less attention than other approaches, and our discussion will reflect this fact.

Several attempts have been made to fabricate co-planar bridges [50],[51] using $YBa_2Cu_3O_{7-\delta}$ electrodes and Au interlayers. Functioning Josephson devices were produced, but their SNS nature was never systematically verified through careful comparisons with proximity effect theory. Indeed, other attempts to fabricate similar devices [52] have cast doubt on the possibility that true SNS junctions can actually be produced in this way. Instead, it was argued [52] that all results can be better interpreted in terms of unintentional superconducting shorts between the two electrodes. Fig. 10a shows $I_c(T)$ for a co-planar $YBa_2Cu_3O_{7-\delta}$-Au-$YBa_2Cu_3O_{7-\delta}$ bridge [511. The data resemble the grain boundary junction data in Figs. 4-6, and show none of the upward curvature with decreasing temperature expected from Eqns. (5), even though $L/\xi_n(T) > 4$ at $77\ K$.

The statement that high-~ planar microbridge SNS structures are relatively unattractive for practical devices is based on conventional theory, which predicts very short coherence lengths at the temperatures of interest. Some experimental $I_c(T)$ data from planar bridge and sandwich junctions can be partially interpreted in terms of SNS theory, but only by invoking a decay length L_0 in Eqns. (5) that is much larger than the normal coherence lengths given by Eqns. (6) and (7) [50], [54]. In several cases, this decay length was found experimentally to be essentially independent of temperature [53]. This is not predicted by conventional proximity effect theory and led some authors to invoke the idea of a "long range proximity effect" *[53] -[56]*. There have been attempts to explain long range proximity effects theoretically [57], as we will discuss further in Section III. Of immediate significance, however, is that data from a planar $HoBa_2Cu_3O_{7-x}$-$La_{1.5}Ba_{1.5}Cu_3O_{7-y}$-$HoBa_2Cu_3O_{7-x}$ junction (Fig. 10b) *[53]* again closely resemble the data taken on grain boundary weak links shown in Figs. 4-6.

SNS Edge Junctions

Immediately after the discovery of high-~ oxide superconductors, it was recognized that the materials are highly anisotropic, with transport occurring far more easily along the a-b planes than in the c-direction. Consequently, the circuit uses of films with the c-axis parallel to the substrate are very limited because wiring cannot turn corners without a major change in transport properties. Moreover, film growth occurs more naturally and evenly with the c-axis normal to the substrate. Thus, circuit-oriented work is usually done with c-axis films, which tends to favor in-plane junction geometries.

The desire for a co-planar geometry not requiring deep-submicrometer lithography led to a renewal of interest in edge junctions. Here, a sloped edge is formed in an epitaxial high-T_c superconductor film for use as the base electrode. A metallic or quasi-metallic interlayer and a superconducting counterelectrode are subsequently deposited to complete the device *[58], [59]*. The resulting edge, or ramp, junction structure is illustrated schematically in Fig. 9c. Edge junctions are well-known in low-~. materials [60]. Edges appropriate for devices of this geometry can be formed by a variety of methods, but the one most generally-applicable relies on ion beam etching (ion milling) [60]. Ion milling can also be applied to counterelectrode patterning [61], since this etching method is applicable to any material.

For a variety of materials-related reasons, including lattice matching, oxygen variation across an interface, and differential thermal expansion, quasi-metallic oxides have been a common choice for interlayer materials in high-T_c *SNS* junctions. Examples of cuprate interlayers include non-superconducting (cold-deposited) $YBa_2Cu_3O_{7-\delta}$ *[59]* and $PrBa_2Cu_3O_{7-\delta}$ *[62] -[64]*. Examples of cubic oxide metallic interlayers include *Nb*-doped $SrTiO_3$ *[65]*, $CaRuO_3$ *[66]*, and $SrRuO_3$ *[67], [68]*.

Figures 11 and 12 show the temperature dependence of I_c for several representative junctions with oxide interlayers. The quasi-linear nature of $I_c(T)$ is clear. Figs. 11 b and 11c compare two $PrBa_2Cu_3O_{7-\delta}$ junctions with $L = 20$ and 8 *nm,* respectively (the actual published data were I_cR_n, but R_n is very nearly temperature independent). The two junctions differ only slightly in I_cR_n at $T=O$ despite the 150% difference in L. The similarity of these data sets to each other, and to the data for the other junction types is remarkable. Similarly, Figs. 12 b-1 2d compare several $SrRuO_3$ junctions which show $I_c(T)$ behavior in the narrow range characteristic of grain boundary junctions (recall Figs. 4-6).

According to conventional proximity effect theory, I_c should depend exponentially on L for *SNS* junctions. Moreover, the temperature-dependent length L_0 in the exponent of

Eqn. (5) should result in a significant upward concavity in $I_c(T)$ which is absent in almost all of the available data. Also, the shape of the normalized I_c (7') curves hardly changes from device to device in spite of the large variation expected from a steep length dependence. These issues will be discussed in more detail in Section V. For now, we merely recognize that it is difficult to reconcile these observations with conventional proximity effect theory.

The general similarity of these data strongly support the idea that these nominally *SNS* devices may not be proximity effect junctions at all. Recall that attempts to make $YBa_2Cu_3O_{7-\delta}$ tunnel junctions resulted in devices dominated by pinholes which behaved very similarly to grain boundary junctions. It is clear that we should consider the same possibility for many reported *SNS* junctions.

Not all SNS edge junctions have linear or quasi-linear I_c (T) dependence. Recently, $PrBa_2Cu_3O_{7-\delta}$ interlayer devices with extremely shallow edges were produced [70] for which $I_c \propto (T_c - T)^2$ over the entire temperature range. Other recent devices exhibit a clearly exponential-like temperature dependence [64], [71], as shown in Fig. 13. Note the difference between the data from these two devices of differing lengths, as well as the striking difference between these data and that taken from the nominally similar devices, depicted in Figs. 11 b and 11c. A similar apparent exponential temperature dependence has been reported for a-axis oriented sandwich junctions [72]. These results will be discussed more fully in Section V.

SN'S Edge Junctions

An ideal interlayer material should allow a low-resistance contact between the S and N layers which preserves the integrity of both of their crystal structures. The entire structure must be stable through film growth, processing, and cryogenic cycling. The sensitivity of high-T_c materials to such factors as processing, composition, and film structure suggests using S and N materials that are closely-matched structurally. Indeed, substituted versions of high-~ superconductors with reduced T_c have received considerable recent attention as interlayers. Examples are $(Y,Pr)Ba_2Cu_3O_{7-x}$ [73], *Co*-substituted- $YBa_2Cu_3O_{7-\delta}$ [74], and *Ca*-substituted-$YBa_2Cu_3O_{7-\delta}$ [75]. These junctions, designated SN'S, are operated at temperatures above T_{cn}, the critical temperature of the **N'** interlayer. Conventional theory predicts that **SN'S** devices will exhibit an I_c that is exponentially-dependent on temperature for $T_{cn} < T < T_c$. Some of these *SN'S* devices provide the most convincing demonstration of proximity effect behavior obtained to date in high-T_c junctions [20]. We defer detailed discussion of these devices, however, until Section V.

SNS Step-Edge Microbridges

Ordinary metals are incompatible with sandwich or ordinary edge junctions with high-~. electrodes because reaction and interdiffusion during growth preclude stable interfaces. However, an alternative to planar bridges has been developed which allows Au, Ag, and other conventional metals to be used as N layers while providing for deep-submicrometer device lengths using ordinary lithography. In this structure, an epitaxial high-T_c superconductor film is deposited at an angle over a step deliberately cut into the substrate (or insulating epitaxial layer). If the deposited film is thin enough, it can be discontinuous, forming two separate superconducting banks. The normal interlayer is then deposited, bridging the banks. This second deposition is typically performed *in situ* to preserve the cleanliness of the exposed film edges. The bridge is then subtractively patterned. The resulting structure is illustrated schematically in Fig. 9d. It is expected that transport into and out of the N-layer is dominated by the exposed a-b planes at the edges of the superconducting films. With this technique, the bridge length L is roughly the step height, typically 100 nm. Good proximity coupling between the banks then requires $\xi_n >> 10\ nm$ at 77 K. Although several successful device demonstrations have been made using this approach [52], [76]-[81], the issue remains whether or not the junction behavior can be described by conventional proximity effect theory.

The temperature dependence of I_c for several noble metal bridges is illustrated in Figs. 14-16, Strictly speaking, the data represented in these figures are actually $V_c = I_c R_n$ but, as R_n is not very temperature-dependent in these samples, the difference between $V_c(T)/V_c(0)$ and $I_c(T)/I_c(0)$ is not important for our purposes. In Fig. 14, the interlayers are Ag [78], an Ag/Au alloy [78], and Au [52], with $L \approx 100\ nm$, determined by the step height and S film thickness, The Ag/Au alloy device had a higher value of $I_c R_n$ at low temperatures than a comparable Ag device (1.0 *versus* 0.6 mV) but a significantly lower apparent T_c. $I_c(T)$ in these bridges is concave downward and more closely resembles the clean point contact dependence of Eqn. (4) than the expected SNS dependence of Eqn. (5a). The differences in shape between these normalized I_c (7') curves and those of most of the junctions discussed so far also deserve mention, although the basic temperature dependence is still close to linear.

Robertazzi eta/. [52] argued that it is unlikely that the dominant conduction path in these junctions is through the normal metal and, as in co-planar noble metal bridges, the Josephson behavior is due to unintended superconducting filaments shorting the banks. It was also argued that excess Au or Ag on top of the superconducting films provides a parasitic shunt path, resulting in reduced values for R_n, and hence $I_c R_n$. Elimination of this excess metal resulted in significant reduction of the parasitic shunt conductance. Rosenthal et al. [80] exploited this idea to achieve $I_c R_n = 10\ mV$ at 4.2 K, the highest

value yet reported in a microfabricated junction. Fig, 15 shows three I_c (T) curves for two Au bridges. The data in Fig. 15a [79] closely resemble typical grain boundary data of Fig. 4. The sample in Fig. 15b [80] had significant parasitic shunt conductance, and $I_cR_n \approx 0.8\ mV$ at low temperatures. When this excess metal was removed by ion milling, I_cR_n was increased to **8** mV **[80].** Note from Fig. 15c, however, that the temperature dependence of I_c changed as well, resembling the data of Fig. 14.

Unusually high I_cR_n products in Au step-edge devices were also reported by Dong et al. **[81].** Fig. 16a shows I_c (T) for a bridge with a low value of $I_cR_n \approx 0.4\ mV$ at 4.2 K, the low value resulting from parasitic shunting. Fig. 16b and 16C show similar data for two bridges with $I_cR_n \approx 3$ and 8 mV. Note that the latter data resemble data from grain boundary junctions.

Fig. 17 shows data from a step-edge microbridge in which $CaRuO_3$ was used in place of a noble metal [82]. Note the similarity of this data to that from noble metal devices, despite the differences in materials and, consequently, ξ_n. Furthermore, notice that this $CaRuO_3$ step-edge data is similar to that of the $CaRuO_3$ edge junction in Figure 12a.

From Figs. 14-16, we see that the behavior of $I_c(T)$ in noble metal microbridges is reminiscent of that of grain boundary and point contact junctions, with some of the best (highest I_cR_n) junctions having $I_c/I_c(0)$ similar to that of grain boundary devices. None of these devices exhibit the SNS-like behavior of Eqns. (5), although we expect that $L >> \xi_n(T_c)$ for many, if not all, of the junctions. In addition, the variations that do exist in the shape of the normalized I_c (7') curves are not easily accounted for by intentional differences in device structure such as different bridge lengths.

SNS Junction Summary

Summarizing the varied results obtained on high-T_c SNS devices: (1) Many curves from devices of presumably differing lengths are very similar to each other despite the sensitivity of the shape of normalized $I_c(T)$ curves to changes in L/L_0 implied by Eqns. (5) (recall that L_0 is typically ξ_n). (2) The $I_c(T)$ data for many high-T_c SNS devices closely resemble those of grain boundary junctions. (3) An exponential behavior of $I_c(T)$ is not representative of most of the devices reported in the literature to date.

D. Quasi-Exponential Behavior

One of the most striking characteristics of SNS junctions with $L >> \xi_n(T_c)$ is the exponential dependence of $I_c(T)$ implied by Eqns. (5) - (7). The $PrBa_2Cu_3O_{7-\delta}$ edge junction data of Fig. 13 provides a possible example of such a dependence, We will

encounter more examples when we discuss $SN'S$ junctions in detail in Section V. However, there are a few other exceptions to the prevailing trend of quasi-linear temperature dependence of I_c.

Fig. 18 shows $I_c(T)$ data for five high-~ junctions with various materials and structures that are suggestive of exponential behavior. Figure 18a shows data representative of several *Ag* bridges [79] that apparently suggest the expected exponential temperature dependence characteristic of the proximity effect. These junctions have smaller $I_c R_n$ values than those of Fig. 15 although the devices were fabricated in the same laboratory. One might suppose that this could be accounted for by a larger L/ξ_n in these *Ag* devices, but the physical structure of the junctions does not account for the difference in behavior. The junction lengths are not significantly different, the Fermi velocities of *Ag* and *Au* are very similar, and the mean free path in both cases should be limited by the noble metal thickness. In fact, although the curve in Fig. 18a can probably be fit by *SNS* theory *[79],* we shall see that the functional dependence of $I_c(T)$ for the junctions of Fig. 18 may not be exponential at all. Fig. 18b - 18e shows data for a co-planar *Au* bridge [83], a $YBa_2CoCu_2O_7$ edge junction [84], a $Bi_2Sr_2CaCu_2O_8$-$Bi_2Sr_2CuO_y$-$Bi_2Sr_2CaCu_2O_8$ sandwich junction [85], and a $Hg_2Ba_2Ca_2Cu_3O_{10}$ grain boundary junction [86], respectively. These data represent what we will term "quasi-exponential" behavior of I_c (T).

What is interesting about these data is that the simple empirical power law dependence $(T_c - T)^{2.5}$ describes the critical currents very well. We offer no immediate explanation for this particular power law, emphasizing only that it is an impressive coincidence that five different types of junctions, including a grain boundary device, with three different electrode materials should behave so similarly. This coincidence, coupled with the virtual absence of other highly nonlinear dependence, suggests that there is a common explanation for the data of Fig. 18. Nevertheless, we argue that this common explanation is unlikely to be based on conventional proximity effect theory, which would manifest itself differently for the different geometries of these devices.

E. Summary

Many high-T_c grain boundary, tunnel, and *SNS* junctions, using a variety of superconducting, insulating, and normal materials, have been fabricated. In general, the behavior of $I_c(T)$ is surprisingly similar across the various device types. It is interesting that the behavior of both nominally tunnel and *SNS* junctions is similar to that of grain boundary junctions. Also intriguing is that the $I_c(T)$ data for most of these devices can be described by point contact and tunneling theories if the superconducting gap is reduced below its BCS value. Nevertheless, our primary goal here will be not to

argue *for* any particular mechanism describing much of the SNS junction data in the literature, but rather argue *against* the application of conventional proximity effect theory to describe most of the data. That $I_c(T)$ data from certain high-T_c $SN'S$ devices is well-described by classical theory [20] strengthens the case against conventional behavior for the other SNS junctions. We will therefore examine the data from this section more closely after reviewing conventional proximity effect theory.

III. THEORY OF SNS JOSEPHSON JUNCTIONS

In this section we describe conventional proximity effect theory, which successfully explains the behavior of low-T_c SNS junctions. We will cover each of the important physical mechanisms that can influence SNS behavior while striving to focus on general results that should transcend any particular theoretical approach.

Traditional theoretical investigations of Josephson weak links are based on the BCS theory of superconductivity [19]. It is far from clear, however, that junctions having high-T_c superconducting electrodes should obey the resulting predictions in detail. For example, while it is generally assumed that the superconducting energy gap A in a high-T_c material has the BCS temperature dependence, there is no clear indication that this is, in fact, true. Conversely, unconventional behavior in Josephson and tunnel junctions has been suggested as a means to investigate unresolved issues, such as the symmetry of the order parameter, in high-T_c materials [14]. In any case, we will need to use caution in applying conventional proximity effect theory to high-T_c devices.

Many low-T_c devices, particular those with semiconductor interlayers, have intrinsically 2-dimensional (2d) geometries, which can affect the details of electron transport [87]. In contrast, high-T_c materials have anisotropic transport properties and films in which the favored current direction lies in the plane of the substrate are common. As a result, we will focus on 1 d device geometries here.

A. de Gennes Dirty Limit Theory

Long SNS Junctions

In 1964, de Gennes [88] produced one of the first systematic theoretical investigations of the proximity effect. This early work still provides an intuitive basis for understanding the proximity effect and the behavior of SNS junctions. As with subsequent treatments of the proximity effect, the starting point for the theory of de Gennes was the self-consistent expression for the spatially-varying pair potential obtained by Gor'kov from

the microscopic BCS theory **[89].** The junction critical currents are then calculated using the phenomenological Ginzburg-Landau theory, which generally applies at temperatures down to $\approx 0.3 T_c$. We will find the de Gennes theory to be consistent with the appropriate limiting cases of more general theoretical approaches, differing only by factors of order unity.

de Gennes established that, on the N side of an SN contact, the superconducting order parameter (or wavefunction) decays exponentially over a material- and temperature-dependent distance, the normal coherence length ξ_n. This length ranges from unit cell dimensions in dirty metals at relatively high temperatures to micrometers or larger in clean metals at low temperatures. Most of de Gennes's results were obtained under the single-frequency approximation, using only the lowest Matsubara frequency in the Fourier expansion of the Fermi-Dirac distribution. This assumption greatly simplifies the analysis and leads to simple analytical expressions, the price paid being that the results are applicable only for long junctions ($L >> \xi_n$, where L is the spatial separation of the superconducting electrodes). Because ξ_n is small in the materials used in many high-T_c devices, the long junction approximation is not a serious limitation, particularly at temperatures of order 77 K. In addition, de Gennes focused exclusively on the dirty limit in both the S and N layers, $\ell << \xi$, where ℓ and ξ are the mean free path and coherence length. For T_{cn} =0, the dirty limit coherence length in N is given by Eqn. (7). de Gennes's theory is actually more general, and its extension to finite T_{cn} will be discussed later.

An SNS junction can be viewed as two back-to-back SN contacts with the coupling strength, as manifested through I_c, determined by the degree of overlap of the wavefunctions of the superconducting electrodes. Evaluating the behavior of the order parameter near the SN interface, de Gennes [88] found that $I_s = I_c \sin\phi$ with

$$I_c(T;L) = \frac{\pi}{4eR_n}\frac{|\Delta_i|^2}{kT_c}\frac{L/\xi_{nd}}{\sinh(L/\xi_{nd})} \cong \frac{\pi}{2eR_n}\frac{|\Delta_i|^2}{kT_c}\frac{L}{\xi_{nd}}e^{-L/\xi_{nd}}, \qquad (8)$$

where L is the bridge length and Δ_i is the superconducting gap at the normal interlayer interface, As previously mentioned, this result is strictly valid only near T_c, the critical temperature of the bulk superconducting banks. Device critical currents have been calculated or measured for dirty SNS junctions with low-T_c electrodes in various circumstances, and universally display an exponential behavior, $I_c \propto \exp(-L/\xi_{nd})$ in long junctions over a broad range of temperatures below T_c. The explicit exponential dependence on junction length and implicit exponential-like dependence on temperature (recall that $\xi_{nd} \propto T^{-1/2}$) are the most distinctive signatures of I_c in an SNS device.

We note several other *key* points relevant to Eqn. **(8).** First, as a result of the single-frequency approximation, Eqn. **(8)** is valid only for $L>>\xi_{nd}$. There is no difference between $u/\sinh u$ and $2ue^{-u}$ over the range of validity. Second, we have assumed that the entire resistance of the junction is due to the normal interlayer N; $R)$, $= \rho_n L//l$, where ρ_n is the resistivity and $\mathcal{A}$ is the cross-sectional area of N. Therefore, the dependence of I_c on L is purely exponential. Third, the temperature dependence of I_c is dominated by that of the normal coherence length ξ_{nd} appearing in the exponential factor, except extremely close to T_c, where the prefactor dominates. Fourth, nearly all practical Josephson devices have thick superconducting electrodes. As a result there is no significant depression of T_c in the bulk superconducting electrodes due to the proximity effect [90], [91]. The device T_c is therefore identical to that of the electrodes in the absence of any N interlayer. Fifth, it is customary in conventional superconducting theory to ignore the temperature dependence of quantities such as R_n. This is usually justified for temperatures of interest for low-T_c devices, typically below 10 K. It is not necessarily justified for high-T_c superconductors over their larger and higher operating temperature range. This consideration is especially important if D_n, the diffusion constant in N, is temperature-dependent, since it determines ξ_{nd}, which appears in the exponent in Eqn. (8). Finally, we note that R_n appears in Eqn. (8) only because it was conveniently substituted for $\rho_n L/\mathcal{A}$. Thus, Eqn. (8) is actually a prediction for the critical current density J_c of the form Eqn. (5 b), with $J_{co} = \pi\Delta_i^2/(2ekT_c\rho_n\xi_{nd})$ and $L_0 = \xi_{nd}$. As previously stated, the only length dependence of J_c is in the exponential factor.

Intrinsic Gap Depression in Electrodes.

The penetration of superconductivity into a normal material near an SN interface is one manifestation of the proximity effect. Accompanying the finite value of the order parameter in N is its reduction in S; $\Delta_i<\Delta_\infty$, where $\mathrm{A_i}$ is the value of the pair potential at the SN interface and Δ_∞ is its vaiue deep in the bulk of the superconductor. From Eqn. (8), we see that I_cR_n increases monotonically with Δ_i. Therefore, rigid boundary conditions, defined as $\mathrm{A_i}= \Delta_\infty$, will result in the largest I_cR_n values for SNS junctions in the absence of extrinsic interface resistance (discussed below), Simply put, $\mathrm{A_i}$ will be negligibly depressed and A will be constant throughout s in the best SNS devices.

The effect of intrinsic $\mathrm{A_i}$ depression on I_c has been addressed by several authors [88], [92]. The magnitude and, near T_c, the temperature dependence of I_c depend crucially on $\mathrm{A_i}$. de Gennes [88] used the Ginzburg-Landau equation [93] to describe the spatial variation of the order parameter in S near the interface. Letting x be the distance into S away from the SN interface, we define

$$\delta \equiv \frac{\Delta(x)}{\Delta_\infty} \tag{9}$$

so that the Ginzburg-Landau equation for the order parameter becomes:

$$\xi_{sd}^2 \nabla^2 \delta + \delta - |\delta|^2 \delta = 0 \tag{10}$$

where ξ_{sd} is the temperature-dependent Ginzburg-Landau coherence length in S. Note that it is not strictly necessary to introduce the dirty limit for the superconducting banks at this point. However, de Gennes formulated the interracial boundary conditions for the dirty limit only, and so we focus on this limit now. Near T_c, $\xi_s = \xi_{sd} = 0.855(\xi_o \ell_s)^{1/2}(1 - 7'/<)^{-1,12}$, where $\xi_o = \hbar v_s / \pi\Delta(0)$ is the clean zero-temperature coherence length, ℓ_s is the mean free path, and v_s is the Fermi velocity, all in S [94].

Multiplying by $\nabla\delta$ and integrating yields:

$$\delta^4 - 2\left[\left(\frac{\xi_{sd}}{b}\right)^2 + 1\right]\delta^2 + 1 = 0, \tag{11}$$

where

$$b \equiv \left|\frac{\nabla\delta}{\delta}\right|^{II} = \left|\frac{\mathrm{VA(x)}}{\mathrm{A(x)}}\right|^{\text{“}} \tag{12}$$

The order parameter at the interface, $x=0$, is given by $\delta_i = \delta(x = \mathrm{O})$, which depends intimately upon the boundary conditions at the SN interface. We can find δ_i by treating Eqn. (11) as an algebraic equation, with $b(x=\mathrm{O}) \equiv b_i$, known as the extrapolation length. Note that b_i can be viewed geometrically as the distance in which the pair potential would go to zero in N if the rate of decay into the normal region continued linearly from that on the superconducting side of the interface, The value of δ_i is then:

$$\delta_i^2 = 1 + \left(\frac{\xi_{sd}}{b_i}\right)^2 - \left[\left(\frac{\xi_{sd}}{b_i}\right)^4 + 2\left(\frac{\xi_{sd}}{b_i}\right)^2\right]^{1/2}. \tag{13}$$

For the dirty limit, de Gennes [88] obtained $b,= (\rho_n /p,)\xi_{nd}$. A natural interface parameter in proximity effect theory [92], [95],[96] is:

$$\gamma \equiv \left(\frac{\mathcal{N}_n \rho_s}{\mathcal{N}_s \rho_n}\right)^{1/2} = \frac{\mathcal{N}_n}{\mathcal{N}_s}\left(\frac{D_n}{D_s}\right)^{1/2} \tag{14}$$

where $\mathcal{N}$ is the *single spin* density of states at the Fermi level. The term ξ_{sd}/b_i in Eqn. (13) can be expressed as:

$$\frac{\xi_{sd}}{b_i} = \frac{\rho_s \xi_{sd}}{\rho_n \xi_{nd}} \; -\frac{}{2}\gamma\left(\frac{\hbar\pi}{T_c - T}\right)^{1/2} \tag{15}$$

We note that this ratio, multiplied by (~/T)"*, is the interface parameter Γ in [95] (in [92], $\Gamma = \gamma(1 - T/T_c)^{-1/2}$).

The value of A_i given by Eqn. (13) is illustrated in Fig. 19. For an "ideal" *SN* contact with little mismatch in transport properties, $\gamma \cong 1$. However, this "ideal" contact is undesirable because Δ_i, and hence I_c, is reduced.

In fact, I_c is optimized in the rigid boundary condition limit $A_i = \Delta_\infty$ or $\delta_i = 1$. This optimization is achieved, according to Eqn. (13), when $b_i >> \xi_{sd}$, consistent with the absence of a gradient of the pair potential in the banks. Physically, rigid boundary conditions occur under some conditions of extreme mismatch in transport properties between the S and *N* materials, so that $\gamma << 1$. In an *SNS* junction, I_c is determined by the value of the order parameter in N . It is thus possible to have $\Delta_i = \Delta_\infty$ in S and still have a device with a small critical current. For example, rigid boundary conditions often apply to interfaces with insulators but I_c is dramatically lower in most *SINIS* junctions compared to typical SNS ones, becoming negligibly small if the insulator is more than a monolayer or so thick. As a result, we find that rigid boundary conditions are a necessary, but not sufficient, condition for maximizing I_c and $I_c R_n$.

de Gennes [88] was most interested in the opposite extreme limit of soft boundary conditions: $hi << \xi_{sd}$ or $\gamma >> 1$. From Eqn. (13) we find

$$\delta_i^2 = \left(\frac{\Delta_i}{\Delta_\infty}\right)^2 \cong \frac{1}{2}\left(\frac{b_i}{\xi_{sd}}\right)^2 = \frac{2}{\pi^2}\frac{1}{\gamma^2}\frac{T_c - T}{T} \qquad (b_i << \xi_{sd}) \tag{16}$$

in this limit. The order parameter at the interface, A_i, is significantly depressed, resulting in a reduction of I_c. Clearly the boundary parameter y contributes significantly to the reduction of critical current; $I_c \propto 1/\gamma^2$. In addition, we note that A_i has an additional temperature dependence beyond that of Δ_∞, which contributes to a further reduction of I_c. It should be emphasized, however, that Eqn. (16) represents only one

extreme limit of the more general de Gennes theory.

The sensitivity of I_c to the behavior of A, is compounded when the electrodes are made from high- T_c materials. One of the hallmark characteristics of a high-T_c superconductor is a remarkably short coherence length ξ_s [97], which can be on the order of the unit cell size. It has been suggested that this creates another mechanism by which the pair potential can be suppressed at an interface [98]. We start by considering an *SI* interface. At such an interface, de Gennes [88], [99] showed that the extrapolation length is given by:

$$\frac{1}{b_i} \cong \frac{2}{\xi_o^2} \int_{-\infty}^{\infty} \frac{\Delta(x)}{\Delta_\infty} \left[1 - \frac{\mathcal{N}_s(x)}{\mathcal{N}_s} \right] dx \qquad (17)$$

where ξ_0 is the clean, zero-temperature coherence length in the superconductor. The density of states $\mathcal{N}_s(x)$ differs from its bulk value $\mathcal{N}_s$ only within about a lattice constant, a_o, of an interface. Consequently, the integrand is nonzero only in this small spatial region, where it changes from O to 1, so that $b_i \approx \xi_o^2 / a_o$ In typical superconductors, $\xi_o >> a_o$, so $b_i >> \xi_o$. This means that $b_i >> \xi_s$ except within an extremely small temperature range near T_c. However, if $\xi_o \approx a_o$, then $b_i \approx \xi_o$, and the temperature range over which $b_i << \xi_s$ can be substantial, From Eqn. (16), we know that $b, << \&$ implies an additional temperature dependence, beyond that of Δ_∞, for I_c near T_c. Thus, a junction with high-T_c superconducting electrodes can have a depressed A, at the interfaces regardless of the quality of device fabrication. In principle, this gap reduction at an interface can be minimized, or even eliminated, by a proper choice of junction materials [100].

Device Critical Currents Near **T_c.**

Studies of $I_c(T)$ near T_c are common because temperature is a readily-accessible experimental variable. There is, however, a tendency to overuse such information in attempting to determine the nature of high-T_c devices. For example, it is occasionally claimed that a particular device must be SNS because $I_c \propto (T_c - T)^2$ near T_c, even though this behavior is only one limit of *SNS* theory and can occur in other (non- *SNS)* structures. As we shall see, fitting $I_c(T)$ near T_c tends to be an unconvincing means of elucidating the nature of a junction.

For long $(L >> \xi_n)$ *SNS* junctions, $I_c(T)$ *is* dominated by the temperature-dependent factor L/ξ_{nd} in the exponent in Eqn. (8). *Any* long device obeying conventional proximity effect theory must have a clear exponential-like I_c (T) dependence over most of the temperature range below T_c. Very close to T_c, however, the prefactor in Eqn. (8)

dominates, and $I_c \propto \Delta_i^2$. Recall from BCS theory that $\Delta_\infty \propto (T_c - T)^{1/2}$ near T_c [24]. Then, for rigid boundary conditions $(b_i >> \xi_{sd})$, $A_i = \Delta_\infty$ and $I_c \propto (T_c - T)$. In contrast, for soft boundary conditions $(b_i << \xi_{sd})$, A_i is given by Eqn. (16), and $I_c \propto (T_c - T)'$.

Mathematically, there is always a region near T_c in which Eqn. (16) is a good approximate solution to Eqn. (13), due to the divergence of ξ_{sd}/b_i at T_c. Thus, in principle, $I_c(T)$ always exhibits soft boundary behavior near T_c. Experimentally, however, one cannot approach arbitrarily close to T_c. "Near T_c" is, in practical terms, the region within a few percent of T_c, or a few kelvins for $T_c \cong 90\,K$. One cannot expect accurate measurements closer than a few tenths of a percent or so of T_c. From Eqn. (13), we find numerically that for $0.001 < 1 - T/T_c < 0.01$, the critical current is proportional to $(T_c - T)^a$, with $1 < \alpha < 2$ (corresponding to $0 < y < \infty$), as shown in Fig. 20, Thus, proximity effect behavior is compatible with a variety of possible power laws very close to T_c.

Not only does proximity effect theory fail to predict a unique power law dependence of I_c (T) near T_c, but *other* mechanisms exist which are compatible with the *same* power laws. For example, a linear dependence, $I_c \propto (T_c - T)$, is obtained for tunnel junctions [23], point contacts [25],[26] and SNS junctions with rigid boundary conditions [6],[96]. A quadratic dependence $I_c \propto (T_c - T)^2$ can be obtained when the order parameter in S is suppressed at an *SN* interface due to the proximity effect (soft boundary conditions) [88] or at an *SI* interface due to a small ξ_s [98]. Other dependence are possible as well, not all associated with electron transport. In the case of flux flow, $I_c(T) \propto (T_c - T)^{\alpha}$, with α =1 .5, 2, or 2.5 [101]. Thus, the behavior of $I_c(T)$ near T_c is, by itself, of little value in determining the nature of a junction.

In this context, several experimental difficulties in near-~ studies of $I_c(T)$ should be mentioned, To begin, it is very difficult to measure I_c accurately as $T \to T_c$ because thermal fluctuations dominate in this temperature regime. Furthermore, the numerical value of T_c must be precisely determined, otherwise it is possible to fit different $(T_c - T)^a$ dependence with the *same* data [102]. Finally, of course, the device properties must be uniform enough throughout the junction that a single T_c is meaningful.

In summary, we reiterate that all long proximity effect devices should exhibit an exponential-like dependence of critical current over a broad temperature range below T_c. Though detailed studies of $I_c(T)$ within a few percent of T_c provide information about the boundary conditions within SNS theory, it is not possible to draw definite conclusions about the nature of any junction from such data alone.

B. **Microscopic Theories**

The results of de Gennes apply to arbitrary metallic contacts involving long (L>> ξ_n), dirty SNS junctions attemperatures nottoo far below T_c. Fortunately, these limitations are not overly restrictive for us since the typical N material in a high-~. SNS device has a short normal coherence length at the operating temperatures of greatest interest. While long junctions provide the clearest signature of proximity effect behavior, short devices are important for practical applications. It is therefore useful to examine junction behavior outside the limits of de Gennes' theory,

More general theoretical approaches are required to deal with arbitrary bridge length and temperature. These approaches are usually based on a more tractable form of Gor'kov's results, the Usadel equations [1 03]. The Usadel equations describe dirty superconductors, but are not restricted to temperatures near T_c, as are the more familiar Ginzburg-Landau relations used by de Gennes. Using this approach, the theory of SNS junctions was extended to encompass arbitrary bridge length (by abandoning the single-frequency approximation) and the entire temperature range below T_c. Likharev's pioneering work [6],[1 04] covered the limit of rigid boundary conditions and is a special case of the more general subsequent work of Kupriyanov and co-workers, who dealt with the proximity effect in the superconductor [92], the effects of interracial barriers [96], finite electron-electron interactions in the N interlayer [1 05], and depairing effects due to large currents in the S electrodes [106]. The latter can be important in short junctions if the condition $\gamma << L/\xi_{nd}(T_c)$ is not met.

The results of Likharev [104] for rigid boundary conditions are illustrated in Fig. 21, which shows the temperature dependence of $I_c R_n$ for various junction lengths. Also shown are curves obtained from de Gennes's theory, Eqn. (8), which follow Likharev's predictions quite closely for temperatures above roughly $0.3T_c$ for $L>2\xi_{nd}(T_c)$. Fig. 22 compares the shape of the temperature dependence of I_c to the linear dependence of Eqn. (1). Clearly, only values of L close to $4\xi_{nd}(T_c)$ are quasi-linear.

Although the general results obtained via the Usadel equations are not simple analytic expressions, the important limiting cases are tractable. For example, for long, dirty junctions under rigid boundary conditions not too far below T_c, Likharev [6],[1 04] and Kupriyanov and Lukichev [92] found that

$$I_c(T;L) = \frac{2}{\pi e R_n}\frac{|\Delta_\infty|^2}{kT_c}\frac{L/\xi_{nd}}{\sinh(L/\xi_{nd})} \cong \frac{4}{\pi e R_n}\frac{|\Delta_\infty|^2}{kT_c}\frac{L}{\xi_{nd}}e^{-L/\xi_{nd}} \qquad (0.3T_c < T < T_c) \qquad (18)$$

Not surprisingly, this expression differs from Eqn. (8), the prediction of de Gennes, by

only a constant of order unity.

In investigating high-< SNS junctions, it is common practice to use Eqn. (8) or Eqn. (18) to infer a value of ξ_{nd} at 4.2 K. Typically, the dependence $I_c(L)$ for junctions obeying $L>>\xi_n(T)$ is fit to the dependence $\exp[-L/\xi_{nd}(T)]$. However, 4.2 K is less than 50/0 of $T_c \cong 90\,K$, and these equations are not valid at such low reduced temperatures,

In order to examine the critical current at very low temperatures, we therefore look at the microscopic theories in the limit $T/T_c << 1$. Within Likharev's theory, for long junctions with $L>>\xi_{nd}(T_c)$, conventional SNS theory does not predict an exponential dependence for I_cR_n on L for $T \to 0$. Instead, the theoretical prediction [6],[1 04] can be approximated by:

$$I_c(T;L) \cong 29\frac{\Delta_\infty(0)}{eR_n}\left(\frac{\xi_{nd}(T_c)}{L}\right)^2 \qquad (T< 0.05q;L26\&(q)). \tag{19}$$

Since $\Delta_\infty(0) \propto k\,T_c$ and $\xi_{nd}^2(T_c) \propto 1/T_c$, we find from Eqn. (19) that at low temperatures $J_c = 8.15\hbar D_n/(e\rho_n L^3)$ *independent of the magnitude of the gap* or other properties of the electrodes.

In many experiments, the behavior of I_c, not that of I_cR_n, is examined. As in the case of Eqn. (8), R_n appears in Likharev's results for I_c only as a result of the substitution $\rho_n L/\mathcal{A} = R_n$. Thus, $I_cR_n = \rho_n L\,J_c$ and Eqns. (18) and (19) are really predictions for J_c. For $L>>\xi_{nd}(T)$ and $T>0.3T_c$, Eqn. (18) is equivalent to Eqn. (5 b), with the only length dependence of J_c in the factor $\exp(-L/\xi_{nd})$. We have found empirically that the purely exponential dependence of Eqn.(5b) is a good approximation to theory for *all* temperatures, provided that $5<L/\xi_{nd}(T_c)<12$. (This approximation does not work for larger L at lower temperatures due to the slower power law decrease in J_c discussed above.) The temperature dependence of the parameters L_0 and J_{co} are shown in Figs. 23 and 24, respectively, along with the predictions of E qn. (8). Figure 23 allows us to infer a value for $\xi_{nd}(T_c)$ from the value of L_0 obtained from low-temperature exponential fits of $J_c(L)$. In fact, we see from Fig. 23 that fitting $J_c(L)$ to the exponential dependence of Eqn.(5b) at low temperatures yields not $\xi_{nd}(T)$, but rather $L_0 = 3.18\xi_{nd}(T_c)$. For $T = 4.2\,K$ and $T_c = 90\,K$, the commonly-made assumption that $\xi_{nd}(T_c) = (\hbar/\sim)\,L_o^2 = 0.216\,L_0$ actually *underestimates* $\xi_{nd}(T_c) = L_0/3.18$ by 31 o/o. Finally, we note that empirically $J_{co} \to 0.70\,\Delta_\infty(0)/(e\rho_n\xi_{nd}(T_c))$ as $T \to 0$.

One might expect that an *SNS* junction would be equivalent to a pure superconducting point contact in the limit $L \to 0$. In fact, dirty *SNS* theory does indeed converge with dirty point contact theory [25] in this limit. For example, Eqn.(4) for dirty point contacts

represents the L =0 limit of *SNS* theory, so that the L =0 curves in Figs. 21 and 22 are identical to curve b in Fig. 1.

Clearly, *SNS* theories do not, in general, predict a quasi-linear $I_c(T)$. We noted in conjunction with Fig. 2 that varying the value of $\Delta(0)/kT_c$ dramatically alters the shape of normalized I_c (T) curves for tunnel junctions and point contacts. The same reasoning applies to short *SNS* junctions as well. However, we are interested primarily in the limits applicable to Eqn. (8), namely T>0.3T_c and $L>>\xi_n$ (T). Under these conditions, the ratio $\Delta(0)/kT_c$ is only a numerical prefactor that does not alter the shape of normalized $I_c(T)$ curves.

As we have already mentioned, *all* of de Gennes's results, covering the limit $L>>\xi_n$, for temperatures not too far below T_c, are special cases of the more general calculations of Kupriyanov and co-workers. For rigid boundary conditions, the de Gennes result, Eqn. (8) with $A_i = \Delta_\infty$, differs from the more general one, Eqn. (18), only by factor of $\pi^2/8 \cong 1{,}23$. For the limit of soft boundary conditions, the de Gennes result, obtained by using Eqn. (16) in Eqn. *(8),* differs from that of Kupriyanov and Lukichev [92] in the same limit only by a factor of 0.62.

C. The Effect of Interface Resistance

Extrinsic Gap Depression in the Electrodes

Our earlier conclusion that rigid boundary conditions are desirable was reached assuming the *SN* interface to be a good contact. Impurities, defects, chemical reactions, layer interdiffusion, and other extrinsic effects can affect the value of the order parameter near an interface. These causes can weaken the superconducting phenomenon at the interface thereby depressing A, and softening the boundary conditions, Given the complex chemical and structural nature of high-T_c materials, extrinsic effects and their influence on I_c may be both common and observable.

Let us consider the theoretical consequences of A_i depression caused by extrinsic effects. The de Gennes approach to calculating I_c, based on the Ginzburg-Landau equations, is easily generalized to allow for arbitrary boundary conditions. We define:

$$A = \frac{|\psi_n|_{x=0}}{|\psi_s|_{x=0}}, \tag{20}$$

where ψ, the Ginzburg-Landau order parameter, is proportional to the pair potential: $\psi = \left[\pi m_s/(4e^2\hbar kT_c\rho_s)\right]^{1/2} \Delta$ *[89],* where m_s is the electron mass in S. Since δ_i in Eqn. (9)

can be expressed as:

$$\delta_i = \frac{|\psi_s|_{x=0}}{114\chi+-}, \tag{21}$$

we find from Eqn. (8) that for long dirty junctions [16],[1 07]:

$$I_c(T;L) = \frac{\pi}{4eR_n}\frac{|\Delta_\infty|^2}{kT_c}\delta_i^2 A^2 \frac{\rho_n m_s}{\rho_s m_n}\frac{L/\xi_{nd}}{\sinh(L/\xi_{nd})} \qquad (L >> \xi_n). \tag{22}$$

In the case of specular scattering at the *SN* interfaces, $A^2 = \rho_s m_n / \rho_n m_s$, giving precisely Eqn. (8) [107]. In other situations, A is determined by the properties of the interface, including those due to extrinsic effects. In principle, the value of A can be determined by independent experiments. As always, the special case of rigid boundary conditions is defined by 6,=1.

Interface Resistance

Generally, $|T|^2$, the quantum-mechanical transparency of a single *SN* interface, is close to unity because the contact is between two metals. However, extrinsic effects can create significant interracial scattering or an insulating barrier, I, between the S and N regions, reducing $|T|^2$ and virtually assuring rigid boundary conditions, A(x)= Δ_∞, in S. At the same time, the value of the order parameter in N is dramatically reduced. The net effect is a reduction of I_c and, ultimately, $I_c R_n$. This is an example in which achieving $A_i = \Delta_\infty$ at the *SN* interface fails to guarantee high junction performance. In fact, the presence of interface resistance in an *SNS* device is generally detrimental.

As discussed by Robertazzi *et al.* [52], a Josephson supercurrent reflects a coherent process. In an S1S tunnel junction, $I_c \propto |T|^2$ [108]. In a nominally SNS junction, there are *two* barriers, or tunnel junctions, in the actual *SINIS* structure. Therefore $I_c \propto (|T|^2)^2$. (Of course, for long devices there is an *additional* $\exp(-L/\xi_{nd})$ depression of I_c due to the loss of coherence in N.) The normal resistance in the *SIS* case is proportional to $1/|T|^2$ [109],[1 10] while, in the *SINIS* case, $R_n = (\rho_n L + 2r_c)/\mathcal{A}$, where r_c is the specific contact resistance, with $r_c \propto 1/|T|^2$. Therefore, $I_c R_n$ is independent of $|T|^2$ in the *SIS* case, but is approximately proportional to $|T|^2$ in short contact-dominated *SNS* junctions in which R_n is determined primarily by r_c. In longer devices, $I_c R_n$ is much smaller than this short link limit because of the exponential decrease of I_c with increasing L, which more than compensates for the linear increase in R_n due to $\rho_n L$.

This argument can be phrased more quantitatively [107]. Using the approach outlined above, $\delta_i = 1$ and $A \propto |T|^2$. Since $|T|^2 << 1$ for even a monolayer of typical insulator, $A << 1$ and, as shown by Eqn. (22), $I_c R_n$ *is* drastically reduced from its optimum value if an insulator is present at the *SN* interface. In addition, an extra prefactor $(1+ 2r_c / \rho_n L)$ must be included in Eqn. (22) to account for contact resistance. Note that $I_c R_n$ is proportional to $\exp(-L/\xi_n)$ in long junctions, whether *SNS* or *SINIS*.

This discussion, based on a Ginzburg-Landau approach, is consistent with the general treatment of *SINIS* junctions in the dirty limit by Kupriyanov and Lukichev [96]. Defining an interface parameter

$$\gamma_b = \frac{r_c}{\rho_n \xi_{nd}(T_c)}, \tag{23}$$

they considered long, dirty junctions, with $\gamma << 1$ (assuring rigid boundary conditions for any γ_b):

$$I_c(T;L) = \left(\frac{4\pi kTC}{\Delta_\infty}\right)^2 \left(1 + \frac{2r_c}{\rho_n L}\right)\left(\frac{4}{\pi e R_n}\frac{|\Delta_\infty|^2}{kT_c}\frac{L}{\xi_{nd}} e^{-L/\xi_{nd}}\right) \qquad (L >> \xi_n(T_c)) \tag{24}$$

where $R_n = (\rho_n L + 2r_c)/\mathcal{A}$. The coefficient C is determined from

$$\frac{\Delta_\infty}{\pi kT} C^4 + 4(1-g)C^3 - 6\frac{\Delta_\infty}{\pi kT} C^2 - 4(1+g)C + \frac{\Delta_\infty}{\pi kT} = 0, \tag{25}$$

with $g = \gamma_b (T/T_c)^{1/2}\left[1 + (\Delta_\infty / \pi kT)^2\right]^{1/2}$. Eqn. *(24)* resembles the de Gennes and Likharev results discussed earlier, except that R_n now includes a contact resistance and there is an additional factor of $(4\pi kTC/$ A.)*. Note that C is maximized for $T \to 0$, and therefore $0 \le C \le \sqrt{2} - 1$.

Let us examine the implications of Eqn. (25). Because proximity effect theory applies to metals we expect that $\rho_n < 10\,\Omega - \mu m$. Noting that ξ_{nd} decreases as ρ_n increases, we find in all cases that $\rho_n \xi_{nd}(T_c) < 0.01\,\Omega - \mu m^2$ for T_c near $90\,K$. Since we anticipate that even in the best metallic contacts, $r_c > 0.01\,\Omega - \mu m^2$, we see from Eqn. (23) that $\gamma_b > 1$. As a result, in a typical *SIN* contact $\gamma_b >> 1$. In this low transparency limit, g>> 1 so that

$$\left(\frac{4\pi kTC}{\Delta_\infty}\right)^2 \cong \frac{1}{g^2} = \frac{1}{\gamma_b^2}\frac{T_c}{T}\frac{(\pi kT)^2}{(\pi kT)^2 + \Delta_\infty^2} \cong \frac{1}{\gamma_b^2}. \tag{26}$$

The prefactor $(4\pi kTC/\Delta_\infty)^2$ contains the effect of interface scattering on J_c. The final result is a valid approximation over a broad temperature range since the temperature-dependent factor multiplying $1/\gamma_b^2$ only increases from 0.93 to 1 for $0.5< T/T_c<1$. Figure 25 shows the accuracy of our approximation under the more restricted temperature range $T \to T_c$.

In Eqn. (24), the last factor in parentheses is identical to Eqn. 18, Likharev's rigid boundary condition result for long junctions, except that R_n now includes the contact resistance which is also reflected in the middle factor in parentheses. As before, Eqn. *(24)* can be interpreted as an expression for J_c in the form of Eqn. (5 b), with J_{co} given by Likharev's result multiplied by $(4\pi kTC/\Delta_\infty)^2$, or $1/\gamma_b^2$ near T_c for $\gamma_b>>1$. In this limit, $J_{co} = 4\Delta_\infty^2 \rho_n \xi_{nd}(T_c)/(\pi e k T_c r_c^2)$.

The most important conclusion to be drawn from our discussion of *SNS* junctions with imperfect interface transparency is that, for a given value of $L/\xi_{nd}(T_c)$, *the shapes of normalized* $I_c(T; L)$ *curves are the essentially the same for both SNS and SINIS devices.* Because boundary resistance is typically not very temperature-dependent, the exponential factor $\exp(-L/\xi_{nd})$, dominates the temperature dependence of I_c as long as $L>> \xi_n$. Therefore, spatially-homogeneous interracial properties cannot explain non-exponential $I_c(T)$ dependence in long junctions.

In contrast, we emphasize that the *absolute magnitudes* of $I_c R_n$ anti J_c are dramatically smaller in the *SINIS* case for $\gamma_b>>1$ than in the SNS case. For *SINIS* devices $I_c \propto 1/\gamma_b^2$ and $R_n \propto r_c \propto \gamma_b$, and so it follows that $I_c R_n \propto 1/\gamma_b$. This result is consistent with our earlier one in terms of $|T|^2$, since the factor of $1/\gamma_b^2$ in Eqn. (24) implied by Eqn. (26) can be identified with the factor $A' \rho_n m_s/\rho_s m_n$ in Eqn. (22).

Although we have argued that $\gamma_b>>1$ is likely to hold in *SINIS* junctions, it is interesting to consider the case of small γ_b. In the limit $T \to T_c$, $\Delta_\infty \to 0$ and the relevant solution to Eqn. (25) is $C \cong \Delta_\infty/[4\pi kT(1 + g)]$ so that $4\pi kTC/\Delta_\infty \cong 1- \gamma_b$, as shown in Fig. 25. Thus, $I_c \propto (1 - \gamma_b)^2$ and $I_c R_n \propto (1 - \gamma_b)^2[1+2\gamma_b \xi_{nd}(T_c)/L] \cong (1 -- \gamma_b)^2$. Clearly, even an arbitrarily small value of γ_b (arbitrarily high barrier transparency) will slightly reduce I_c and $I_c R_n$ from the optimum rigid boundary condition values obtained by de Gennes and Likharev. Of course, it is possible for the reduced $I_c R_n$ value in an *SINIS* device to exceed that which results from soft boundary conditions in an *SNS* device, since in the latter case $I_c R_n \propto 1/\gamma^2$ for $\gamma>>1$.

Spatially-Inhomogeneous Interfaces

The idealized contacts discussed in the preceding section were assumed to be spatially

homogeneous with the contact resistance r_c reflecting a constant value of barrier transparency, $|T|^2$. This is an inadequate model for many fabricated devices, in which $|T|^2$ can fluctuate widely over the contact areas, its local value having little to do with the value of microscopically observable quantities such as r_n. This has been clearly demonstrated with low-T_c tunnel junctions [1 11],[1 12] and superconductor-semiconductor contacts [17],[1 13].

The simplest inhomogeneous *SINIS* contacts can be understood using a lumped element model. Consider an *SINIS* device in which the transparency of the *SN* interfaces is inhomogeneous. We can picture the SN contacts as consisting of two parallel channels, one for the regions of high barrier transparency (a small resistor) and one for those of low transparency (a large resistor). Because most of the applied current will flow through the small resistor, this high-transparency channel dominates the total conductance of the system.

In a superconducting device, the small-resistance branch dominates the critical current as well as normal conductance. In other words, the inhomogeneity simply reduces the effective area of the *SN* contacts. As a result, within our two-channel model, interface inhomogeneity results in higher device resistance, in conjunction with lower critical current, compared to a homogeneous high-transparency device. Of course, $I_c R_n$ is essentially the same in the two cases. In an *SNS* device having homogeneous interfaces with $\delta_i = 1$ and $|T|^2 \cong 1$, the $I_c R_n$ product is optimal. Because r_c is low, such a device will typically have an impractically small R_n. A spatially-inhomogeneous, low-transparency layer *I* at one or both *SN* interfaces partially blocks current flow, reducing I_c and increasing R_n, keeping $I_c R_n$ constant. Although such a higher-resistance device may be more practical, it is not clear that such an *SNS* device is more desirable than a point contact array with no *N* interlayer present at all.

Our discussion has based on the simplest possible two-channel model. The more-transparent channel dominated transport of both normal current and supercurrent and the less-transparent channel was effectively opaque. We can generalize the model by allowing the less-transparent channel to contribute to the total device current by increasing its transparency and possibly its fraction of the total contact area. We saw in the previous section that in the *SINIS* picture, less-transparent regions contribute more to the normal conductance, which varies as $|T|^2$, than to the critical current, which varies as $(|T|^2)^2$. Thus, the less-transparent regions can contribute significantly to the total device conductance without contributing significantly to I_c. This explains why an inhomogeneous *SINIS* junction with maximum local transparency $T_{max}{}^2$ can have an $I_c R_n$ product that is *smaller* than a homogeneous one whose interface transparency is $|T_{max}|^2$ over the entire device area.

Although this two-channel model can be made more realistic by allowing a spread of $|T|^2$ values, it is still oversimplified. Diffusive transport in the N interlayer in a $SINIS$ device means that high-transparency regions of one SN contact interact with both high-and low-transparency regions of the other contact. Nevertheless, the preceding discussion does demonstrate that, in realistic cases of devices having inhomogeneous SN interfaces, $I_c R_n$ can be no larger than the optimal limiting value predicted for an SNS or $SINIS$ device with homogeneous contacts having $\delta_i = 1$ and $|T|^2 \cong 1$. Introducing contact inhomogeneity does not *improve* $I_c R_n$ and in many cases *reduces* it.

Finally, we emphasize that, under conventional proximity effect theory, the presence of a thick N interlayer $(L >> \xi_n)$ must result in the familiar exponential dependence $I_c \propto \exp(-L/\xi_n)$ regardless of the nature of the SN interfaces (whether homogeneous or inhomogeneous). This is inconsistent with the quasi-linear $I_c(T)$ dependence most often observed in high-T_c devices. Previous discussions of the role of the SN interfaces [1 14] failed to recognize that the normal layer does not contribute significantly to the supercurrent in typical high-T_c SNS and $SINIS$ junctions. In other words, most devices under consideration are SNS in name only.

Limits on Ic

We have seen that, in both SNS and $SINIS$ proximity effect-coupled junctions, it is the minimum value of the superconducting order parameter (or wavefuncton) that determines, and limits, I_c. Contributing factors to the value of I_c are: (1) the value of A in the bulk of the S electrodes (assuming thick S layers with $A = \Delta_\infty$), (2) the reduction, created by the proximity effect, of the order parameter in S as the SN boundary is approached, (3) the reduction of the order parameter in crossing the SN boundary, and finally, (4) the reduction of the order parameter as it decays exponentially in N as $\exp(-L/\xi_n)$.

Soft boundary conditions are responsible for factor *(2)*. Rigid boundary conditions, perhaps due to an extreme mismatch in transport properties between S and N, allow for factor (2) to be overcome. The presence of an SN interracial barrier allows factor (3) to significantly reduce the critical current as $I_c \propto 1/\gamma_b^2$ (recall that $\gamma_b >> 1$ for any realistic interracial tunnel barrier).

The effect of the various boundary conditions is summarized in Table 1. Expressions for J_{c0}, the prefactor in Eqn. (5 b), are included in order to show the effects of the boundary parameters y and γ_b on J_c. The de Gennes expressions are listed for the two pure SNS cases. For consistency, the $SINIS$ result differs from that obtained from

Eqn. (24) by the factor $\pi^2/8$ discussed earlier.

D. Greater Model Sophistication

So far, our discussion of *SNS* theory has been limited to the special case of devices whose N interlayer is in the dirty limit with $T_{cn}=0$. Neither of these conditions is required for the proximity effect, and the study of high-~. devices motivates a relaxation of these restrictions. At elevated temperatures ($T \cong 77\,K$) ξ_{nc} becomes very short and the clean limit ($\ell_n >> \xi_{nc}$) is more likely to be encountered in the interlayer. In addition, although N interlayers that undergo a superconducting transition are rarely encountered in low-T_c devices, there has been a focus on high-T_c devices based on such materials. This interest results from the fact that doping cuprate superconductors can reduce T_c, allowing for N interlayers which are structurally well-matched to the S electrodes. Thus, we need to go beyond the more common dirty limit, T_{cn} =0 models.

Fortunately, the original de Gennes result, Eqn. (8), is valid regardless of the value of T_{cn}, provided the proper expression for ξ_{nd} is used. In contrast, Eqn. (8) is not expected to apply in the clean limit since it was derived using dirty limit boundary conditions. Nevertheless, calculations of I_c for long junctions with an arbitrary mean free path in N [1 15], including microscopic calculations carried out in the clean limit [1 16], give results similar to Eqn. (8). In particular, $I_c \propto \exp(-L/\xi_n)$ as before, assuming that an appropriate expression is used for the normal coherence length. Consequently, we will obtain general expressions for ξ_n and use Eqn. (8) to describe I_c in the long junction limit (L>> ξ_n), with the caveat that the results should be viewed more skeptically as the dirty limit approximation is relaxed. This approach should hold in the cases of greatest present interest.

Coherence Lengths

Cuprate superconductors are highly anisotropic. In some cases, *SNS* junctions are fabricated using doped cuprates as N interlayers. We thus must allow for a possible quasi-2d interlayer when modeling the devices. Although we will examine expressions for the normal coherence length in both 3d and 2d materials, we will find that there is little difference between the two cases. In fact, the expressions for ξ_n with nonzero T_{cn} in 2d are mathematically simpler than their 3d counterparts.

Very general expressions for ξ_n, valid for arbitrary T_{cn} and ℓ_n, have been obtained. For 3d metals in the single-frequency approximation, ξ_n is given by [1 17]:

$$\frac{1}{2}\ln\frac{T}{T_{cn}} = \frac{\mathcal{K}}{\frac{\xi_{nc}}{\xi_n} - \frac{\xi_{nc}}{\ell_n}\mathcal{K}} - 1 \qquad \text{(3d, general case)} \qquad (27a)$$

where

$$\mathcal{K} = \tanh^{-1}\left(\frac{1}{\xi_n}\frac{\xi_{nc}\ell_n}{\xi_{nc}+\ell_n}\right) \qquad (27b)$$

(Recall that the single-frequency approximation is valid in the long junction limit only.) The analogous result for 2d materials [1 18] in the single-frequency approximation is:

$$\xi_n = \xi_{nc}\left(\frac{1+\frac{2}{\ln(T/T_{cn})}}{4+\ln(T/T_{cn})+\frac{2\xi_{nc}}{\ell_n}}\right)^{1/2} \qquad \text{(2d, general case).} \qquad (28)$$

For T_{cn} =0 and arbitrary mean free path we obtain from Eqns. (27):

$$\xi_n \tanh\left(\frac{\ell_n}{\xi_n}\right) = \frac{\xi_{nc}\ell_n}{\xi_{nc}+\ell_n} \qquad (3d,\ T_{cn} = O) \qquad (29)$$

(this result can also be derived directly for T_{cn} = 0 [1 16]), The analogous result for 2d materials is:

$$\xi_n = \left(\frac{1}{\xi_{nc}^2} + \frac{1}{\xi_{nd}^2}\right)^{-1/2} \qquad (2d,\ T_{cn} = O)\ . \qquad (30)$$

Because the 3d result, Eqn. (29), only gives ξ_n implicitly, it is easier to use the 2d result, Eqn. (30), as an approximation [1 19] since it agrees with Eqn. (29) to better than *6%* for all values of ℓ_n. Fig. 26 illustrates the dependence of ξ_n on ℓ_n for the 3d T_{cn} =0 case, comparing the exact and approximate expressions.

For finite T_{cn} in the dirty limit ($\ell_n << \xi_{nc}$) Eqns. (27) and (28) both give the result originally derived by de Gennes [88]:

$$\xi_n = \xi_{nd}\left(1+\frac{2}{\ln(T/T_{cn})}\right)^{1/2} \cong \left(\frac{\hbar D_n}{\pi k(T-T_{cn})}\right)^{1/2} \qquad (2d \text{ and } 3d,\ \ell_n << \{),(.). \qquad (31)$$

The approximation in Eqn. (31) is valid for $(T - T_{cn})/T_{cn} << 1$. Allowing T_{cn} to approach O in the approximate expression violates this condition and results in a value for ξ_n that exceeds the correct dirty limit formula by a factor of $\sqrt{2}$.

For finite T_{cn} in the clean limit, Eqns. (27) yield the implicit relationship for 3d materials:

$$\frac{1}{2}\ln\frac{T}{T_{cn}} = \frac{\xi_n}{\xi_{nc}}\tanh^{-1}\left(\frac{\xi_{nc}}{\xi_n}\right) - 1 \qquad (3d, \ell_n >> \xi_{nc}). \tag{32}$$

For 2d materials in the clean limit:

$$\xi_n = \xi_{nc}\frac{1 + 2/\ln(T/T_{cn})}{\left[1 + 4/\ln(T/T_{cn})\right]^{1/2}} \cong \frac{\hbar v_n}{2\pi k T_{cn}}\left(\frac{T_{cn}}{T - T_{cn}}\right)^{1/2} \qquad (2d, \ell_n >> \xi_{nc}). \tag{33}$$

As in the dirty limit, the approximation in Eqn. (33) is valid for $(T - T_{cn})/T_{cn} << 1$. Again, it fails in the limit $T_{cn} \to 0$, predicting that $\xi_n(T_c)$ diverges as $1/T_{cn}^{1/2}$ rather than approaching $\xi_{nc}(T_c)$ as given by Eqn. (6). We point this out explicitly because the approximations shown in Eqns. (31) and (33) continue to be applied over wide temperature ranges in place of the exact results [73],[1 20], compromising the associated analysis.

As expected, the familiar results given by Eqns. (6) and (7) follow immediately from Eqns. (29), (30), or (31) in the dirty limit and Eqns. (29), (30), (32), and (33) in the clean limit for $T_{cn} = 0$. In general, all of the many expressions for the order parameter decay length in normal metals found in the literature agree in the appropriate limits. Note however that Eqns. (27) and the results that follow from them differ from some earlier results [115],[121] which work in the dirty limit but approach $\xi_{nc}/\sqrt{3}$, rather than ξ_{nc}, in the clean limit. The discrepancy resulted from an inaccurate approximation to the Usadel equations [1 17]. Finally, Eqn. (30) is equivalent to Eqn. (28) even when T_{cn} *O, provided that the exact expressions for the coherence lengths given by Eqns. (31) and (33) replace ξ_{nd} and ξ_{nc}, respectively.

We close by emphasizing that the clean and dirty limit expression Eqns. (6) and (7) for the case $T_{cn} = 0$, and Eqns. (31) - (33) for arbitrary T_{cn}, are *upper* limits for the actual value of ξ_n. If the clean limit applies, then the dirty limit expression overestimates ξ_n, and *vice* versa. This was never a significant issue with low-T_c materials because it is difficult to achieve the clean limit for the temperature range of interest in low-~. thin film structures. However, it is possible to encounter both the clean and dirty limits in high-T_c structures, so careful consideration of the proper expression for ξ_n is required.

Ic in the Clean Limit

We have repeatedly stressed that all theories discussed thus far apply to devices in the dirty limit. It is possible, however, to encounter high-~. devices which are well out of this regime, particularly at higher operating temperatures. For example, $\ell_n \approx \xi_{nc}$ in high-T_c SNS devices with noble metal interlayers at temperatures not too far below T_c.

We can begin to approach experimental results from such devices using the microscopic theory developed by Kupriyanov [1 16]. This calculation of $I_c(T)$ is valid for clean, ballistic junctions $(\ell_n >> \xi_{nc}, L)$ under rigid boundary conditions $(v_n << v_s)$. Once again, the ubiquitous exponential relationship $I_c \propto \exp(-L/\xi_n)$ is obtained for long $(L >> \xi_{nc})$ devices.

Kupriyanov's results for $I_c R_n$ as a function of temperature in clean junctions are illustrated in Fig. 27. We note that the normal state resistance of such a device is determined by Sharvin's formula $R_n \mathcal{A} = 2/(e^2 \mathcal{N}_n v_n)$ [122],[1 23] because $\ell_n >> L$. Fig. 28 compares the shapes of normalized $I_c(T)$ curves to the linear dependence of Eqn. (1). Clearly, only very short devices (small values of L) yield quasi-linear $I_c(T)$ curves. In the limit $L \rightarrow 0$, these devices are equivalent to clean point contacts and this theory converges with that of Ref. [26]. The $L = 0$ curves in Figs. 27 and 28 are therefore identical to curve c in Fig. 1.

E. Resonant Tunneling Models

The term "long range proximity effect" identifies junctions in which proximity effect coupling apparently occurs over distances many times (perhaps orders of magnitude) longer than those expected from the conventional normal coherence length. Experimental evidence for long range proximity effect coupling usually consists of an exponential dependence of I_c on L, $I_c \propto \exp(-L/\xi_n^*)$, where ξ_n^* is a scaling length in the range 10-100 nm. The scaling length in this relationship is often virtually independent of temperature. In principle, within conventional proximity effect theory ξ_{nd} would be temperature-independent if $D_n \propto T$. However the theory does not apply to systems characterized by such non-metallic behavior.

Devayatov and Kupriyanov [57] have developed a theory for nominally SNS structures in which the N interlayer is an oxide with a composition close to a metal-insulator transition. Their model assumes transport between the superconducting electrodes by resonant tunneling, rather than direct metallic conductivity. It does not depend on induced superconductivity in the interlayer material. Indeed, the use of the term

"proximity effect" merely refers to the notion that the superconducting wavefunction can exist outside of a superconductor near an interface.

Assuming that the interlayers are direct narrow gap semiconductors in which transport is dominated by localized states, a characteristic decay length can be found [57]:

$$\xi_n^* \cong \alpha = \frac{\hbar}{[2m(V-\mu)]^{1/2}} \tag{34}$$

where v is the potential at the bottom of the conduction band and μ is the chemical potential. For $m = m_e$, the free electron mass, and a realistic bandgap of $V - \mu = 1\,eV$, α =0.2 nm, an extremely short distance. Conversely, in order to account for the observed exponential dependence of I_c, the conduction band edge must be very close to the Fermi level. For example, if α =10 nm, then $V - \mu = 0.4$ meV, a very small energy.

The calculation of the critical current using this theoretical approach has been successfully used to fit quasi-linear $I_c(T)$ data in high-~ grain boundary junctions and edge junctions with non-metallic interlayers [57]. We note, however, an important theoretical constraint: $1 < L/\alpha < (V-\mu)/kT_c$ For T_c =90 K, this constraint means that $V - \mu > 8\,meV$ even for $L = a$. According to Eqn. (34), this implies that $\alpha < 2.2\,nm$. Actually, even this is an overestimate of the maximum allowable a. The value of a is inferred from an exponential relationship of I_c and L, which only exists for $L >> a$ (long junctions). In this limit, applying the constraint $L/\alpha < (V-\mu)/kT_c$ reduces the maximum possible value of a to well below 2 nm. The extremely small inferred values of a appear to rule out applying this theory to junctions with L exceeding several nanometers.

Nevertheless, the resonant tunneling approach can account for an exponential length dependence of I_c with approximately temperature-independent scaling length over distances longer than those usually associated with tunneling ($\approx 1nm$). Evidently, resonant tunneling can occur in devices having nondegenerate semiconducting interlayers. However, the required sub-meV bandgaps will have significant effects on normal state transport properties. Therefore, it must be verified that these transport effects occur in a particular sample if resonant tunneling theory is to explain proximity effect-like behavior.

Many high-T_c SNS junctions are based on interlayers whose behavior is metallic, well away from any metal-insulator transition, and cannot be explained by a resonant tunneling approach. In fact, many high-T_c SNS junctions, including "long range

proximity effect" ones, have essentially the same temperature dependence as those of high-T_c grain boundary and tunnel junctions. This observation should motivate a search for a *common* origin for the behavior of these different types of junctions, rather than to develop explanations on a case-by-case basis. In fact, the resonant tunneling mechanism is interesting precisely because it can also be applied to grain boundary junctions [57].

The preceding discussion serves to point out that the conduction mechanisms in the interlayer are important. The tunneling (SIS) and direct metallic conduction (SNS) limits are well-understood theoretically. Semiconductor and oxide interlayers with compositions near a metal-insulator transition may not fail neatly into either of these limits, yet still give rise to Josephson effects.

IV. LOW-T_c PROXIMITY EFFECT DEVICES

In this section, experimental results on SNS devices with low-T electrodes are briefly reviewed. Our purpose is to demonstrate that conventional proximity effect theory has been rigorously tested experimentally. In addition, several investigations of SNS' junctions, where S is a high-T_c and S' a low-~ superconductor, have also been performed. These experiments, which are necessarily limited to low temperatures, appear to establish that the conventional proximity effect can occur with at least a single high-T_c electrode.

A. Low-T_c SNS Junctions

As we have repeatedly discussed, the most distinctive predicted signature of an SNS junction is the exponential-like behavior of $I_c(T)$ in the case $L >> \xi_n(T_c)$. This behavior is clearly visible in experimental data obtained over many years on low-T_c SNS junctions. For example, in early work on $Pb-Cu-Pb$ sandwich junctions, Clarke [124] studied the dependence of I_c on temperature, interlayer thickness, mean free path (varied by alloying the Cu with Al), and the presence of an oxide at the SN interfaces. This systematic work was successfully interpreted in terms of what we now refer to as the conventional theory of the proximity effect, establishing an exponential $I_c(T;L)$ with the expected normal coherence length.

Sandwich junctions with metallic interlayers are of limited technological interest because of their inherently low resistances and large critical currents. As modern microelectronic technology was applied to superconducting devices in the 1970's, SNS microbridge weak links were introduced. For example, Fig. 29 shows $I_c(T)$ for a $Pb-Cu-Pb$

microbridge [125]. The normalized data are well-fit by conventional rigid-boundary *SNS* theory [6],[1 04] using $L/\xi_{nd}(T_c)$ =8 as a fitting parameter. No attempt was made to fit the magnitude of I_cR_n on the inset plot, but the agreement with theory is satisfactory. In fact, it was reported [126] that $I_c \propto (T_c - T)^2$ near T_c, as expected from conventional soft boundary condition theory. It is certainly possible to fit the entire I_c (7') curve by choosing a value of γ appropriate for soft boundary conditions. However, the crucial point is that I_c is obviously dominated by the exponential factor, while the boundary conditions are of secondary importance. This is illustrated not only by the data shown, but also by the fact that longer bridges (larger L/ξ_n) exhibited steeper temperature dependence consistent with $I_c \propto \exp(-L/\xi_n)$. Conventional *SNS* theory accounts for the magnitude and shape of I_c (7') at all temperatures, although $L/\xi_{nd}(T_c)$ must be used as a fitting parameter because the device dimensions were not accurately known.

In subsequent work on similar $Pb-Cu-Pb$ microbridges [127], $I_c(L)$ at various temperatures was fit to the conventional critical current form of Eqn. (5a), yielding values for $\xi_n(T)$ which were in good agreement with the dirty limit expression for the normal coherence length, Eqn. (7). Although the magnitude of the prefactor $I_c(0)$ in Eqn. (5a) was not fit to theory in Ref. [127], both the magnitude and temperature dependence of I_c in $Nb-Au-Nb$ and $Nb-Cu-Nb$ microbridges have been satisfactorily described using a Ginzburg-Landau approach appropriate for soft boundary conditions [16].

Since most low-T_c *SNS* junction investigations have been aimed at producing practical devices, however, efforts to understand the physics of the device behavior included considerable attention to non-stationary junction behavior. As a result, while the numerical value of ξ_n and the exponential behavior of I_c were comparatively well-understood, detailed investigations of the magnitude of I_c were not carried out. In fact, virtually all research on low-T_c *SNS* devices was conducted prior to the complete microscopic theory described in Section III. Nevertheless, it is clear that the primary predicted feature, the exponential dependence of $I_c(7'; L)$, is common in low-~ SNS devices. Indeed, careful research has shown that the characteristic length in the exponent is the expected normal coherence length obtained from calculations.

There is little early experimental work on the role of interface resistance in SNS devices with metallic interlayers because interface resistance in proximity effect structures was recognized as detrimental [28]. Subsequently, interest was generated in using semiconductors (Sin) as interlayers in *SSmS* devices in order to achieve practical device resistances [17]. Such devices act as *SNS* junctions as long as there are free carriers in the *Sm* layer. However, interface resistance is almost unavoidable in *SSmS* devices due to Schottky barriers or a large mismatch in Fermi wavevectors between S and *Sm*.

Experiments have only shown the expected exponential dependence of I_c on T and L for dirty limit devices with Si [128],[1 29] and $InAs$ [130],[1 31] interlayers. Knowledge of carrier density, effective mass, and mobility in the Sm interlayer allow ξ_n to be calculated. Although agreement between the calculated and fitted values of ξ_{nd} has been claimed for junctions with p- Si interlayers[1 28], it has been pointed out [1 32] that the complex band structure of p– Si was not properly considered, leading to an overestimate of ξ_{nd}. It is also probably significant that $I_c R_n$ values in at least some Si-coupled devices[1 07],[1 29] were experimentally measured to be larger than expected from conventional theory. Clearly, $SSmS$ devices are not nearly as well understood as metallic SNS ones. Nevertheless, the expected exponential dependence of I_c on T (in individual devices) and on L (in sets of similar devices), using the same $\xi_{nd}(T_c)$, has been demonstrated. Thus, these basic signatures of the proximity effect are observed in semiconducting, as well as metallic, interlayers.

Although $I_c(T)$ in low-T_c SNS bridges has never been shown to follow the quasi-linear dependence associated with high- T_c weak links, this type of dependence has been observed in all-Nb weak links with a narrow superconducting constriction linking two massive superconducting banks. An example is shown in Fig. 30 [133]. This device is evidently a reasonable approximation to an ideal clean point contact, as described by Eqn. (4).

B. SNS' Junctions

Thus far, we have focused our entire discussion on SNS junctions with nominally-identical S electrodes because these structures are of greatest experimental and practical interest. However, many theoretical papers treat the possibility of different superconducting electrodes. This case, designated SNS', is of present interest because there have been several experimental investigations of SNS' junctions in which S is a high-T_c superconductor and S' a low-T_c one. (Of course, the symmetry of the order parameter may differ between the low- and high-T_c electrodes, further complicating the interpretation of the data.) We will not attempt to review this subfield, which includes efforts involving $SNIS'$ junctions in tunneling studies and SN bilayers for contact resistance studies. We will only mention work which examines SNS' Josephson junctions for the purpose of establishing that the proximity effect does indeed occur in systems involving high- T_c superconductors. We note, however, that such investigations cannot examine the proximity effect in the temperature range of primary technological interest since they are confined to temperatures at which the low-T_c electrode is a superconductor. In addition, these experiments cannot establish that conventional proximity effect theory can account for the behavior of all-high-~ SNS junctions.

Gijs *et al. [134],[1* 35] fabricated $YBa_2Cu_3O_{7-\delta}$-Ag-Pb sandwich junctions and interpreted their results using an approach similar to that of de Gennes, modified for non-identical electrodes. Some of their junctions showed quasi-linear temperature dependence over a fairly wide temperature range, while others showed a rapid increase in I_c (T) at low temperatures that was qualitatively consistent with conventional proximity effect theory. However, these experiments did not provide quantitative fits to theory using measured inter-layer thicknesses and calculated coherence lengths. Similar experiments on $YBa_2Cu_3O_{7-\delta}$-Ag/Au-Pb sandwiches were interpreted in terms of an *SINI'S'* model [136], but the junctions studied had a quasi-linear $I_c(T)$ dependence and no systematic investigations involving long junctions were performed.

Tarte *et a/.* [137],[1 38] have performed systematic investigations of $YBa_2Cu_3O_{7-\delta}$-Ag-Pb sandwich junctions and also interpreted them using de Gennes's theory modified for non-identical electrodes. In this work, the Ag thickness was intentionally varied to span the range from short to long SNS' junctions. Although the entire range of temperatures below the critical temperature of Pb was not examined, junction critical currents increased rapidly with decreasing temperature, with the rate of increase much larger in long junctions than in short ones as expected from Eqns. (5). This systematic study represents the most convincing evidence to date for conventional proximity effect behavior in SNS' junctions and is very much in the spirit of the approach we advocate for examining all-high-T_c junctions.

V. COMPARATIVE STUDY OF HIGH-T_c JUNCTIONS

In Section II we saw that the normalized $I_c(T)$ curves for most high-T_c junctions of various types are remarkably similar. In many examples, I_c approximately follows the linear temperature dependence of Eqn. (1) over the entire temperature range below T_c. This holds for a variety of junction geometries and interlayer materials over a broad range of bridge lengths. We now explore specific data in more detail, showing that conventional proximity effect theory is not consistent with the observed behavior of most of these nominally *SNS* devices.

It is obviously necessary to be cautious in comparing high-T_c experimental results to a theory developed for low-T_c junctions. Nevertheless, it is sensible to look for conventional behavior in existing devices as a starting point for understanding the nature of the high-~, junctions, Recall that conventional superconducting tunneling behavior is exhibited in at least some high-T_c structures, as illustrated by the data in Fig. 8, supporting the notion that conventional theory is relevant. In addition, the recent systematic results on SNS' junctions discussed in Section IV give reason to believe that

conventional SNS behavior might be expected.

A. Experimental Issues

Junction Length Scales

Several important length scales determine the behavior of an SNS weak link, including the mean free path ℓ_n and coherence length ξ_n in N, the bridge length (electrode separation) L, the junction width W, and the Josephson penetration depth A,. As we saw earlier, the analysis of SNS junctions is most straightforward in long devices in the dirty limit ($\ell_n << \xi_n << L$), although some departure from the dirty limit can be accommodated. It is also desirable that the junctions be narrow ($W < 2\lambda_J$) so that the current distribution is uniform and I_c reflects the critical current density, J_c, which is a more fundamental parameter. Fortunately, most devices that we consider meet these constraints.

We have seen that the temperature dependence of ξ_n is not simply $1/T$ or $1/T^{\text{“}2}$ unless the junction is clearly in the extreme clean ($\ell_n >> \xi_{nc}$) or dirty ($\ell_n << \xi_{nc}$) limits, respectively. However, ξ_n is easily calculated in its general form if v_n and ℓ_n are known. It can also be determined experimentally. In the limit $L >> \xi_n$, conventional proximity effect theory predicts a purely exponential dependence of I_c on L regardless of the behavior of the SN contacts. Thus, ξ_n is determined by the slope in a semilog plot of $I_c(L)$. However, even this simple approach requires further discussion.

There have been few careful high-temperature device studies where ξ_n is inferred from $I_c(L)$ data at several different temperatures and carefully compared to theory. This is partially because such a study is difficult in practice. For example, an exponential dependence of $I_c(L)$ requires that $L >> \xi_n$ *at the measurement temperature.* Because ξ_n diverges as T_{cn} is approached from above, the temperature range over which ξ_n satisfies this criterion is reduced. Recall also that, while $I_c(L)$ can be exponential below $0.3T_c$, the exponent no longer gives ξ_n directly. Moreover, the temperature regime is restricted from above by the fact that the critical current must vanish as T_c is approached. Finally, the actual interlayer thickness is not typically known with precision because of thickness calibration difficulties, inhomogeneities in the deposition film thickness, and an uncertain junction length in the transport direction for structures such as edge geometries.

Combining the issues of a restricted measurable temperature range and the uncertainty in the value of L, the central difficulty for $I_c(L)$ studies is apparent. Junctions of many different lengths need to be fabricated to meaningfully extract ξ_n from the data.

However, this length range is limited: We must choose a single temperature where each L is large enough so that the junction is in the long limit, but short enough to have an experimentally measurable I_c. Generally speaking, this yields a range of about 30 nm between the shortest and longest bridge lengths. The uncertainty in L, however, can be 5 nm or more, a significant fraction of the range. Consequently, the resulting extracted values of ξ_n must be viewed with some skepticism. Despite the difficulties with this type of study, there is a major need for more experiments along this direction with special emphasis on establishing controlled fabrication processes.

Finally, the simple exponential relationship $I_c = I_{co}\exp(-L/\xi_n)$ limits the absolute range of L. In a typical experiment, the critical current density at $4.2\,K$, extrapolated to $L=0$, is **50** $mA/\mu m^2$ **[64], [66].** The area of a typical photolithographically-defined edge junction is $\approx 1\ \mu m^2$. Thus, an upper limit for I_{co} is about 50 mA. The minimum (thermal fluctuation-limited) measurable Josephson current is roughly $ekT/\hbar$, or about 1 μA at 77 K. Inverting Eqn. (5a), we thus see that to even observe a critical current at 77 K, the ratio $L/\{_n$ should be less than about 10. (Ideally, we should have used a value of I_{co} at 77 K in this estimate, but there is little $I_c(L)$ data available at this temperature. Nevertheless, since I_c is lower near T_c, the true upper limit on L/ξ_n is smaller still.)

This rough upper limit of $L<10\xi_n(T)$ for even observing a device supercurrent at 77 K has a major impact on the range of L. Recall from the discussion following Eqns. (6) and (7) that ξ_n is less than 15-30 nm at 77 K for typical noble metals. We thus find that an upper limit on L is a few hundred nanometers for SNS junctions made with interlayers of Au or Ag. Because the Fermi velocity is at least an order of magnitude smaller in typical oxide metals, 30 nm is a reasonable upper limit on L for oxide-based SNS junctions.

Noise Rounding

This paper deals exclusively with the stationary properties of Josephson junctions and does not confront any of the interesting and important issues associated with junction phase dynamics and finite voltages. Experimental measurements of the critical current, however, require dealing with the current-voltage characteristics of the device. In most cases, the measurement of I_c consists of determining the largest value of current for which the voltage is immeasurably small. The sharp break from zero to finite voltage in a typical Josephson junction makes this a particularly simple matter. However, when I_c is small, such that the Josephson coupling energy $\hbar I_c$ /2e is comparable to kT, thermal fluctuations result in the appearance of a finite dc voltage across a junction at current levels below the intrinsic critical current of a junction [22]. Fortunately, many junctions are well-described by a simple circuit model and the intrinsic critical current can be

deconvolved from the measured $I-V$ characteristics [22]. This extraction process is routine practice with low- T_c devices. It has also been shown that some high-T_c junctions are well-described by the standard noise-rounding model over the entire range of temperatures below T_c [139]. High-T_c junctions not described by the model present a problem since accurate measurements of I_c are required for our analysis. Fortunately, the experimental difficulties associated with small critical currents are generally an issue only near T_c, outside the temperature range of primary interest,

Magnetic Field Modulation of Critical Current

When a magnetic field threads the junction plane of an *SIS* tunnel junction, the magnetic energy associated with a flux quantum Φ_0 matches the Josephson coupling energy when the flux is spread out (in the direction orthogonal to the current flow) over a distance known as the Jospheson penetration depth [21]:

$$\lambda_J = \left[\frac{\Phi_0}{2\pi\mu J_c(d + 2\lambda_L)}\right]^{1/2}, \tag{35}$$

where μ is the permeability of the insulating layer, d is the tunnel barrier thickness, and λ_L is the London penetration depth of the electrodes. If the junction width w is much greater than A,, transport in the junction will be effected by the local magnetic fields created by the current itself. In this wide junction limit, the transport characteristics can be dominated by the dynamic behavior of the flux quanta (Josephson vortices) in the device,

In contrast, the magnetic fields caused by the currents in the junction can be neglected for $W <$ A,. The response of the critical Josephson current I_c to an external magnetic flux Φ in the plane of the junction then contains information about the distribution of the supercurrent over the junction area [140]. For a rectangular *SIS* junction, $I_c(\Phi) \propto \sin x / x$, where x = $\pi\Phi/\Phi_0$, a Fraunhofer pattern. The zeroes of the function correspond to integral numbers of flux quanta threading the junction. In general, $I_c(\Phi)$ is related to the Fourier transform of the spatial distribution of the critical current density in the junction. Because only the magnitude of I_c is measurable, absolute phase information is lost and the spatial variation of the critical current density cannot be unambiguously determined from the magnetic field response. Nevertheless, it is possible to determine the macroscopic scale over which the supercurrent flows in an average sense [141]. Consider, for example, a rectangular junction with the supercurrent distribution determined by tiny pinholes through the insulating barrier. If the pinholes are uniformly distributed over the junction area, the $I_c(\Phi)$ characteristics of the rectangular device will approach the ideal Fraunhofer pattern despite the

microscopic nonuniformities in current distribution [1 11],[1 12]. Thus, we can infer from $I_c(\Phi)$ data the macroscopic (averaged) distribution of the supercurrent flow and not the microscopic distribution.

The meaning of $I_c(\Phi)$ for an idealized planar tunnel junction is clear. Real devices, however, are more complex. First, flux in the form of Abrikosov vortices can be trapped in the superconducting electrodes themselves, affecting the critical current of the device [142]. Moreover, the overlapping, non-planar, structures associated with many high-T_c junctions pose special problems. It has been demonstrated, for example, that a spatial modulation of the critical current in a high-T_c edge junction can be attributed to the presence of Abrikosov vortices in the overlapping counterelectrode [1 43].

Clearly, we must use caution when interpreting $I_c(\Phi)$ data in terms of local current distributions. The magnetic field response has been used to infer that many high-T_c junctions have highly nonuniform current distributions [39]. Indeed, the interpretation of $I_c(\Phi)$ data has played a major role in constructing models of the junctions based on inhomogeneous interlayer or barrier regions.

B. Parameter Estimates

In order to make detailed comparisons between theory and experiment, it is important to calculate ξ_n accurately. This requires three basic material parameters of the N interlayer: Its critical temperature T_{cn}, Fermi velocity v_n, and mean free path ℓ_n. Here we summarize the values of these quantities for relevant interlayers. Although T_{cn} is easily obtained by direct measurement, the other two parameters may not be as accurately known, particularly in the case of anisotropic oxide films. We will proceed by making reasonable estimates for the better-known parameters and calculating others as required. We also comment on other important parameters in the theory, such as the interface parameters γ and γ_b.

Coherence Lengths

In noble metal interlayers such as Au and Ag, the important parameter values are unambiguous. Of course, T_{cn} =0 and, assuming a spherical (isotropic) Fermi surface, we can use the Drude model of conductivity [144] to obtain

$$v_n = \frac{\hbar(3\pi^2 n)^{1/3}}{m} \tag{36}$$

and

$$\ell_n = \frac{m v_n}{e^2 n \rho_n}. \qquad (37)$$

In these expressions, n is the carrier density, m is the effective electron mass, and ρ_n is the resistivity. Table 2 lists values for carrier concentration, Fermi velocity, and resistivity for Cu, Au, and Ag under the assumption that m is the free electron mass m_e, with ℓ_n taken to be 100 nm. (Note that the bulk mean free path is extremely long in pure noble metals below 100 K, so that ℓ_n is determined by the film thickness, which we take to be 100 nm for the tabulated parameter values) Also listed are the values of ξ_{nc}, ξ_{nd}, and ξ_n at 77 and 4.2 K, obtained using Eqns. (6), (7), and (30), respectively.

We next examine the ruthenates $CaRuO_3$ and $SrRuO_3$, both of which have been used as interlayers. These materials are oxides with T_{cn} = O. We begin with $CaRuO_3$ because it is a simple isotropic metal that is reasonably well understood [145]. Table 2 lists relevant parameter values as well as the coherence lengths at 77 and 4.2 K. The resistivities listed are obtained from data on 200 nm -thick films [66] and are given approximately by $p_n(T)$ =2.07 Ω –M+(O.0160 $\Omega - \mu m/K)T$.

The resistivity can also be expressed as:

$$\rho_n = \frac{1}{2e^2 \mathcal{N}_n D_n}, \qquad (38)$$

an expression that is generally applicable independent of the details of the band structure if the single-particle density of states, $\mathcal{N}_n$, is measured or calculated independently, Recalling that the 3d diffusion constant is given by $D_n = v_n \ell_n/3$, ℓ_n can be determined if ρ_n, V_n, and $\mathcal{N}_n$ are known. In fact, the mean free path in $CaRuO_3$ obtained from Eqn. (37) agrees with that deduced from the density of states as measured by electron-energy-loss spectroscopy [1 45], underscoring the material's simple 3d metallic nature.

Parameter values for $SrRuO_3$ are also found in Table 2 [145]. As before, the isotropic metallic nature of the material is demonstrated by the agreement between estimates made using the carrier concentration, n, and those using the density of states, $\mathcal{N}_n$. Bulk $SrRuO_3$ differs from bulk $CaRuO_3$ by undergoing a ferromagnetic phase transition at a Curie temperature of about 160 K [146]. This transition has been used to explain kinks in $\rho_n(T)$ curves measured on $SrRuO_3$ films as thin as 10 nm [67]. For the temperatures of interest for SNS devices, we use the measured linear resistivity [67], $\rho_n(7') = 0.52$

$\Omega - \mu m + (0.0098\,\Omega - \mu m/K)T$.

Finally, there is the popular class of N interlayers whose crystalline structure is similar to $YBa_2Cu_3O_{7-\delta}$. As several of these materials are actually substituted forms of $YBa_2Cu_3O_{7-\delta}$, it isuseful toexamine theparameter values of $YBa_2Cu_3O_{7-\delta}$ as a starting point. The carrier concentration in pure $YBa_2Cu_3O_{7-\delta}$ is approximately 5x 1027 m^{-3} [42],[1 47], or about one carrier per unit cell. Consequently, the standard 3d relationship for the Fermi wavevector yields $k_n = (3\pi^2 n)^{1/3} = 5.3\times 10^9\, m^{-1}$. However, the cuprates are highly anisotropic and so we should consider estimates which are based on 2d treatments. Since the c-axis lattice constant is 1.16 nm [148], the sheet carrier concentration is N_{sq} =5.8x $10^{18}\, m^{-2}$ which, in turn, yields a 2d Fermi wavevector of $k_n = (2\pi N_{sq})^{1/2} = 6.0\times 10^9\, m^{-1}$ Notice that the difference between the 3d and 2d wavevector estimates is small so our estimates are not very dependent on the assumed dimensionality. The accepted effective carrier mass for a-b plane transport is about 5 m_e [42], and a reasonable estimate of the in-plane Fermi velocity is $v_n = \hbar k_n / m$ =1 .4x 105 m/s, which is about the same as that found in the ruthenate materials discussed above.

In order to calculate the mean free path using Eqns. (37) or (38), the resistivity is required. For pure $YBa_2Cu_3O_{7-\delta}$, $\rho_n \propto T$. The value of ρ_n at a given temperature varies with purity and defect density; $\rho_n \approx 1\ \Omega - \mu m$ at 100 K. Eqn. (37) then leads to ℓ_n =5 nm at 100 K. Table 2 lists estimates for relevant parameter values at 77 K based on these values. Checking the consistency of the estimate of the mean free path using the density of states relation (38), we obtain ℓ_n =4.5 nm at 100 K for $2\mathcal{N}_n$ =3x $10^{28}\, eV^{-1}m^{-3}$ [148], a reasonable match.

In interlayers based on $YBa_2Cu_3O_{7-\delta}$, chemical substitution can be used to reduce T_c. In $YBa_2Cu_3O_{7-\delta}$ the relationship between T_c and n is parabolic [149]. In the case of $YBa_2Cu_{3-y}Co_yO_{7-\delta}$, Co is substituted onto Cu sites, decreasing n and yielding $T_{cn} \cong 50\,K$. As a result, for $YBa_2Cu_{2.79}Co_{0.21}O_{7-\delta}$ the carrier concentration is roughly 75% of that in $YBa_2Cu_3O_{7-\delta}$. In $Y_xCa_{1-x}Ba_2Cu_3O_{7-\delta}$, Ca is substituted onto Y sites, yielding $T_{cn} \cong 50\,K$ again. However, the carriers added by the Ca ions are compensated by the creation of O vacancies [149]. As a result, we will use the carrier concentration characteristic of pure $YBa_2Cu_3O_{7-\delta}$ in our parameter estimates for $Y_xCa_{1-x}Ba_2Cu_3O_{7-\delta}$.

Changes in n, as well as defect scattering, affect ρ_n. Given n, ρ_n, and T_{cn}, we can obtain ℓ_n and ξ_n. In calculating ξ_n, we use a 2d treatment of the layered cuprate interlayers. Comparison with the results of a 3d treatment indicates that the differences are insignificant for this discussion. We further assume the same lattice constant and carrier mass as in pure $YBa_2Cu_3O_{7-\delta}$. Table 2 lists transport parameters and coherence lengths for $YBa_2Cu_{2.79}Co_{0.21}O_{7-\delta}$ and $Y_{0.7}Ca_{0.3}Ba_2\ Cu_3O_{7-\delta}$.

As the required parameters for the doped interlayers are not known with precision, it is important to understand the validity of the estimates given in Table 2. Figure 31 shows $\xi_n(T)$ for ρ_n=1, 3, and 10 $\Omega-\mu m$, the range of interest for oxide interlayers. For comparison, the corresponding curves for T_{cn}=0 are also shown. Clearly, finite T_{cn} substantially enhances ξ_n, which is a few nanometers over the temperature range of interest and varies by roughly a factor of 2 for the order of magnitude change in ρ_n. Doping changes would shift the curves up or down in proportion to v,,. Reducing ℓ_n (increasing ρ_n) results in a shift towards the dirty limit, but the effect on the shape of the curves is not major. For the finite T_{cn} curves in Fig. 31, the ratio ξ_{nd}/ξ_{nc} ranges between 1.4-1.8, 0.81-1, and 0.45-0.56 for ρ_n=1, 3, and 10 $\Omega-\mu m$, respectively, indicating that departure from the dirty limit is not excessive for ρ_n above roughly 3 $\Omega-\mu m$. Finally, it is instructive to estimate the effects of ion substitution by calculating ξ_n under three different assumptions: (1) doping changes only ℓ_n and not n, (2) doping changes only n and not ℓ_n, and (3) doping changes both parameters. (In Table 2, it is assumed that both ℓ_n and n are affected by doping.) Although the system tends towards different (clean and dirty) limits in the three cases, the final computed values of ξ_n are similar over the temperature range of interest ($T_{cn}<T<T_c$) and vary less than 20°/0 from each other at 77 K. From these observations, we conclude that the normal coherence length is a few nanometers regardless of how Co and Ca doping affect the properties of $YBa_2Cu_3O_{7-\delta}$.

Interface Parameters γ and γ_b

The interface parameter γ depends on the resistivities and densities of states in the S and N layers; y = $(\mathcal{N}_n\rho_s/\mathcal{N}_s\rho_n)^{1/2}$, as indicated by Eqn. (14). Rigid boundary conditions ($\gamma<<1$) are favored by high resistivity N layers with low carrier concentrations (relative to S). Soft boundary conditions are favored in the opposite extreme. Although the density of states should not depend strongly on temperature, p is temperature-dependent for many materials used in high-T_c devices.

Consider junctions with oxide interlayers first. In $YBa_2Cu_3O_{7-\delta}$ the resistivity is proportional to temperature. This relationship holds in some doped cuprate interlayers as well, although often ρ_n exceeds ρ_s. For other oxides, such as the ruthenates, $\rho_n>>\rho_s$, with ρ_n much less temperature-dependent than ρ_s. Moreover, for 3d, $\mathcal{N}_n$ is proportional to m^2v_n and so $\mathcal{N}_n$ will not be significantly larger than $\mathcal{N}_s$. As a result, in typical high-T_c junctions with oxide interlayers, y <1 and the boundary conditions tend towards rigid.

The other SNS junctions of interest are those with noble metal interlayers. In this case,

$\mathcal{N}_n >> \mathcal{N}_s$, and $\rho_n << \rho_s$, except possibly at very low temperatures, Therefore, $\gamma >> 1$, and soft boundary conditions should apply in the absence of interracial barriers. This means that $I_c R_n$ should be reduced in proportion to $1/\gamma^2$.

As discussed in Section Ill, the parameter γ only dominates junction properties in the limit of high SN interface transparency, $\gamma_b << 1$. However, recall that $\gamma_b > 1$ even for the best metallic contacts to high-~ electrodes. The presence of a tunnel barrier will further increase the contact resistance, leading to the expectation that $\gamma_b >> 1$. Thus, we expect that rigid boundary conditions will hold in most cases of interest and that γ_b will be the more important interface parameter. Note, however, that the absence of a barrier *locally* (a pinhole in an interracial barrier, for example) implies that $\gamma_b = 0$ there.

C. Examination of Specific Junction Types

We now examine several experimental studies of high-~. SNS junctions within the theoretical framework developed in Section Ill. We emphasize again that this is a representative, not exhaustive, survey of the field to date.

Noble Metal Step-Edge Junctions

The best understood normal interlayers are noble metals. For such materials, v_n falls in the range 1-2x 10^6 m/s, so that ξ_{nc} is 15-30 nm at 77 K. As discussed earlier, ξ_{nc} represents an upper limit for normal coherence length. Estimates of ξ_n for representative noble metals are listed in Table 2 (using a film thickness of 100 nm as the value of ℓ_n). It is interesting that ξ_n does not change dramatically when the interlayer thickness, and hence ℓ_n, is reduced. For example, halving ℓ_n from 100 to 50 nm only reduces ξ_n by 13-1 8°/0 from the values listed in the table. Thus, although ℓ_n may be reduced by defects in actual inter-layers, our analysis will not be greatly affected. Noble metal interlayer films thinner than a few tens of nanometers are unlikely to be electrically continuous and hence are not of interest here,

At low enough temperatures, all SNS junctions are in the dirty limit because ξ_{nc} diverges, assuring that $\ell_n << \xi_{nc}$. It is therefore convenient to define a crossover temperature T_x at which $\xi_{nc}(T) = \xi_{nd}(T)$. For a 3d material,

$$T_x = \frac{3\hbar v_n}{2\pi k \ell_n} \tag{39}$$

From Eqn. (30), we find that ξ_n (7') is within 10% of $\xi_{nc}(T)$ for $T > 3.43 T_x$ and within 10°/0 of $\xi_{nd}(T)$ for $T < 0.36 T_x$. It is useful to refer to Fig, 26 in examining these limits. For a

100 nm thick Ag or Au film, $T_x \cong 51K$. As a result, we can only confidentially apply dirty limit theory to such noble metal SNS junctions for temperatures less than approximately 18 K. Thus, while most noble metal low-T devices are in the dirty limit for all temperatures of interest, applying this same limit to noble metal high-<. junctions is of no value except at low reduced temperatures.

The same 100 nm thick Ag or Au film will meet our criterion for the clean limit only for $T>175\ K$, beyond the critical temperature of any known superconductor. Thus, noble metal devices are not well-described by either the dirty or clean limits at $77\ K$. However, the clean limit coherence length is relevant to the temperature dependence of the critical current. The expression [1 16]

$$\frac{1}{\xi_n} = \frac{1}{\ell_n} + \frac{1}{\xi_{nc}} \qquad (\ell_n > \xi_{nc}) \tag{40}$$

is accurate to within 5% for $\ell_n > \xi_{nc}$, or $T>T_x/3$, as shown in Fig. 32. This means that the exponential relationship between I_c and $L/\xi_{nc}(T)$ expected in the clean limit holds: $I_c \propto \exp(-L/\xi_n) \cong \exp(-L/\ell_n)\exp(-L/\xi_{nc})$. Because the temperature dependence of ℓ_n is weak, the additional prefactor has little effect on the *shape* of normalized $I_c(T)$ data.

The details of electron transport in step-edge microbridges are not well-understood. For example, it is difficult in most cases to ascertain the minimum distance, L, between the S electrodes. As shown in Fig. 9d, it depends on at least the step height, electrode film thickness, edge angle, and deposition angle. Reported step heights vary from roughly 60 nm to as large as 400 nm, and S electrode thicknesses are typically 50-200 nm. The S film is deposited at an angle in order to produce two electrodes separated by a break at the step. We will not discuss here the fabrication issues connected with non-line-of-sight deposition which could produce unintended shorts. Instead, we will simply assume that the superconducting electrodes are electrically isolated in the absence of the noble metal film. Indeed, it is common to attempt to verify this isolation with control experiments.

Junctions with the base electrode film exceeding the step height have been fabricated [150]. This geometry minimizes L, which is given by the horizontal separation of the electrodes in Fig. 9d, $d_{step} \tan \mathrm{O}$, where d_{step} is the step height and O is the angle of incidence for the superconductor deposition (6' = O corresponds to normal incidence). For $6 \cong 45$", $L \cong d_{step}$. Thus, since the typical minimum step is $60\ nm$, *we see* from Table 2 that all noble metal step-edge junctions fabricated to date should be long with $L/\xi_n(T_c)>4$. Moreover, L is even greater in junctions having electrodes thinner than the step height. As this thin-electrode case is the more common fabrication choice,

$L/\xi_n(T_c)$ should be greater still. Clearly, an exponential temperature dependence of I_c should be ubiquitous among all these devices,

In Figs. 14-16, we saw that $I_c(T)$ is quasi-linear for most noble metal step-edge SNS bridges. Despite the fact that $L>>\xi_n(T_c)$, there is little experimental indication of the expected exponential-like temperature dependence and the expected changes in shape of I_c (7') with changing $L/\xi_n(T_c)$. This observation holds for both pure Ag and Au bridges as well as Au-Ag alloyed bridges, in which the alloying should cause the junctions to be closer to the dirty limit.

Let us next consider $I_c(L)$. Fig. 33 shows data at 4.2 K for several bridges [151]. The data are actually I_cR_n, but the normal state resistance displays little temperature dependence, I_c can be fit to the exponential form of Eqn. (5a). At 4,2 K, the Ag and Au-Ag bridge data of Fig. 33 reveal that &=44.1 and 18,3 nm, respectively. The dirty limit applies at this low temperature and, as we saw in Section Ill, theory predicts that $L_0 \cong 3.18\xi_n(T_c)$, yielding $\xi_{nd}(T_c) = 13.9$ and 5.75 nm for Ag and Au-Ag, respectively. The Ag value for $\xi_{nd}(T_c)$ is about half that estimated in Table 2, a clear inconsistency between theory and experiment.

We now compare Ag and Au-Ag bridges by examining I_cR_n. The low-temperature values of I_cR_n for Ag and Au-Ag junctions obtained from the fits of Fig. 33 are 0.112 mV and 3.72 mV, respectively. From Eqns. (24)-(26), we see that $I_{co}R_n$ is proportional to $\gamma_b^{-\alpha}$, where α = 1 in junctions in which the contact resistance r_c dominates R_n and a =2 in junctions in which the bulk resistance of the interlayer dominates R_n. (Recall that we expect $\gamma_b>>1$ for typical metallic contacts to high-T_c superconductors.) Now, $\gamma_b = r_c/(\rho_n \xi_{nd}(T_c))$. From Eqns. (7) and (38) we see that $\xi_{nd}(T_c) \propto (\mathcal{N}_n\rho_n)^{-1/2}$, and therefore, $\gamma_b \propto r_c\mathcal{N}_n\xi_{nd}(T_c)$. Assume that r_c is the same for Ag and Au-Ag interlayers deposited on $YBa_2Cu_3O_{7-\delta}$. Since, the density of states, $\mathcal{N}_n$, is virtually identical in the two interlayers, we thus find that the ratio of $I_{co}R_n$ between Ag and Au-Ag devices should be the ratio of $[\xi_{nd}(T_c)]^{-\alpha}$ in the devices. However, the experimentally-obtained $I_{co}R_n$ ratio is 0.030, while the ratio of $[\xi_{nd}(T_c)]^{-\alpha}$ using the fitted values obtained above is 0.41 if $\alpha = 1$ and 0.17 if a =2. Thus, there is a significant discrepancy between experiment and theory.

Figure 34 shows the dependence of normalized critical current on reduced temperature for an investigation [150] of Au bridges in which 85 nm -thick electrodes were deposited onto steps varying from 80 to 140 nm in height. When $d_{step} = 80\,nm$, the electrode thickness d_{film} exceeds the step height d_{step} and $L \cong d_{step}$. When $d_{film} < d_{step}$, we estimate that $L^2 \cong d_{step}^2 + (d_{step} - d_{film})^2$ for θ ==45°. Thus, for $d_{film} = 85\,nm$ and d_{step} =80, 110, and 140 nm, we estimate that $L \cong$ 80, 113, and 150 nm, respectively, Assuming that $\ell_n \cong L$

and $\xi_{nc}(T_c)$= 19.0 nm, we therefore conclude from Eqn. (40) that $L/\xi_n(T_c)$ =5.2, 6,9, and 8.9 for the three step heights. Clearly, $L>>\xi_n(T_c)$ and the reduced length varies by nearly a factor of 2. Thus, we expect a dramatic exponential-like dependence of I_c on temperature, with much more upward curvature in the longer devices. Instead, we see in Fig. 34 that the shape of the normalized $I_c(T)$ data varies only slightly. Although the qualitative trend is towards greater upward curvature in the longer devices, the amount of upward curvature and variation from device to device is much smaller than expected. Similar results were obtained from studies of step-edge junctions in which the Au film morphology was altered by changing the Au deposition temperature [152].

Finally, let us examine data on the length dependence of I_c for these Au step-edge devices [150]. $I_c(L)$ data at 4.2 K is available for the junctions in which $d_{film}>d_{step}$, so that $L \cong d_{step}$. Recall that the dirty limit should apply at this low temperature, If we attempt to fit the data to the exponential dependence of Eqns. (5), we require that $L_0 \cong$ 10 nm. This, in turn, implies that $\xi_n(T_c)$= Lo/3.18=3 nm, much smaller than the values of either $\xi_n(T_c)$ or $\xi_{nd}(T_c)$ estimated from Table 2.

We thus conclude that the available experimental data on noble metal step-edge SNS bridges are clearly inconsistent with conventional theory in both temperature and length dependence. If, however, these devices are not SNS in nature, it is far from clear how they function for there is no clear alternative explanation, Further investigation of the step-edge bridge geometry is worthwhile in light of the excellent performance reported for magnetometer [76], [77] and high frequency [80] devices based on it.

Oxide Metal Edge Junctions: Ruthenates

Edge junctions having oxide metal interlayers with T_{cn} =0 form another class of devices for which experiments can be compared to theory in detail. Most oxide edge junctions reported to date have resistances that greatly exceed that attributable to the bulk N-layer, so interracial resistance dominates. However, we have seen that contact resistance affects only the *magnitude* of I_c and not the qualitative signatures of the proximity effect. Here we demonstrate that the data available on these junctions is inconsistent with conventional proximity effect theory. We will also see that there is direct evidence for pinholes through the N interlayers in some of these devices.

We begin by discussing $YBa_2Cu_3O_{7-\delta}$ edge junctions with $CaRuO_3$ interlayers [66], [69]. From Table 2 we see that $CaRuO_3$ is in the dirty limit for all temperatures below T_c (approximately 90 K) with $\xi_{nd}(T_c) \cong 0.8$ *nrn, so* conventional SNS junction models should apply. However, $I_c(T)$ data for $CaRuO_3$ edge junctions are quasi-linear. For example, the data shown in Fig. 12 were taken from a device with L =10 nm, implying that

$L/\xi_{nd}(T_c) \cong 12$. Under conventional proximity effect theory, such a long junction must exhibit exponential I_c (T) behavior, In fact, comparing the data to Likharev's theory [6],[1 04] reveals that a much better match is achieved for $L/\xi_{nd}(T_c)$ =4 rather than $L/\xi_{nd}(T_c)$ = 12, as shown in Figure 35. Clearly, the bridge in question does not obey conventional theory unless the interlayer is actually one-third as thick as claimed.

We saw earlier that to observe a critical current requires L less than roughly $10\xi_{nd}$ (T). Considering the large estimated reduced length $L/\xi_{nd}(T)$, no supercurrent should be observed at 77 K in the junction under discussion. In fact, at 77 K $\xi_{nd}(T) \cong 0.9\,nm$ and we thus expect a supercurrent to be apparent only for $L<9\,nm$. Despite this, there are reports of finite critical currents at 77 K in $CaRuO_3$ edge junctions having L as large as 30 nm [66], implying that L/ξ_{nd} (73>33. Again, in light of the exponential dependence of I_c on L in conventional proximity effect theory the discrepancy between theory and experiment is quite large, and supercurrent transport appears to take place over physically impossible distances.

Studies of the critical current as a function of length for $CaRuO_3$ devices have also been reported [66]. Data taken at 4.2 K are shown in Fig. 36. There is a large, presumably exponential, change in J_c as L increases from 10 to 50 nm. However, the large scatter in the data, roughly 2.5 decades for L =30 nm, makes it impossible to convincingly establish a specific relationship between J_c and L. More fundamentally, the fact that two junctions differing in nominal length L by a factor of 2 can exhibit the same critical currents indicates a large inhomogeneity in interlayer thickness and raises the question of whether or not *any* of the device interlayers are continuous. Even if the scatter is neglected, the data are not easily reconciled with conventional theory, Using the values of ρ_n and ξ_{nd} in Table 2, $J_c(L)$ can be calculated from Eqn. (5 b). Thus, Fig, 36a was obtained using $J_{co} = 0.70\,\Delta_\infty(0)/(e\rho_n\xi_{nd}(T_c)) = 3.6\,A/\mu m^2$ and $L_0 = 3.18\xi_{nd}(T_c)$ =2.6 nm, with $2\Delta_\infty(0)/kT_c$=3.53. Note that this calculation assumes high SN interface transparency, γ_b<1. Larger values of γ_b would result in much smaller critical currents. This would result in a reduction in J_{co} to a value more in line with the data, but J_c at finite L would then become far to small, Thus, despite evidence that the device resistance is dominated by interface resistance, the data are clearly not compatible with γ_b>>1,

Figure 36b is a two-parameter fit to the data of the form Eqn. (5 b), which results in $J_{co} = 31\,mA/\mu m^2$ and $L_0 = 5.6\ nm$, The smaller fitted value of J_{co} might be understood as resulting from interface resistance or inhomogeneity, however the 120% discrepancy in ξ_{nd} values is harder to explain. In addition, the larger L_0 value obtained from the fit implies that $\xi_{nd}(T_c) = 1.7\ nm$. Even with this larger value of $\xi_{nd}(T_c)$, $L/\xi_{nd}(T_c)$ ran9es up to 28, incompatible with a finite critical current at 77 K in the longer devices. For

example, Ref. [66] reports a reasonably sized critical current density of approximately 20 $\mu A/\mu m^2$ at $77\ K$ for L =30 nm where L/ξ_{nd} (7') should be 17. These discrepancies are not surprising in view of the unexpected quasi-linear behavior of I_c (T).

We saw in Section Ill that conventional theory predicts that at very low temperatures, for $L/\xi_{nd}(T_c)>12, J_c \propto 1/L^3$, a dependence that is much slower than exponential. Thus, theory predicts an exponential $I_c(T)$ dependence over a wide temperature range but a power-law length dependence at low temperatures for these very long (L>> $\xi_{nd}(T_c)$) junctions. Obviously, neither prediction is compatible with the reported $CaRuO_3$ data,

Difficulty in reconciling $CaRuO_3$ device measurements with theory is not limited to edge junctions. Comparisons between theory and experiment using $CaRuO_3$ step-edge devices [82] are equally puzzling. For the device of Fig, 17, $d_{step} \cong 100\ nm$ and d_{film} =80 nm, implying $L \cong 100\ nm$ and $L/\xi_{nd}(T_c)>120$. Proximity coupling in such a junction is impossible to reconcile with conventional theory, as is the quasi-linear (rather than exponential) I_c (7') dependence,

Similar inconsistencies between theory and experiment have been obtained on edge junctions with $SrRuO_3$ interlayers [67]. The relevant lengths are listed in Table 2 and again the dirty limit applies at all temperatures of interest, with $\xi_n(T_c) \cong 1.2\ nm$. For a typical reported device length of 20 nm, the reduced length $L/\xi_{nd}(T_c)>16$. As before, conventional proximity effect theory predicts that $I_c(T)$ should exhibit an exponential temperature dependence with no observable I_c at higher temperatures. Nevertheless, data such as that presented in Fig. 12 again has a quasi-linear temperature dependence, In fact, we find that the best match of the data in Figure 12 to theory is achieved for $L/\xi_{nd}(T_c) \cong 4$, just as in the $CaRuO_3$ edge junction case. Aside from the large discrepancy between inferred and predicted normal coherence lengths, another remarkable issue emerges: Although the $CaRuO_3$ and $SrRuO_3$ devices are characterized by different ξ_n and different ranges of L values, the best match of theory and experiment yields the *same* reduced length $L/\xi_{nd}(T_c)$! This observation can hardly be accepted as coincidence.

The results of a study of $I_c(L)$ at 4.2 K for $SrRuO_3$ SNS devices are shown in Fig. 37 [67]. Again, the large scatter in the data suggests that the possibility of discontinuous interlayers merits strong consideration. Even if we ignore the large scatter, however, the data are not easily reconciled with conventional theory, Using the values of ρ_n and ξ_{nd} in Table 2, $J_c(L)$ can be calculated from Eqn. (5 b). The resulting curve would lie well above the data shown. We note, however, that R_n of both $CaRuO_3$ [66] and $SrRuO_3$ [67] devices is dominated by interface resistance, suggesting that γ_b>>1. Although taking γ_b into account does not improve agreement between theory and experiment in

the $CaRuO_3$ case, a large value of γ_b should be considered for $SrRuO_3$ devices. From Table 2, we obtain $\rho_n = 0.56\,\Omega - \mu m$ at 4,2 K and $\xi_{nd}(T_c) = 1.3$ *run.* Device resistance data [67] shows that $r_c >> \rho_n L$, implying that $R_n \cong 2r_c / \mathcal{A}$. The spread in R_n values is large, but r_c is on the order of 10 $\Omega - \mu m^2$. Thus, from Eqn. (24), $\gamma_b \approx 104$. This results in predicted I_c values far smaller than the reported data. Figure 37a was obtained assuming an *SINIS* structure, using $J_{co} = 0.70\Delta_\infty(0)/(\gamma_b^2 e\rho_n \xi_{nd}(T_c))$ **=5.6** $mA/\mu m^2$ and $L_0 = 3.18\xi_{nd}(T_c) = 4.2\ nm$. In order to obtain the J_{co} value, we chose $\gamma_b^2 = 1000$, smaller than the above estimate. The discrepancy might be explained by interface inhomogeneity. Figure 37b is a two-parameter fit to the data of the form Eqn. (5 b), resulting in $J_{co} = 1.2\ mA/\mu m^2$ and $L_0 = 8.5$ *nm,* or twice the calculated value. The discrepancy between theory (including the fitting parameter γ_b^2) and the $I_c(L)$ data is relatively small given the scatter in the data. As with $CaRuO_3$ devices, the real problem of theoretical interpretation lies in the extrapolation to higher temperature, since the observed quasi-linear temperature dependence of the critical current cannot be reconciled with conventional proximity effect theory.

Twenty-four of the twenty-nine $SrRuO_3$ devices with L =25 or 30 *nm* were reported to have "zero" critical current [67], with $J_c < 1\,\mu A/\mu m^2$ ($I_c < 1\,\mu A$) at 4.2 K. Without correcting for noise rounding, and allowing for the possibility of external noise affecting the measurements, this small value is close to the minimum observable I_c at this temperature, If the critical current density data for $L \geq 25\,nm$ have the same spreads as that for smaller junction lengths, then the failure to observe a critical current in over 80% of the junctions with $L \geq 25\,nm$ is simply consistent with the rest of the data shown,

Antognazza and co-workers [67] offer a more exotic explanation for why most of the longer junctions have no observable critical current, For *SNS* junctions with ferromagnetic interlayers, $I_c(L)$ has been predicted to either oscillate [1 53] or exhibit a critical thickness [154],[1 55]. In either case $I_c(L)$ *goes* to zero at some critical value L_c. In most ferromagnetic materials, the Curie temperature (160 K in bulk $SrRuO_3$) *is* larger than T_c. Analytic expressions for $I_c(L)$ are available in this case for dirty limit junctions [153], the situation of interest here. However, Ref. [67] incorrectly argues from an expression [155] for c/can limit junctions having ferromagnetic interlayers with *small* Curie temperatures (much less than T_c). Furthermore, *ad hoc* replacements of ξ_{nc} by ξ_{nd} and L_c by a dirty limit value [154] were made, It was then concluded that L_c must be 25 nm, since $I_c(L)$ apparently vanishes at that thickness. However, L_c in this model is directly proportional to ξ_{nd} and the claimed experimental values of these quantities are inconsistent with each other. This line of reasoning, based on inappropriate theoretical expressions, provides little support for the exotic claim that these $SrRuO_3$ junctions are an example of ferromagnetic *SNS* devices.

Transmission electron microscopy (TEM) studies of $CaRuO_3$ edge junctions [1 56] have revealed direct shorts through 5 nm thick interlayers. The number of *observed* shorts decreased as barrier thickness increased and shorts were thought to be "generally absent" in edge structures with interlayer thicknesses exceeding 30 nm. Similar TEM evidence for pinholes through $SrRuO_3$ interlayers exists [1 *57]*. These observations suggest that shorts exist through the interlayers in most of the junctions in Fig. 36. A proximity effect interpretation is therefore clearly inappropriate. Considering the small areas probed by TEM, it is reasonable to postulate pinhole shorts through the interlayers in all the reported junctions. Thus, despite persistent claims of their SNS behavior [66], [67], ruthenate edge junctions are better described by a pinhole model [15], the interlayer pinholes having been observed directly.

Oxide Metal Edge Junctions: Cuprates (T_{cn}=0)

Transport in cuprate materials is not as well understood as in noble metals or oxide metals such as the ruthenates. Nevertheless, cuprates have attracted considerable attention as interlayers for SNS junctions because of their chemical and structural compatibility with the high-T_c electrode materials. For example, lattice-matching is useful for allowing epitaxial growth of the counterelectrode. In addition, the matching of thermal expansion coefficients over the entire temperature range encountered in device growth and operation helps to preserve the integrity of the desired structure.

We saw in Section II that SNS edge junctions have been fabricated with interlayers of non-superconducting $YBa_2Cu_3O_{7-\delta}$ *[59],[1* 58] by depositing the interlayer at a lower-than-normal temperature ($\cong$530 "C). In such devices, J_c depends exponentially on length at low temperatures, with ξ_{nd} estimated from experiment to be roughly 2 nm [59]. However, as in the ruthenate case, $J_c(T)$ data are quasi-linear and do not change shape when L increases. Thus, these junctions also fail to conform to the predictions of conventional proximity effect theory.

The most commonly-employed cuprate interlayer material with T_{cn}=0 has been $PrBa_2Cu_3O_{7-\delta}$. This material is structurally very similar to $YBa_2Cu_3O_{7-\delta}$ and is anisotropic. However, $PrBa_2Cu_3O_{7-\delta}$ *is* not superconducting and has transport properties varying from insulating to metallic depending on fabrication conditions and transport direction. We see from Eqns. (7) and (37) that, within conventional proximity effect theory, ξ_{nd} decreases with increasing resistivity and carrier density as $1/(\rho_n^{1/2}n^{1/6})$. Thus, if the interlayer changes from metallic towards insulating, the accompanying resistivity increase results in a smaller coherence length. This has serious consequences for the application of conventional proximity effect theory. For example, in a representative oxide metal such as $CaRuO_3$, ξ_{nd} at 77 K is 0,88 nm (see Table 2). Increasing the

resistivity by a factor of 100 decreases ξ_{nd} to less than 0.1 *nrn* if n is unchanged. If n were reduced in achieving this resistivity increase, ξ_{nd} would be larger, but even a simultaneous two order of magnitude reduction in n would yield a ξ_{nd} below 0.2 *ntn,* still on the order of a single lattice spacing. Thus, conventional proximity effect theory cannot account for supercurrent in junctions with interlayers approaching a metal-insulator transition. Moreover, conventional theory, which assumes metallic transport in the interlayer, cannot apply to non-metallic N materials.

Sandwich $YBa_2Cu_3O_{7-\delta}$ junctions with $PrBa_2Cu_3O_{7-\delta}$ interlayers were first fabricated with each layer having its c-axis normal to the substrate [62]. Supercurrent were observed in junctions up to 50 nm -thick at temperatures exceeding 40 K. Although no $I_c(T)$ data are available, the junction resistance above T_c increased dramatically with decreasing temperature, consistent with a non-metallic interlayer. The interlayer resistance was on the order of $10^6\,\Omega-\mu m$, so conventional proximity effect theory does not apply, as discussed above. In fact, it is likely that the supercurrent resulted from pinholes in the interlayer film itself. Subsequently, supercurrent were observed in similar c-axis $PrBa_2Cu_3O_{7-\delta}$ sandwich junctions as thick as 130 nm *[1* 59], with an exponential dependence of J_c on L for L>75 nm. In these devices, the scaling length Lo at 4,2 K was inferred to be 15 nm, This large "coherence length" and the roughly linear dependence of $I_c(T)$ cannot be reconciled with proximity effect theory, especially considering the non-metallic nature of the interlayer. However, the data from these devices are again qualitatively consistent with the effects of pinholes.

Barrier *et a/.* [1 60] demonstrated $PrBa_2Cu_3O_{7-\delta}$ sandwich junctions using films whose a-saxes were normal to the substrate. In their devices, J_c scaled exponentially with interlayer thickness from 30 to 150 nm at 10 K with a scaling length on the order of 25 nm. Subsequently, Hashimoto *et a/,* [72] fabricated similar devices in which the magnetic field dependence of I_c approximated the ideal dependence expected from a uniform interlayer. As mentioned in Section II, $I_c(T)$ for these junctions was consistent with the exponential dependence of Eqn. (5), with $L_n \propto T^{-1/2}$, as expected from dirty-limit proximity effect theory. The authors [72] inferred $\xi_{nd} \cong 30\,nm$ from the data at 4.2 K. However, the large apparent resistivity of the interlayer ($\cong 4000\,\Omega-\mu m$) indicates a much shorter coherence length under conventional proximity effect theory. The authors estimated 1 nm, but of course the theory is invalid for such large, non-metallic values of resistivity. The possibility of interface resistance was not considered in estimating the bulk interlayer resistivity. If the device resistance were dominated by the interfaces and the interlayer were metallic, a coherence length comparable to those listed for oxides in Table 2 might be expected. Unfortunately, these deduced values of ξ_n are still considerably smaller than those inferred from the $I_c(L)$ data. Thus, while the $I_c(T)$ data are suggestive of proximity effect behavior, the deduced length scale is inconsistent with

theory. A critical current scaling length of 30-40 nm at 4.2 K has also been obtained in a-axis junctions with $Pr_{0.55}Y_{0.45}Ba_2Cu_3O_{7-x}$ interlayers [161]. Although $I_c(T)$ data were not discussed, the interlayer resistivity was claimed to exhibit behavior consistent with variable range hopping rather than metallic conductivity. In such a case, proximity effect theory would not be expected to apply. Since the interlayer resistivities in Refs. [72] and [160] were even *higher* than those in Ref. [161], the successful application of proximity effect theory to the former devices is even less likely.

$PrBa_2Cu_3O_{7-\delta}$ sandwich junctions with interlayers in the (103) orientation have also been fabricated [162]. In these junctions, $I_c(T)$ behaved anomalously below 65 K [163]; it *decreased* with decreasing temperature. In contrast, the I_cR_n product increased with decreasing temperature, due to the exponential increase in junction resistance. This behavior was attributed to the semiconducting nature of the interlayer. Similar behavior has not, however, been reported in low-T_c junctions having semiconductor interlayers.

Co-planar bridge junctions (Fig. 9a) with $HoBa_2Cu_3O_{7-x}$ electrodes and $PrBa_2Cu_3O_{7-\delta}$ interlayers behaved similarly to other types of $PrBa_2Cu_3O_{7-\delta}$ devices [1 64]. These structures exhibited $J_c \cong 10\ nA/\mu m^2$ at *4.2 K* in devices with L as large as 100 nm. Although such J_c values are not inconsistent with the sandwich junction results for ab-plane transport, they are not reconcilable with conventional proximity effect theory given the non-metallic behavior of the interlayer.

Several groups have fabricated edge junctions with $PrBa_2Cu_3O_{7-\delta}$ *[63], [64], [70],[1 65]-[168]* or $(Y,Pr)Ba_2Cu_3O_{7-x}$ *[1 69]* interlayers. Recall that transport in edge junctions is predominantly along the ah-planes, parallel to the substrate. The most extensive work in this system has been done by Gao et *a/.* [166] -[168], In their devices, $J_c(L)$ was exponential at 4.2 K for $5<L<30\ nm$, yielding a scaling length $LO \approx 5\text{-}8\ nm$. However, $J_c \propto (T_c - T)^2$ over a wide range below T_c regardless of $l.$, a dependence expected only very near T_c. The exponential-like temperature dependence predicted for long junctions was not observed. Thus, despite the apparent exponential scaling of $J_c(L)$ at low temperatures, these devices are not described by conventional proximity effect theory. The resistances of these devices [165]-[1 68] were also peculiar. The inferred resistivities were in the range 4000-8000 $\Omega - \mu m$, implying non-metallic interlayers. We would therefore expect R_n to increase with decreasing temperature. Instead, the measured device resistances were relatively insensitive to temperature. This inconsistency suggests that *SN* interface resistance is responsible for the large R_n of these $PrBa_2Cu_3O_{7-\delta}$ devices. Recall that a large interface resistance, coupled with the short coherence length inherent in a $PrBa_2Cu_3O_{7-\delta}$ interlayer, implies an extremely small wavefunction overlap in the N region, and ıence a small I_c. The large critical currents

actually observed are therefore consistent with transport through pinholes rather than proximity coupling across the interlayer.

We have already noted (see Fig. 13) that Barrier *et al.* [64], [71] obtained $J_c(T)$ curves on $PrBa_2Cu_3O_{7-\delta}$ edge junctions that were qualitatively consistent with the exponential-like dependence expected from conventional theory. This qualitative agreement consists of $J_c(T)$ data that exhibit dramatic upward curvature which increases with junction length. However, the scaling length of 9 nm inferred from $J_c(L)$ data at 4.2 K is quantitatively inconsistent with proximity effect theory given the high interlayer resistivity of 300 $\Omega - \mu m$. One possible explanation for this inconsistency is interlayer inhomogeneity. The junctions could be SNS in nature but with supercurrent transport dominated by interlayer regions significantly thinner than the expected thickness. It is worth noting that a patchy interlayer is distinct from an interlayer with pinholes. Nevertheless, a patchy interlayer is undesirable from the standpoint of making reproducible, manufacturable devices.

Although numerous groups have fabricated working junctions with $PrBa_2Cu_3O_{7-\delta}$ interlayers in a variety of geometries, we have seen that there is tremendous variation in the basic properties of the devices. The temperature dependence of the critical current can be linear, quadratic, or exponential. Occasionally, $I_c(T)$ has even been observed to decrease with decreasing temperature. The junction resistance usually increases with decreasing temperature. In some cases, however, it is relatively temperature-insensitive. Consequently, the reported data are difficult to reconcile both qualitatively with each other and quantitatively with proximity effect theory. Indeed, it is even difficult to justify applying conventional theory to these high-resistivity (possibly non-metallic) interlayer devices.

The non-metallic nature of typical $PrBa_2Cu_3O_{7-\delta}$ interlayers has been explicitly recognized [161],[162] in attempting to account for supercurrent that cannot be explained by conventional proximity effect theory. In Section III, we briefly discussed extensions of *SNS* theory to cover junctions in which transport through the interlayers is the result of resonant tunneling processes *[57]*. It is natural to expect that such models might be applied to at least some of the available results on $PrBa_2Cu_3O_{7-\delta}$ junctions. Recall, however, that is difficult to theoretically justify the large observed values of the scaling length L_0. Indeed, the resonant tunneling theory does not necessarily explain supercurrent in junctions whose interlayers are thicker than those encountered in conventional proximity effect models. However, the theory may provide the basis for understanding transport in some junctions with thin non-metallic interlayers, and such junctions are of special interest because their inherently large R_n is a desirable feature in many applications [16].

Experimental results on **edge junctions** with $DyBa_2Cu_3O_{7-x}$ **electrodes and** $PrBa_2Cu_{3-x}Ga_xO_{7-\delta}$ interlayers [1 70] appear to be consistent with resonant tunneling transport, The addition of Ga to $PrBa_2Cu_3O_{7-\delta}$ significantly increases its resistivity. Junctions made with x ranging from O to 0.4 exhibit good I_c modulation in magnetic fields applied parallel to the plane of the interlayer (normal to the page in Fig. 9c). The critical current density followed Eqn. (5 b), $J_c = J_{co}\exp(-L/\mathrm{L},))$, with J_{co}=30 $mA/\mu m^2$ and L_o=4-5 nm at 4.2 K, independent of x. (Note that the 4-5 nm value assumes that transport is along the ab-planes in the 18-22° ramp structure. If the thickness of the interlayer normal to the substrate is used, L_O=2 nm.) It is remarkable that J_c *is* independent of x despite the orders of magnitude differences in resistivity for the different interlayer compositions. Such behavior is not encountered in the (metallic) proximity effect. In fact, the value of LO may be the scaling length a of the resonant tunneling model discussed in Section Ill.

The resonant tunneling model [57] predicts the behavior of the current-voltage characteristic in the normal state [171] as well as the superconducting one. For example, the zero-bias conductance should vary exponentially with interlayer thickness with the same characteristic decay length as the supercurrent. Such behavior has been reported in $PrBa_2Cu_3O_{7-\delta}$ edge junctions with $YBa_2Cu_3O_{7-\delta}$ electrodes [172]. The observed temperature dependence of both the decay length and the normal conductance were consistent with theory. In fact, the specific predictions of resonant tunneling theory for the normal state conductance are useful in determining the applicability of this particular model and in providing key parameter values. Both the superconducting and normal state measurements discussed suggest that reproducible junctions operating in a resonant tunneling regime have been produced. Moreover, these junctions potentially reveal a promising direction for understanding and improving high-T_c devices. Note, however, that resonant tunneling is not a general explanation for most other past results: it does not account for extraordinarily long decay lengths and does not apply to metallic interlayers.

Oxide Metal Edge Junctions: Cuprates (T_{cn}>0)

In most experimental investigaitons of the proximity effect T_{cn}, the transition temperature in N, is zero, However, SN' S junctions, where N' is a superconductor above its transition temperature (~. > T>T_{cn}>0), are of present interest because substitutionally-doped forms of the $YBa_2Cu_3O_{7-\delta}$ electrode material can be used as interlayers. Small dopant concentrations in $YBa_2Cu_3O_{7-\delta}$ can significantly lower the material's transition temperature with only small changes to its lattice constant, allowing it to function as an interlayer that is well-matched to the electrodes.

In his original theoretical investigations of the proximity effect, de Gennes allowed for $T_{cn} \neq 0$. Consequently, we can use Eqn. (8) in conjunction with the general expressions for ξ_n presented in Section IIID when examining $SN'S$ data. As usual, since de Gennes's theory is strictly applicable in the dirty limit only, we will proceed with the caveat that our analysis is more suspect if there is a large deviation from this limit

$(Y, Pr)Ba_2Cu_3O_{7-x}$ exhibits a finite critical temperature for Y fractions exceeding 0.45 [1 73], and $YBa_2Cu_3O_{7-\delta}$ edge junctions have been fabricated with $Pr_{0.4}Y_{0.6}Ba_2Cu_3O_{7-x}$ interlayers having $T_{cn}=40\ K$ [73]. These devices were analyzed using conventional proximity effect theory: $I_c(L)$ was fit to Eqn. (5a) at several temperatures and $\xi_n(T)$ was determined from the value of the exponent. This procedure resulted in an inferred $\xi_n(T)$ that increased from 10 to 15 nm between T_c and T_{cn}. Although no generally-applicable expression for $\xi_n(T)$ was employed in the analysis, it was concluded that $\ell_n >> \xi_n > 10\ nm$. The resistivity of the N' layers was approximately $1\ \Omega - \mu m$, which is inconsistent with such a long mean free path or coherence length. Kogan and Simonov [1 18] responded to this work by recalling the existence of a general expression for ξ_n valid for arbitrary ℓ_n and T_{cn} in 3d [1 17] and reported their derivation of a general 2d result as well. However, they too were led to an unreasonably long mean free path when analyzing the data.

The critical current of one of these $Pr_{0.4}Y_{0.6}Ba_2Cu_3O_{7-x}$ junctions with a 125 nm-thick interlayer increased rapidly with decreasing temperature down to 48 K, close to the expected value of T_{cn} [73]. Surprisingly, the rate of increase of $I_c(T)$ was even *more* rapid below this temperature. It is significant that almost all of the variation in the inferred $\xi_n(T)$ occurred *below* T_{cn}. Of course, proximity effect theory does not even apply when the interlayer is in the superconducting state. Consequently, the behavior of these $Pr_{0.4}Y_{0.6}Ba_2Cu_3O_{7-x}$ edge junctions could not be explained by conventional proximity effect theory.

Char *et al.* have demonstrated *SNS* edge junctions with substituted-$YBa_2Cu_3O_{7-\delta}$ interlayers [1 *74]: $Y_{0.7}Ca_{0.3}Ba_2Cu_3O_{7-\delta}$ and $YBa_2Cu_{2.79}Co_{0.21}O_{7-\delta}$ interlayers had low bulk resistances and negligible *SN* interface resistance. Small interface resistances in $PrBa_2Cu_3O_{7-\delta}$ *SNS* edge junctions had been reported previously [63], [64]. However, the unusually low resistivity of the substituted-$YBa_2Cu_3O_{7-\delta}$ interlayers put an even lower limit on the magnitude of the contact resistance. In principle, low interface resistance improves the probability of observing proximity effect behavior because the critical current is larger in the absence of boundary resistance, More importantly, unlike $PrBa_2Cu_3O_{7-\delta}$, substituted-$YBa_2Cu_3O_{7-\delta}$ is a *metallic* interlayer which increases the chances that a straightforward application of the de Gennes proximity effect theory will

be successful. However, Char and co-workers did not attempt such analysis in the original investigations [74], [75], [174]. Indeed, there were only three values of L reported for each interlayer material and there was no significant range of temperatures for which measurable critical currents existed for all three L values. Therefore, the type of analysis discussed above for $Pr_{0.4}Y_{0.6}Ba_2Cu_3O_{7-x}$ junctions could not be performed and $\xi_n(T)$ could not be directly determined.

From Table 2, we find that the departures from the dirty limit are not large for the doped cuprate interlayers of interest. It is therefore reasonable to assume that Eqn. (8), using an appropriate general formula for ξ_n, will adequately describe $I_c(T; L)$. (Recall that the general formula for ξ_n is given by Eqn. (30) using Eqn. (31) to express ξ_{nd} and Eqn. (33) to express ξ_{nc}.) Using the available device parameters [74], [75], we were thus able to *calculate* [20], rather than merely fit, $I_c(T; L)$ for the substituted-$YBa_2Cu_3O_{7-\delta}$ interlayer devices, In these calculations, Eqn. **(8)** was employed with T_c=88 K, T_{cn}=50 K, and 2A(0) / kT_c=3.53. (Deviations from BCS theory for the gap value only affect the constant prefactor in Eqn. (8), and then only by a factor of order unity.) The reported resistances and device dimensions were used to calculate ρ_n, which, in turn, yields ℓ_n. The normal coherence length, <n(T), was obtained as described in connection with Fig. 31. Data for $Y_{0.7}Ca_{0.3}Ba_2Cu_3O_{7-\delta}$ junctions [75] are compared with the calculated results in Fig. 38. The agreement is impressive and reflects two important qualitative features: The exponential-like increase of I_c with decreasing temperature and the downward shift in the temperature at which I_c becomes measurable. Figure 39 shows a similar comparison for $YBa_2Cu_{2.79}Co_{0.21}O_{7-\delta}$ junctions [74]. The agreement is not nearly as good as in the previous case, but the qualitative trend of the data is exhibited. We note the absence of arbitrary fitting parameters in both Figs. 38 and 39 and the fact that the fits can be improved by adjusting the values of the physical parameters.

These results, which show the strongest agreement between conventional theory and experiment obtained to date, strongly suggest conventional proximity effect behavior. We note that $I_c(T;L)$ was calculated under the simplifying assumption of rigid boundary conditions. Re-examination of the published data [74] for $I_c(T)$ near T_c showed that this is a reasonable assumption [175] for the $YBa_2Cu_{2.79}Co_{0.21}O_{7-\delta}$-interlayer devices. However, it was not clear from the original data that this was true in the case of the $Y_{0.7}Ca_{0.3}Ba_2Cu_3O_{7-\delta}$-interlayer devices. Indeed, we would expect non-rigid boundary conditions for well-matched electrode and interlayer materials. As we have emphasized throughout this paper, however, the boundary conditions are of secondary importance because the exponential factor in Eqn. (8) dominates the behavior of $I_c(T;L)$ *so* completely, Consequently, it is not surprising that calculations carried out under a variety of assumed boundary conditions show similar satisfactory agreement with experiment. The important result of our analysis [20] is that the agreement between the

calculated and measured $I_c(T;L)$ is as good as any achieved with low- T_c devices and represents strong evidence that the $Y_{0.7}Ca_{0.3}Ba_2Cu_3O_{7-\delta}$-interlayer devices are correctly described by conventional proximity effect theory.

Following the publication of our analysis [20], attempts were made to apply conventional proximity effect theory to other $YBa_2Cu_{3-y}Co_yO_{7-\delta}$ [176],[177] and $Y_xCa_{1-x}Ba_2Cu_3O_{7-\delta}$ [178] edge junction data. For example, I_c data were fit to conventional dirty limit theory for junctions with interlayers having several Co concentrations [176]. In $YBa_2Cu_{3-y}Co_yO_{7-\delta}$ devices, values for ξ_n of 49 nm ($y=0.1$), 12.6 nm ($y=0.2$), and 4.3 nm ($y=0.3$) resulted from fitting $I_c(L)$ at 60 K for $L<55\ nm$. By fitting $I_c(T)$ for fixed L, values of 16.4 nm ($y=0.2$, $L=55\ nm$) and 5.7 nm ($y=0.3$, $L=30\ nm$) were obtained. The decrease in ξ_n with increasing Co concentration is expected, however the extremely long fitted coherence lengths are inconsistent with conventional theory, particularly considering the relatively large measured interlayer resistivities, which exceeded 10 $\Omega-\mu m$. This problem is equivalent to that of the disagreement between experiment and theory evident in Fig. 39. Recall that the theoretical curves in Fig. 39 result from a straightforward *calculation* from conventional proximity effect theory. The data can instead be ***fit*** to theory using longer coherence lengths, however it is difficult to justify the parameter values required.

The I_c data from Co-substituted junctions show less temperature dependence than theory predicts because of the relatively short ξ_n calculated from material parameters. (Recall from Fig. 22 that $I_c(T)$ is steeper for smaller $\xi_n(T_c)$.) It has been speculated by Antognazza and co-workers that magnetic pair breaking affects the coherence length in $YBa_2Cu_{3-y}Co_yO_{7-\delta}$ [177]. The practical effect of such pair breaking is to *shorten* the coherence length further, replacing the factor T in Eqn. (7), the usual expression for ξ_{nd}, with $T+T_o$ where T_o is the lifetime associated with magnetic scattering [28]. Adding the magnetic pair-breaking effects does, however, reduce the temperature dependence of ξ_n and hence I_c. As a result, this procedure can provide a superficially better fit to the data if an anomalously large value of D_n is used to re-lengthen $\xi_n(T_c)$. Such a model is *ad hoc,* however, and was applied *only* to the $YBa_2Cu_{3-y}Co_yO_{7-\delta}$-interlayer devices with the *largest Co* concentration (the proposed model contained no magnetic scattering for lower Co concentrations) [177].

Other problems occur in this analysis [177]. The critical current was calculated using an expression similar to, but not identical with, Eqn. (8), Soft boundary conditions were assumed. Inexplicably, the temperature dependence of the prefactor in their expression was $(T_c-T)^*$ *over the entire temperature range.* As we saw in Section III, the correct form is $\Delta^2(T)(T_c-T)$; the simple quadratic form is an acceptable approximation only within 10% of T_c, where $A(T) \propto \sqrt{T_c-T}$. Moreover, all calculations were carried out

using the extreme clean or dirty limits for ξ_n rather than the general form associated with Eqn. (30).. For the clean limit, the *approximate* form of ξ_{nc} given in Eqn. (33) was used in place of the exact formula. Consequently, the calculated results are valid only at temperatures near T_{cn}, where A(T) is not proportional to $\sqrt{T_c - T}$. Finally, it was unpersuasively argued that the clean limit applied to $YBa_2Cu_{3-y}Co_yO_{7-\delta}$ junctions with y=0.12 and 0.21 whereas the dirty limit applied to the y=0.42 sample. For the clean limit to be valid, the condition $\xi_{nd} >> \xi_{nc}$, or $D_n >> \hbar v_n^2/(2\pi kT)$, must hold. Using $v_n \approx 10^5$ m/s this implies that $D_n >> 2\times 10^{-4} m^2/s$ for T=60 K. Now, using $\rho_n = 1\Omega - \mu m$ and $2\mathcal{N}_n = 3\times 1028\, eV^{-1}m^{-3}$, *we see* from Eqn. (38) that $D_n \approx 2\times 1\ 0^{-4}\, m^2/s$ for *pure* $YBa_2Cu_3O_{7-\delta}$. It is not reasonable to postulate much *larger* values for the diffusion constant in substituted- $YBa_2Cu_3O_{7-\delta}$, as required by the clean limit criterion. As a result, the analysis of Antognazza *et al. is* not internally consistent. Moreover, while the magnetic pair breaking hypothesis is intriguing, it is unsupported by the experimental data.

Attempts were also made by Antognazza and co-workers [178] to analyze the same $Y_{0.7}Ca_{0.3}Ba_2Cu_3O_{7-\delta}$-interlayer edge junction data shown in Fig. 38. The analysis assumes soft boundary conditions and the extreme clean limit. Again, the calculations contain the same inconsistencies just discussed, The $(T_c - T)^2$ prefactor is only valid within 10°/0 of T_c. The approximate form for ξ_n is only valid near T_{cn}, the opposite end of the temperature range. Finally, the clean limit requires $D_n >> \hbar v_n^2/(2\pi kT)$. Thus, a value of v_n=2× 105 m/s implies an unreasonably large diffusion constant, $D_n >> 8\times$ 10-4 m^2/s at T=60 K.

These authors also propose a "percolation model" as an alternative explanation of the $Y_{0.7}Ca_{0.3}Ba_2Cu_3O_{7-\delta}$ junction data [178]. The interlayer is assumed to consist of many '(grains," each having a different T_c. When one or more of these grains form a continuous superconducting path through the interlayer, an additional supercurrent can flow. A particular *ad hoc* distribution of transition temperatures must thus be assigned to the grains in order to explain the nonlinear $I_c(T)$. It was stated [178] that the grain size was approximately 20 nm, implying that the grains are as thick as some of the interlayers. It was left unexplained how grains many coherence lengths in size act as Josephson weak links. An appropriate test of this percolation model would be careful studies of $I_c(B;T)$. These measurements would presumably demonstrate the dramatic temperature dependence of the macroscopic spatial distribution of J_c that is an integral part of the model. Of course, superconducting shorts through the interlayer are precisely what is meant by "pinholes," which were already invoked to explain the quasi-linear temperature dependence in many nominally *SNS* junctions [15], (Obviously, such pinholes are presumably much smaller than 20 nm.) It is ironic that these authors, who have consistently promoted a proximity effect interpretation of their earlier results

[66], [67],[1 14],[1 74] which are more easily explained by interlayer shorts, are advancing a pinhole model for $Y_{0.7}Ca_{0.3}Ba_2Cu_3O_{7-\delta}$ devices, where conventional proximity effect theory readily accounts for the available data,

Summary

It is clear from this discussion that at present there is no compelling evidence for conventional proximity effect behavior in high-T_c SNS junctions whose interlayers have T_{cn}=0. In the case of the ruthenate edge junctions, the evidence for pinholes (supercurrent paths *through* the interlayer) is overwhelming: The pinholes have been observed directly. The behavior of other types of devices is more intriguing. Noble metal step-edge bridges also fail to exhibit conventional proximity effect behavior, but there is no clear evidence for transport via paths other than the normal metal bridge itself, Of course it is possible that thin, possibly filamentary, superconducting shorts couple the two electrodes. Indeed, such paths are expected for superconducting films deposited at pressures high enough to allow considerable scattering of the deposited species *en route* to the substrate. However, control experiments designed to reveal unintended shorts connecting the step-edge electrodes have failed to produce evidence for their existence. Cuprate interlayers with T_{cn}=0, such as $PrBa_2Cu_3O_{7-\delta}$, exhibit a range of transport behavior depending on deposition conditions. These interlayers can be non-metallic and therefore devices made with them cannot be described by conventional proximity effect theory. However, other $PrBa_2Cu_3O_{7-\delta}$ films appear to be metallic and yield devices with exponential-like $I_c(T)$ behavior, although the inferred coherence lengths are unreasonably long. There is a great need for more definitive experimental data on high-~, devices with each of these normal interlayer materials.

Results on devices whose interlayers have $T_{cn} \neq$ O provide the best available evidence to date for conventional proximity effect behavior in high-~ junctions. In the case of $YBa_2Cu_{3-y}Co_yO_{7-\delta}$ interlayers, junction behavior is qualitatively consistent with expectations, although the coherence length required to fit the data tends to be longer than material parameters justify. In the case of $Y_xCa_{1-x}Ba_2Cu_3O_{7-\delta}$ interlayers, a reasonable quantitative agreement with theoretical predictions has been demonstrated, This evidence for proximity effect behavior is encouraging enough to motivate careful and consistent attempts to analyze high-~. SNS junction data using conventional theory as a starting point.

Vi. SUMMARY

Two basic themes emerge from a careful examination of the available high-< junction

critical current data. First, most high-T_c junctions behave very similarly, exhibiting a quasi-linear dependence of I_c on temperature regardless of constituent materials, fabrication techniques, and device geometry. Second, these data cannot be reconciled with the well-established and well-tested conventional proximity effect theory.

Data from some SN' S devices, in which the interlayer N' is a substituted form of the electrode material, provide significant exceptions to these observations. Ca- and Co-substituted edge junctions differ markedly from other high-T_c SNS devices in that $I_c(T;L)$ data obtained from them show the exponential dependence predicted by conventional proximity effect theory. Although their SNS nature cannot be considered absolutely established at the present time, these SN' S junctions provide a clear indication that basic proximity effect ideas can be effectively applied to high- T_c devices. Thus, an understanding of conventional device behavior should expedite the development of a robust high-T_c junction fabrication technology.

A. Experimental Consequences of Conventional Theory

Key Experimental Tests

There is no *a priori* reason to believe that high-T_c SNS junctions are well-described by conventional proximity effect theory. Nevertheless, an appreciation of the primary signatures of conventional theory is essential if a useful connection is to be made between present electrical measurements and future progress in device processing. We therefore review the general features of conventional proximity effect theory.

The proximity effect in an SNS junction is manifested by the spatial overlap of the decaying wavefunctions of the superconducting electrodes. In other words, Cooper pairs "leak' into the normal interlayer. The wavefunctions decay exponentially in long junctions over a distance ξ_n, the normal coherence length. The critical current of the device directly reflects the degree of wavefunction overlap. Therefore, in any long SNS device, the critical current must depend exponentially on electrode separation L and temperature T in a manner consistent with the temperature dependence of ξ_n. It is therefore important in the initial stages of device development to fabricate and analyze long junctions ($L>>\xi_n$). Although such junctions may be impractical for most applications because of their small I_cR_n products, they provide the clearest signatures of the proximity effect. Having established that the devices are truly SNS in nature, it is then possible to optimize the processing and fabricate shorter devices for actual applications.

As we have repeatedly discussed, **three key features of the proximity effect in long**

SNS devices are:

(1) **A dramatic, exponential-like increase of I_c with decreasing T over a broad temperature range below T_c.** Moreover, this temperature dependence should become steeper as junction length L increases. This behavior provides an obvious qualitative indication of indication of proximity effect behavior that is not typical of other types of junctions. Indeed, a quasi-linear temperature dependence in a long *SNS* junction is a strong indication that the device is *SNS* in name only. Because $I_c(T)$ can be studied in a single junction, these data should be critically examined before more exhaustive and quantitative studies of $I_c(T;L)$ are undertaken.

(2) **An exponential dependence of I_c on L.** Establishing this dependence requires data from many junctions. The common practice of fitting a few points to an exponential dependence at a single temperature is inadequate. Ideally, $I_c(L)$ should be fit at several temperatures. The scatter in I_c data for a single value of L is significant; a large scatter is an indication of inhomogeneous interlayers and poor fabrication control.

(3) **A quantitative agreement between calculated and experimentally-obtained exponential decay lengths.** Ideally this quantitative comparison of experiment and theory is performed over a wide range of temperatures. For $T > 0.3T_c$, the decay length Lo, obtained from either $I_c(T)$ or $I_c(L)$, is the normal coherence length ξ_n and is thus easily calculated from fundamental interlayer parameters. At temperatures below 0.3 T_c, the decay length is related to $\xi_n(T_c)$, but $L_o \neq \xi_n$. (This latter point is important because most attempts to determine ξ_n from $I_c(L)$ have been done at 4.2 K.) Of course, only the general expression for $\xi_n(T)$ given by Eqns. (27)-(30), should be used in the calculations unless it is known *a priori* that a device is in the extreme clean or dirty limits.

These general litmus tests for conventional proximity effect behavior follow directly from the basic notion that the Cooper pairs in the superconducting electrodes “leak” into the normal interlayer. These three key features will hold for the clean, dirty, or intermediate regimes, for isotropic or anisotropic materials, for one-, two-, or three-dimensional device structures, and will be independent of the symmetry of the superconducting order parameter in the electrodes. Establishing these features provides strong evidence for the conventional proximity effect in a device, Conversely, failure to establish them, as in devices with length-independent quasi-linear $I_c(T)$, provides strong evidence against such behavior.

Secondary Experimental Issues

In addition tothethree central aspects of proximity effect behavior, other features of typical data areless useful ininitial device characterization. Forexample, the behavior of $I_c(T)$ near T_c is a much overused secondary feature. Such data reflect the prefactor in Eqn. (5). However, as discussed in Section Ill, it is difficult to acquire reliable data near T_c and interpret it. The power-law dependence of 1_c(T) is sensitive to the choice of T_c, which is seldom known with sufficient accuracy. In addition, even under the assumption of s-wave symmetry of the superconducting wavefunctions, there are multiple conventional explanations for any particular power-law dependence. Finally, the prefactor in Eqn. (5) is sensitive to the many complicating issues discussed above that do not influence the basic exponential dependence associated with the proximity effect. As a result, near-T_c data is of limited value and should used only after a device is known to be proximity-coupled from the more general signatures.

The quality of the SN interfaces in a device is an important fabrication issue that can be addressed by more detailed experiments focusing on the prefactor in Eqn. (5). The major interface-related concerns are contact homogeneity and transparency. Although magnetic field modulation of the critical current can be used to probe interface homogeneity, other data such as device resistance must also be examined. The dependence of R_nA on device length is often used to determine whether the bulk resistance of the interlayer or the contact resistance of the interface dominates the junction. If the contact resistance dominates, the SN interfaces are almost certainly inhomogeneous, otherwise the magnitude of the critical current would be impractically small, (Of course, the shape of the *normalized* $I_c(T)$ data would still be exponential-like even if the interfaces were inhomogeneous with a low transparency.) Nevertheless, performing such experiments is premature until the validity of Eqn. (5) and the conventional proximity effect are first established. In other words, we should understand transport across the bulk of the interlayer before examining transport across its interfaces.

B. Interpretation of Existing Results

In the previous section, we summarized the $I_c(T;L)$ behavior expected *if* a particular device were indeed proximity-coupled. Here, we review the implications of the actual data reported on nominally SNS devices.

It should now be obvious that the nominally SNS high-T_c junctions discussed in the literature do not conform to conventional proximity effect theory. This fact is most clearly reflected in the unexpected quasi-linear, rather than exponential-like, $I_c(T)$ data.

Only if $L/\xi_n(T_c)$ is always approximately 4, indicating a relatively short junction, does conventional proximity effect theory predict a quasi-linear $I_c(T)$. It is possible to fit quasi-linear data with conventional tunneling or point contact theories by assuming that the superconducting gap of a high-T_c material has a magnitude or symmetry different from that associated with standard BCS theory. These theories, or one based on resonant tunneling, may be applicable to grain' boundary junctions. However, they are not expected to apply to long *SNS* devices with metallic interlayers.

In fact, the similarity of the $I_c(T)$ data from nominally *SIS* and *SNS* high-~ edge junctions (*SN' S* junctions excepted) to that from grain boundary junctions leads to an important conclusion: **The behavior of** SNS **edge junctions reported in the literature is dominated by pinholes through the N interlayers.** There is further supporting evidence for this claim. As discussed in Section V, the experimentally-measured length dependence of the critical current cannot be reconciled with theory. In devices with short normal coherence lengths, a large *SN* interface resistance precludes a significant critical current; yet I_c is readily observed. Finally, transmission electron microscopy has revealed physical evidence of pinholes in edge junctions. Taken together, these observations clearly indicate that the only potential proximity-coupled high-T_c devices demonstrated to date are of the *SN'* S variety.

By making the interlayers thick enough, it is possible to fill in the pinholes. The result, however, is an inhomogeneous interlayer with large thickness variations. The critical current in an *SNS* device with such an interlayer would be dominated by the thinnest regions in N. This may account for exponential-like $I_c(T)$ behavior in a few reported devices with interlayers that are evidently thinner than intended. Thus, if an interlayer is grown with pinholes, $I_c(T)$ is quasi-linear, as in a grain boundary junction. However, if the interlayer is continuous but extremely in homogeneous, $I_c(T)$ can be exponential-like but with the actual L smaller than intended. (Note that this interpretation differs from the common assertion of a normal coherence length which is longer than that expected from theory.) With this pinhole model, there is a continuum of $I_c(T)$ behavior from quasi-linear to exponential-like.

It is emphasized that pinholes through the bulk interlayer should not be confused with pinholes through a low-transparency *SN* interface. We saw in Section III that the transparency of the *SN* interfaces primarily affects the *magnitude* of the critical current rather than its temperature or length dependence, Indeed, pinholes through a low-transparency barrier are useful because they allow better coupling between the normal and superconducting regions. It is the pinholes through the bulk *N* interlayer that influence the shape of $I_c(T;L)$. This is the primary reason for our emphasis on normalized critical current data.

Because of their different geometry, noble metal step-edge SNS junctions are not straightforwardly described by a pinhole model. Nevertheless, there is strong evidence that their behavior is not governed by the conventional proximity effect. As with the grain boundary and edge devices (both nominally S1S and nominally SNS), these junctions demonstrate quasi-linear $I_c(T)$ behavior. Moreover, the $I_c(L)$ data is inconsistent with conventional theory. Again, it is the failure of *multiple* key tests that indicates that the step-edge junctions are not proximity-coupled. An appropriate explanation for the behavior of noble metal step-edge junctions remains elusive.

Finally we note that SN' S edge junctions are interesting because they follow the trends expected from conventional proximity effect theory. It is evident from quantitative analysis of $I_c(T;L)$ data that uniform, homogeneous interlayers of substituted-$YBa_2Cu_3O_{7-\delta}$ can be grown between $YBa_2Cu_3O_{7-\delta}$ electrodes. In addition, the low values of $R_n\mathcal{A}$ indicate highly transparent SN interfaces. The SN' S results suggest that lattice and thermal-expansion matching between the S and N layers in a high-~ device are of crucial importance. Thus, although Ca- and Co-substituted- $YBa_2Cu_3O_{7-\delta}$ interlayers are too conductive to provide practical device impedances, a matched, but more resistive, N material such as $PrBa_2Cu_3O_{7-\delta}$ may be worthy of further study.

C. Conclusions

The qualitative and partial quantitative agreement between conventional proximity effect theory and measurements on SN' S edge devices supports the primary premise of this paper: It is appropriate to apply conventional theory to high-~ SNS junctions. Major deviations from theoretical predictions most likely indicate materials and fabrication issues with rather than exotic physics associated with the high- T_c nature of the device.

Because the major predictions of proximity effect theory are tied to the normal coherence length $\xi_n(T)$, most of our analysis has focused on this quantity and its influence on device properties. Unfortunately, there have been few experimental studies in which $\xi_n(T)$ is obtained from $I_c(L)$ at several temperatures and carefully compared to theory. Most attempts to determine $\xi_n(T)$ have been carried at 4.2 K. At this low reduced temperature, the length L,, obtained from exponential fits $I_c(L)$ is not ξ_n. In typical experiments, only a few data points for a few L values are obtained. Since the typical electrode separation is imperfectly known (due, for example, to inhomogeneities in the deposited film thickness), the critical current can vary widely for each L. As a result, many experimental values of $\xi_n(T)$ should be viewed somewhat skeptically. There is a clear need for more definitive experimental work in this area. In particular, it is important to establish the consistency of inferred values of $\xi_n(T)$,

obtained from both $I_c(T)$ and $I_c(L)$ data, with theory,

Of course, conventional proximity-coupled junctions are not the only devices worthy of attention. For example, conventional proximity effect theory is not expected to apply if the N interlayer is not metallic. New models, such as those based on resonant tunneling, need to be further developed to describe such devices. It might even be easier to test such models with low-T_c junctions because fabrication is better controlled and understood. In the end, such unconventional devices may be a more appropriate choice for building a high-T_c circuit technology.

Acknowledgment

We appreciate useful discussions with J.B. Barrier, R.A. Buhrman, Al. Braginski, R.H. Cantor, M.S. Colclough, M.S. Dilorio, Z.W. Dong, G.J. Gerritsrna, B.D. Hunt, L.L.H. King, J.T. Kucera, M.Yu. Kupriyanov, D.K. Lathrop, L. F'. Lee, J.A. Luine, M.J. Neal, R.H. One, T.P. Orlando, R.W. Simon and J.Z. Sun. We especially thank M.J. Burns for conversations about the broad issues involved with high-T_c devices and for his careful reading of the original manuscript.

REFERENCES

1. R.P. Feynman, R.B. Leighton, and M. Sands, **The Feynman Lectures on Physics,** Addison-Wesley, New York, 1965, Vol. 3, Chapter 21.

2. T. Van Duzer and C.W. Turner, **Principles of Superconductive Devices and Circuits,** Elsevier, New York, 1981.

3. A. Barone and G, Paterno, **Physics and Applications of the Josephson Effect,** Wiley, New York, 1982.

4. K.K. Likharev, **Dynamics of Josephson Junctions and Circuits,** Gordon and Breach, New York, 1986.

5. T.P. Orlando and K.A. Delin, **Foundations of Applied Superconductivity,** Addison-Wesley, New York, 1991.

6. K.K. Likharev, Rev. Mod. Phys. 51, 101 (1979).

7. M.B. Ketchen, IEEE Trans. Magnetics 27, 2916 (1991).

8. K.K. Likharev and V.K. Semenov, IEEE Trans. Appl. Supercond. 1, 1 (1991).

9. A.W. Kleinsasser, A.C. Callegari, B.D. Hunt, C. Rogers, R. Tiberio, and R.A. Buhrman, IEEE Trans. Magnetics 17,307 (1981).

10, M. Gurvitch, M.A. Washington, and H.A. Huggins, Appl. Phys. Lett. 42,472 (1983).

11. See, for example, IBM J. Res. and Develop. 24, 105-264 (1980).

12. Al. Braginski in **Superconducting Devices and Their Applications,** H. Koch and H. Lübbig, eds., Springer-Verlag, Berlin, 1992, p. 3.

13. Y. Enomoto, M. Suzuki, T. Murakami, T. Inukai, and T. Inamura, Jpn. J. Appl. Phys. 20, L661 (1981).

14. D.J. Scalapino, Phys. Reports 250,329 (1995).

15. K.A. Delin and A.W. Kleinsasser, IEEE Trans. Appl. Supercond. 5,2976 (1 995).

16. R.B. van Dover, A. De Lozanne, and M.R. Beasley, J. Appl. Phys. 52, 7327 (1981).

17. A.W. Kleinsasser and W.J. Gallagher, in **Superconducting Devices,** D. Rudman and S. Ruggiero, eds., Academic Press, Boston, 1990, p. 325.

18. M.Yu. Kupriyanov and K.K. Likharev, Sov. Phys. Usp. 33, 340 (1990) [Usp. Fiz. Nauk. 160,49 (1990)].

19. M. Tinkham, **Introduction to Superconductivity,** McGraw-Hill, New York, 1975.

20. A.W. Kleinsasser and K.A. Delin, Appl. Phys. Lett. 66, 102(1995).

21 T.P. Orlando and K.A. Delin, *op. cit.*, p. 432.

22. V. Ambegaokar and B.I. Halperin, Phys. Rev. Lett. 22, 1364(1969).

23. V. Ambegaokar and A. Baratoff, Phys. Rev. Lett. **10,486** (1963); erratum, **11**, 104 (1963),

24. M. Tinkham, *op cit.*, p. 34.

25. I.O. Kulik and A.N. Omel'yanchuk, JETP Lett. 21, 96 (1975).

26. I.O. Kulik and A.N. Omel'yanchuk, Sov. J. Low Temp. Phys. 4, 142 (1978).

27. T.P. Orlando and K.A. Delin, *op. cit.*, pp. 528 ff.

28. G. Deutscher and P.G. de Gennes in **Superconductivity,** R.D. Parks, cd., Marcel Dekker, New York, 1969, Vol. 2, p. 1005.

29. J.H. Xu, J.L. Shen, J.H. Miller, and C.S. Ting, Phys. Rev, Lett. 73,2492 (1994).

30. M.S. Colclough, C.E. Gough, M. Keene, C.M. Muirhead, N. Thomas, J.S. AbeII, and S. Sutton, Nature 328,47 (1987).

31. P. Chaudhari, D. Dimes, and J. Mannhart, IBM J. Res. and Develop., 33299 (1989).

32, S.E. Russek, D.K. Lathrop, B.H. Moeckly, R.A. Buhrman, D.H. Shin, and J. Silcox, Appl. Phys. Lett. 57, 1155 (1990).

33. I3. Dimes, P. Chaudhari, J. Mannhart, and F.K. LeGoues, Phys. Rev. Lett. 61, 219 (1988).

34. S.M. Garrison, N. Newman, B.F. Cole, K. Char, and R.W. Barton, Appl. Phys. Lett. 58, 2168 (1991).

35 K. Char, M.S. Colclough, L.P. Lee, and G. Zaharchuk, Appl. Phys. Lett. 59, 2177 (1991).

36. Yu. Boikov, Z.G. Ivanov, G. Brorsson, T. Claeson, Supercond. Sci. Technol. 7, 281, (1994).

37. R.W. Simon, J.B. Bulman, J.F. Burch, S.B. Coons, K.P. Daly, W.D. Dozier, R. Hu, A.E. Lee, J.A. Luine, C.E. Platt, and M.J. Zani, IEEE Trans. Magn. 27, 3209 (1991).

38. K. Herrmann, Y. Zhang, H.-M. Muck, W. Zander, and Al. Braginski, Supercond. Sci. Technol. 4,583 (1991).

39. O.K. Lathrop, PhD Thesis, Cornell Univ., 1991 (unpublished).

40. R. Gross in **Interfaces in High-T_c Superconducting Systems, S.** Shinde and D. Rudman, eds., Springer, 1993, p. 176.

41. B.H. Moeckly, PhD Thesis, Cornell Univ., 1994 (unpublished).

42. V.Z. Kresin and S.A. Wolf, J. Supercond. **1,** 143 (1988).

43. See, for example, M. Gurvitch and J. Kwo, in **Advances in Cryogenic Engineering,** A.F. Clark and R.P. Reed, eds., Plenum, N. Y., 1984, Vol 30, p. 509.

44. R.P. Robertazzi, R.H. Koch, R.B. Laibowitz, and W.J. Gallagher, Appl. Phys. Lett. 61,711 (1992).

45. R.B. Laibowitz, J.Z. Sun, V. Foglietti, W.J. Gallagher, and R.H. Koch, Appl. Phys. Lett. 64,247 (1994).

46. D. Grundler, J.-P. Krumme, B. David, and O. Dössel, Appl. Phys. Lett. 65, 1841 (1 994).

47. R. Kleiner, F. Steinmeyer, G. Kunkel, and P. Müller, Phys. Rev. Lett. 68, 2394 (1992).

48. R. Kleiner and P. Müller, Phys. Rev. B 49, 1327 (1994).

49. G. Oya, N. Aoyama, A. Irie, S. Kishida, and H. Tokutaka, Jpn. J. Appl. Phys. 31, 829 (1 992).

50. D.B. Schwartz, P.M. Mankiewich, R.E. Howard, L.D. Jackel, B.L. Straughn, E.G. Burkhart, and A.H. Dayem, IEEE Trans. Magnetics 25, 1298 (1989).

51. M.G. Forrester, J. Talvacchio, J.R. Gavaler, M. Rooks, and J. Lindqvist, IEEE Trans. Magnetics 27, 3098(1991).

52. R.P. Robertazzi, A.W. Kleinsasser, R.B. Laibowitz, R.H. Koch, and K.G. Stawiasz, Phys. Rev. B **46, 8456 (1992).**

53. **Y.** Tarutani, **T. Fukazawa,** U. **Kabasawa, A. Tsukamoto,** M. Hiratani, and K. Takagi, Appl. Phys. Lett. 58,2707 (1991).

54. K. Mizuno, K. Higashino, K. Setsune, and K. Wasa, Appl. Phys. Lett. 56, 1469 (1990).

55. M. Kasai, T. Ohno, Y. Kanke, Y. Kozono, M. Hanazono, and Y. Sugita, Jpn. J. Appl. Phys. 29, L2219 (1990).

56. R. Yuasa, M. Nemoto, S. Fujiwara, H. Furukawa, H. Mukaida, S. Tokunaga, and M. Nakao, Physics C 185-189, 2587 (1991).

57. I.A. Devayatov and M.Yu. Kupriyanov, JETP Lett. 59, 202 (1994) [Pis'ma. Zh. Eksp. Teor. Fiz. 59, 187 (1994)].

58. R.B. Laibowitz, R.H. Koch, G. Koren, A. Gupta, W.J. Gallagher, V. Foglietti, B. Oh, and J.M. Viggiano, Appl. Phys. Lett. 56, 686 (1990).

59. B.D. Hunt, M.C. Foote, and L.J. Bajuk, Appl. Phys. Lett. 59, 982 (1991).

60. A.W. Kleinsasser and R.A. Buhrman, Appl. Phys. Lett. 37, 841 (1980).

61. D.F. Moore, H.P. Dietrich, A.W. Kleinsasser, and J.M. E. Harper, J. Vat. Sci.

Technol. A3, 1844 (1985).

62. C.T. Rogers, A. Inam, M.S. Hegde, B. Dutta, and X.C. Wu, Appl. Phys. Lett. 55, 2032 (1 989).

63. Yu.M. Boguslavskij, J. Gao, A. J.H.M. Rijnders, D. Terpstra, G.J. Gerritsma, and H. Rogalla, Physics C 194, 268 (1992).

64. J.B. Barrier, B.D. Hunt, M.C. Foote, W.T. Pike, and R.P. Vasquez, Physics C 207, 381 (1993).

65. D.K. Chin and T. Van Duzer, Appt. Phys. Lett. 58,753 (1991).

66. K. Char, M.S. Colclough, T.H. Geballe, and K.E. Myers, Appl. Phys. Lett. 62, 196 (1993).

67. L. Antognazza, K. Char, T.H. Geballe, L.L.H. King, and A.W. Sleight, Appl. Phys. Lett. 63, 1005 (1993).

68. A.I. Braginski and E. Sodtke (unpublished work).

69. K. Char, L. Antognazza, and T.H. Geballe (unpublished work).

70. Ml. Faley, U. Poppe, H. Soltner, C.L. Jia, M. Siegel, and K. Urban, Appl. Phys. Lett. 63,2138 (1993).

71. J.B. Barrier (unpublished work).

72, T. Hashimoto, M. Sagoi, Y. Mizutani, J. Yoshida, and K. Mizushima, Appl. Phys. Lett. 60, 1756 (1 992).

73. E. Polturak, G. Koren, D. Cohen, E. Aharoni, and G. Deutesher, Phys. Rev. Lett. 67,3038 (1991).

74. K. Char, L. Antognazza, and T.H. Geballe, Appl. Phys. Lett. 65, 904 (1994).

75. L. Antognazza, K. Char, and T.H. Geballe (unpublished work).

76. M.S. Dilorio, S. Yoshizumi, K-Y. Yang, J. Zhang, and M. Maung, Appl. Phys. Lett. 58, 2552 (1991).

77, M.S. Dilorio, S. Yoshizumi, M. Maung, K-Y. Yang, J. Zhang, and N. Cl. Fan, Nature 354, 513 (1991).

78. R.H. One, J.A. Bean, M.W. Cromar, T.E. Harvey, M.E. Johansson, C. Reintsema, and D.A. Rudman, Appl. Phys. Lett. 59, 1126 (1991).

79. S.J. Berkowitz, PhD Thesis, Boston Univ., 1994 (unpublished).

80. P.A. Rosenthal, E.N. Grossman, R.H. One, and R.L. Vale, Appl. Phys. Lett. 63, 1984 (1 993).

81. Z.W. Dong, P. Hadley, R. Bessling, and J.E. Mooij, Proc. Workshop on HTS Josephson Junctions and 3-Terminal Devices, Enschede, The Netherlands, May 2, 1994.

82. S.-G. Lee, K. Park, Y.K. Park, and J.-C Park. Appl. Phys. Lett. 64, 2028 (1994).

83. B. Ghyselen, R. Cabanel, S. Tyc, D.G. Crete, Z.H. Barber, J.E. Evetts, G. Ben Assayag, J. Gierak, and A. Schuhl, Physics C 198, 215 (1992).

84. G. Koren, E. Polturak, D. Cohen, E. Aharoni, and L. Patlagan, Physics C 221, 157 (1994).

85. K. Mizuno, H. Higashino, K. Setsune, and K. Wasa, Proc. ISS '90, Sendai, Japan, 1990.

86. J.Z. Sun (unpublished work).

87. V.F. Lukichev, A.A. Orlikovsky, and M.Yu. Kupriyanov, in SQUID '85: **Superconducting Quantum Interference Devices and their Applications,** H.D. Halbohm and H. Lübbig, eds., W. de Gruyter, Berlin, 1985, p. 55.

88. P.G. de Gennes, Rev. Mod. Phys. 36,225 (1964).

89. L.P. Gor'kov, Sov. Phys. JETP **10,** 998 (1960).

90. N.R. Werthamer, Phys. Rev., 132, 2440 (1963).

91. J.J. Hauser, H.C. Theuerer, and N.R. Werthamer, Phys. Rev. 136A, 637 (1964).

92. M.Yu.Kupriyanov and V.F. Lukichev, Sov. J. Low Temp. Phys. 8, 526 (1982) [Fiz. Nizk. Temp. 8, 1045 (1982)].

93. T.P. Orlando and K.A. Delin, *op. cit.*, p. 503,

94. M. Tinkham, *op cit.*, p. 111.

95. Z.G. Ivanov, M.Yu. Kupriyanov, K.K. Likharev, S.V. Meriakri, and O.V. Snigirev, Sov. J. Low Temp. Phys. 7,274 (1981) [Fiz. Nizk. Temp. 7,560 (1981)].

96. M.Yu. Kupriyanov and V.F. Lukichev, Sov. Phys. JETP 67, 1163 (1988) [Zh. Eksp. Teor. Fiz. 94, 139 (1988)].

97. V.Z. Kresin and S.A. Wolf, J. Supercond. 1, 143 (1988).

98. G. Deutesher and K.A. Müller, Phys. Rev. Lett. 59, 1745(1987).

99. P.G. de Gennes, **Superconductivity of Metals and Alloys,** W.A. Benjamin, New York, 1966, p. 231.

100. G. Deutesher and R.W. Simon, J. Appt. Phys 69,4137 (1991).

101. A.N. Lykov, Sov. Phys. Usp., 35,811 (1992).

102. D.K Lathrop, PhD Thesis, Cornell Univ., 1991 (unpublished)

103. K.D Usadel, Phys. Rev. Lett. 25, 507(1970).

104. K.K Likharev, Sov. Tech. Phys. Lett. 2, 12 (1976).

105. M.Yu. Kupriyanov, K.K. Likharev, and V.F. Lukichev, Sov. Phys. JETP 56, 235 (1982) [Zh. Eksp. Teor. Fiz. 83,431 (1982)].

106, A.A. Zubkov and M.Yu. Kupriyanov, Sov. J. Low, Temp. Phys. 9, 279 (1983) [Fiz. Nizk. Temp. 9, 548 (1983)].

107. A.W. Kleinsasser, IEEE Trans. Magnetics 27, 2589 (1991).

108. A. Barone and G. Paterno, *op cit*, pp. 25 ff.

109. R. Stratton, J. Phys. Chem. Solids 23, 1 77 (1 962).

110. J.G. Simmons, J. Appl. Phys. 34, 1793 1963).

111. R.E. Miller, W.H. Mallison, A.W. Kleinsa sser, K.A. Delin, and E.M. Macedo, Appl. Phys. Lett. 63, 1423 (1993).

112. A.W. Kleinsasser, R.E. Miller, W.H. Mallison, and G.B. Arnold, Phys. Rev. Lett. 72, 1738 (1 994).

113. W.M. van Huffelen, T.M. Klapwijk, D.R. Heslinga, M.J. de Boer, and N. van der Post, Phys. Rev. B 47, 5170 (1993).

114. K. Char, Bull. Mat. Res. Sot. 19,51 (1994).

115. T.Y. Hsiang and D.K. Finnemore, Phys. Rev. B, 22, 154(1980).

116. M.Yu. Kupriyanov, Sov. J. Low Temp. Phys. 7, 342 (1981) [Fiz. Nizk. Temp. 7, 700 (1981)].

117. V. Kogan, Phys. Rev. B 26, 88 (1982).

118. V. Kogan and A. Yu. Simonov, Phys. Rev. Lett. 68, 2106 (1992).

119. W. Silvert, J. Low Temp. Phys. 20,439 (1975).

120. L. Antognazza, S.J. Berkowitz, T.H. Geballe, and K. Char, Phys. Rev. B 51, 8560 (1995).

121. Y. Krähenbühl and R.J. Watts-Tobin, J. Low Temp. Phys. 35,569 (1979).

122. Yu. V. Sharvin, Sov. Phys. JETP 21, 655 (1965).

123. G. Wexler, Proc. Roy. Sot. 89, 927 (1966).

124. J. Clarke, Proc. Roy. Soc. A 308,447 (1969).

125. J.M. Warlaumont, J.C. Brown, and R.A. Buhrman, Appl. Phys. Lett. 34, 415 (1 979).

126. J.M. Warlaumont PhD Thesis, Cornell Univ., 1980 (unpublished).

127. J.E. Sauvageau, R.H. One, A.K. Jain, K. Li, and J.E. Lukens, IEEE Trans. Magnetics 21,854 (1985).

128. T. Nishino, E. Yamada, and U. Kawabe, Phys. Rev. B33, 2042 (1986).

129. M. Hatano, T. Nishino, F. Murai, and U. Kawabe, Appl. Phys. Lett. 53,409 (1988).

130. H. Takayanagi and T. Kawakami, Phys. Rev. Lett. 54,2449 (1985).

131. T. Kawakami and H. Takayanagi, Appl. Phys. Lett. 46,92 (1985).

132. D.R. Heslinga, PhD Thesis, Univ. of Groningen, 1991 (unpublished).

133. Y. Harada, N. Hirose, Y. Uzawa, M. Sekine, S. Yoshimori, and M. Kawamura, Physics C 185-189, 2555 (1991).

134. M.A.M. Gijs, D. Scholten, Th. van Rooy, and R. Ijsselsteijn, Sol. St. Commun. 71, 575 (1 989).

135. M.A.M. Gijs, M. Okada, R.M. Wolf, and Th. van Rooy, Sol. St. Commun. **81, 609 (1992).**

136. J. Yoshida, T. Hashimoto, S. Inoue, Y. Mizutani, M. Sagoi, and K. Mizushima, Jpn. J. Appl. Phys. 31, 1771 (1992).

137. E.J. Tarte, H.W. Lean, and J.R. Waldram, Physics B 194-196, 1763 (1994).

138. H.W. Lean, E.J. Tarte, J.R. Waldram, Z.H. Barber, and R.E. Somekh, Physics C 224,207 (1 994).

139 B. Mayer, S. Schuster, A. Beck, L. Alff, and R. Gross, Appl. Phys. Lett. 62, 783 (1993).

140. T.P. Orlando and K.A. Delin, *op. cit.*, p. 420 ff.

141. A. Barone and G. Paterno, *op. cit.*, pp. 74 ff.

142. A.A. Golubov and M.Yu. Kupriyanov, Sov. J. Low Temp. Phys. 12, 212 (1986).

143. A. Marx, K.-D. Husemann, B. Mayer, R. Gross, M.A.J. Verhoeven, and G.J. Gerritsma, Appl. Phys. Lett. 64, 241 (1994).

144. N.W. Ashcroft and N.D. Mermin, Solid State Physics, Holt, Rinehart, and Winston, Philadelphia, 1976, p. 1ff.

145. P.A. Cox, R.G. Egdell, J.B. Goodenough, A. Hammnett, and C.C. Naish, J. Phys. C, 16, 6221 (1983).

146. J.M. Longo, P.M. Raccah, and J.B. Goodenough, J. Appl. Phys. 39, 1327, (1 968).

147. A.T. Fiery, A.F. Hebard, R.H. Eick, P.M. Mankiewich, R.E. Howard, and M.L. O'Malley, Phys. Rev. Lett. 65,3441 (1990).

148. W.E. Pickett, Rev. Mod. Phys. **61,433 (1989)**

149. J.T. Kucera and J.C. Bravman, Phys. Rev, B 51, 8582 (1995).

150. C.D. Reintsema, R.H. One, G. Barnes, L. Borcherdt, T.E. Harvey, G. Kunkel, D.A. Rudman, L.R. Vale, N. Missert, and P.A. Rosenthal, IEEE Trans. Appl. Supercond. 5, 3405 (1 995).

151. M.S. Dilorio, S. Yoshizumi, K-Y. Yang, J. Zhang, and M. Maung (unpublished work).

152. N. Missert, L.R. Vale, R.H. One, C.D. Reintsema, D.A. Rudman, R.E. Thomson, and S.J. Berkowitz, IEEE Trans. Appl. Supercond. 5, 2969 (1995).

153. Al. Buzdin and M. Yu. Kupriyanov, JETP Lett. 53,321 (1991) [Pis'ma Zh. Eksp. Teor. Fiz. 53,308 (1991)].

154< S. Kuplevakhskii and 1.1. Fal'ko, Teor. Mat. Fiz. 86, 272 (1991).

155. S. Kuplevakhskii and I.I. Fal'ko, Teor. Mat, Fiz. 84, 146 (1989).

156, E. Olsson and K. Char, Appl. Phys. Lett. 64, 1292 (1994).

157. L.P. Lee (unpublished work).

158, J.A. Agostinelli, J.W. Chwalek, C.J. Baron, G. Lubberts, and C.D. Dowell, Physics C 207, 203 (1 993).

159. B. Ghyselen, M.A. Bari, E.J. Tarte, M.G. Blamire, R.E. Somekh, Y. Yan, and J.E. Evetts, Physics C 230, 327 (1994),

160. J.B. Barrier, C.T. Rogers, A. Inam, R. Ramesh, and S. Bersey, Appl. Phys. Lett. 59,742 (1991).

161. T. Umezawa, D.J. Lwew, S.K. Streiffer, and M.R. Beasley, Appl. Phys. Lett. 63, 3221 (1 993).

162. H. Sate, H. Akoh, and S. Takada Appl. Phys. Lett. 64, 1286(1994).

163. H. Akoh, H. Sate, and S. Takada, IEEE Trans. Appl. Supercond. 5, 2373 (1995)

164. U. Kabasawa, Y. Tarutani, A. Tsukamoto, T. Fukazawa, M. Hiratani, and K. Takagi, Physics C **194**, 261 (1992).

165, G. Koren, E. Polturak, G.M. Reisner, B, Fisher, and L. Patlagan, Physics C 225, 21 (1994).

166. J. Gao, W.A.M. Aarnink, G.J. Gerritsma, and H. Rogalla, Physics C 171, 126 (1990).

167. J. Gao, Yu.M. Boguslavskij, B.B.G. Klopman, D. Terpstra, G.J. Gerritsma, and H. Rogalla, Appl. Phys. Lett. 59, 2754(1991).

168. J. Gao, Yu.M. Boguslavskij, B.B.G. Klopman, D. Terpstra, R. Wijbrans, G.J. Gerritsma, and H. Rogalla, J. Appl. Phys. 72,575 (1992).

169. C. Stölzel, M. Siegel, G. Adrian, C. Krimmer, J. Söllner, W. Wilkens, G. Shultz, and H. Adrian, Appl. Phys. Lett. 63, 2970 (1993).

170. M.A.J. Verhoeven, G.J. Gerritsma, H. Rogalla, anti A.A. Golubov, IEEE Trans. Appl. Supercond. 5, 2095 (1995).

171. L.I. Glazman and K.A. Mateev, Sov. Phys. JETP 67, 1276 (1 988) [Zh. Eksp. Teor. Fiz. 94, 322 (1988)].

172. T. Satoh, M.Yu. Kupriyanov, J.S. Tsai, M. Hidaka, and H. Tsuge, IEEE Trans. Appl. Supercond. 5, 2612 (1995).

173. H.B. Radousky, J. Mater. Res. 7, 1917 (1992).

174. K. Char, L. Antognazza, and T.H. Geballe, Appl. Phys. Lett. 63, 2420 (1993).

175. A.W. Kleinsasser, Appl. Phys. Lett. 66,394 (1995).

76. B.D. Hunt, J.B. Barner, M.C. Foote, and R.P. Vasquez (unpublished work).

77. L. Antognazza, S.J. Berkowitz, T.H. Geballe, and K. Char, Phys. Rev. B 51, 8560 (1995).

178. L. Antognazza, B.H. Moeckly, T.H. Geballe, and K, Char (to be published in Phys. Rev. B, August 1995).

Table 1

Effect of Boundary Conditions on Proximity-Coupled Device Properties

	soft (*SNS*)	Rigid (*SNS*)	B a r r i e r (*SINIS*)
Boundary Parameter	$\gamma >> 1$	$\gamma << 1$	$\gamma_b >> 1$ (in practice)
Order Parameter	$\Delta_i < \Delta_\infty$	$\Delta_i = \Delta_\infty$	$\Delta_i = \Delta_\infty$
$I_c \propto (T_c - T)^a$ (near T_c)	$\alpha = 2$	$\alpha = 1$	0!=1
J_{co} (near T_c)	$\frac{2(T_c /T- 1)\ \pi\Delta_\infty^2}{\pi^2\gamma^2\ \ 2ekT_c\rho_n\xi_{nd}(T_c)}$	$\frac{\pi\Delta_\infty^2}{2ekT_c\rho_n\xi_{nd}(T_c)}$.	$\frac{1}{\gamma_b^2}\ \frac{\pi\Delta_\infty^2}{2ekT_c\rho_n\xi_{nd}(T_c)}$
J_c	low	optimal	low (tunneling required)"
R_n	$\rho_n L / \mathcal{A}$	$\rho_n L / \mathcal{A}$	$(\rho_n L + 2r_c) / \mathcal{A}$
$I_c R_n$	low	optimal	low

Table 2

Representative Interlayer Parameters

Material	in (m_e)	n (m^{-3})	v_n (rn I s)	T_c (K)	T (K)	ρ_n $(\Omega - \mu m)$	ℓ_n (rim)	ξ_{nc} (rim)	ξ_{nd} (rim)	ξ_n (rim)
Noble Metals										
Cu	1	8.42 X 10^{28}	1.57 X106	o	77	0.0066 *	100 *	25	29	19
					4,2	0.0066 *	100*	450	120	120
Au	1	5.97 x 10^{28}	1.40 X106	0	77	0.0083 *	100"	22	27	17
					4.2	0.0083 *	100 *	400	120	**110**
Ag	1	5.85 X 10^{28}	1.39X10^{6}	o	77	0.0084 *	100 *	22	27	17
					4.2	0.0084 *	100*	400	120	110
Ruthenates (cubic **oxides)**										
$CaRuO_3$	4.0	1.76 X 10^{28}	2.33 X 10^{5}	0	77	3.3	0.62	3.7	0.88	0.85
					4.2	2.1	0.98	67	4.7	4.7
$SrRuO_3$	3.6	1.72 x 10^{28}	2.57x10^{5}	o	77	1.3	1.5	4.1	1.4	1.3
					4.2	0.56	3.4	74	9.2	9.1
Cuprates (anisotropic oxides)										
$YBa_2Cu_3O_{7-\delta}$	5.0	5.0 X1027	1.40 X105	90	77	0.77	6.4	---	---	---
$YBa_2Cu_{2.79}Co_{0.21}O_{7-\delta}$	5.0	3.7 X1027	1.21X10^{5}	50	77	3.3	1.7	1.9	1.3	2.3
$Y_{0.7}Ca_{0.3}Ba_2Cu_3O_{7-\delta}$	5.0	5.0 x 10^{27}	1.40 X105	50	77	0.67	7.4	2.2	2.9	3.4

*** Determined under the assumption that ℓ_n is** given by the film thickness of **1** 00 **nm.**

FIGURE CAPTIONS

Figure 1. Theoretical temperature dependencesof I_c normalized to $I_c(0)$ (its value at $T = O)$ for (a) tunnel junction [23], (b) dirty point contact [25], and (c) clean point contact [26], with $2\Delta(0)/kT_c$ = 3.53, For the three cases, $eR_nI_c(0)/\Delta(0) = \pi/2, 0.66\pi$, and π, respectively. The straight line (d) is $I_c / I_c(0)$ = 1 --T/~

Figure 2, Theoretical $I_c / I_c(0)$ versus $T/\sim$. (a) Tunnel junction with $2\Delta(0)/kT_c$ = 1.0. (b) Tunnel junction with $2\Delta(0)/kT_c$ = 1.2. (c) Dirty point contact with $2\Delta(0)/kT_c$ = 1.5. (d) Clean point contact with $2\Delta(0)/kT_c$ = 2.6. Curves (a) - (c) are offset in the vertical direction for clarity,

Figure 3. Schematic diagrams of typical device geometries. S1 and S2 are the superconducting electrodes. (a) Grain boundary junction. (b) Step-edge grain boundary junction. Two grain boundaries form in series in a film grown over a step etched into a substrate. Ideally, one junction has a much smaller critical current than the other and dominates the electrical behavior. (c) Tunnel junction (sandwich geometry),

Figure 4. I_c, normalized to its extrapolated zero-temperature value $I_c(0)$, versus reduced temperature T/T_c for three representative grain boundary junctions. (a) Natural grain boundary in $YBa_2Cu_3O_{7-\delta}$ film [39]. (b) $YBa_2Cu_3O_{7-\delta}$ bicrystal [31]. (c) $YBa_2Cu_3O_{7-\delta}$ bicrystal [40]. The solid curves are I_c /1=(0)= $1 - T/T_c$. The dotted curves are provided as guides to the eye. Curves (a) and (b) are offset in the vertical direction for clarity,

Figure 5. $I_c / I_c(0)$ versus $T/\sim$ for two bi-epitaxial $YBa_2Cu_3O_{7-\delta}$ grain boundary junctions [35]. The solid curves are $I_c / I_c(0)$ = 1- T/T_c. The dotted curves are provided as guides to the eye. Curve (a) is offset in the vertical direction for clarity.

Figure 6. $I_c / I_c(0)$ versus T/ T_c for two representative $YBa_2Cu_3O_{7-\delta}$ step junctions. (a) [37] (b) [38]. The solid lines are $I_c / I_c(0)$ = 1- T/ T_c. Curve (a) is offset in the vertical direction for clarity.

Figure 7. 1,/1,(0) versus $T/\sim$ for three representative $YBa_2Cu_3O_{7-\delta}$-$SrTiO_3$-$YBa_2Cu_3O_{7-\delta}$ edge junctions [45]. (a) Unannealed junction; $J_c(0) = 76\ \mu A/\mu m^2$. (b) oxygen plasma-treated junction; $J_c(0)$ = 400 $\mu A/\mu m^2$. (c) annealed junction; J,(O)= 600 $\mu A/\mu m^2$. The solid lines are $I_c / I_c(0) = 1 - T/T_c$. The dotted curves are provided as guides to the eye. Curves (a) and (b) are offset in the vertical direction for clarity.

Figure 8. $I_c / I_c(0)$ versus $T/\sim$ for c-axis transport in (a) $(Pb,Bi)_2Sr_2CaCu_2O_8$ [49] and (b) $Tl_2Ba_2Ca_2Cu_3O_{10}$ [48] single crystals. The curves are the Ambegaokar-Baratoff dependence, assuming the standard BCS energy gap, $2A(0) = 3.53kT_c$ Curve (a) is offset in the vertical direction for clarity.

Figure 9. Schematic diagrams of typical *SNS* device geometries. S1 and S2 are the two superconducting electrodes. (a) Co-planar bridge. (b) Sandwich junction. (c) Edge (or ramp) junction. (d) Step-edge microbridge, in which S1 and S2 are formed from a single superconducting film deposited at an angle to a step in the substrate so as to result in a break. The supercurrent is dominated by the contacts to the a-b planes of S1 and S2, which lie parallel to the substrate plane.

Figure 10. $I_c / I_c(0)$ versus T/T_c for a two co-planar bridges. (a) $YBa_2Cu_3O_{7-\delta}$-Au-$YBa_2Cu_3O_{7-\delta}$ [51]. (b) $HoBa_2Cu_3O_{7-x}$-$La_{1.5}Ba_{1.5}Cu_3O_{7-y}$-$HoBa_2Cu_3O_{7-x}$ [53]. The solid lines are $I_c / I_c(0) = 1 - T/T_c$. The dotted curves are provided as guides to the eye. Curve (a) is offset in the vertical direction for clarity.

Figure 11. $I_c / I_c(0)$ versus T/T_c for several *SNS* edge junctions with oxide (doped $SrTiO_3$ and cuprate) interlayers. (a) Nb-doped $SrTiO_3$, $L=2.5$ *nm [65]*. (b) $PrBa_2Cu_3O_{7-\delta}$, $L=20$ *nm* [63]. *(c)* $PrBa_2Cu_3O_{7-\delta}$, $L=8$ *nm [63]*. (d) Non-superconducting $YBa_2Cu_3O_{7-\delta}$, $L=5$ *nm [59]*. The solid lines are $I_c / I_c(0) = 1 - T/T_c$. The dotted curves are provided as guides to the eye. Curves (a) - (c) are offset in the vertical direction for clarity.

Figure 12, $I_c / I_c(0)$ versus T/T_c for several SNS edge junctions with cubic oxide interlayers. (a) $CaRuO_3$, $L=10$ *nm* [69]. (b) $SrRuO_3$, $L=20$ *nm [67], (c)* and (d) $SrRuO_3$, $L=30$ *nm [68]*. The solid lines are $I_c / I_c(0) = 1 - T/T_c$. The dotted curves are provided as guides to the eye. Curves (a) - (c) are offset in the vertical direction for clarity.

Figure 13. $I_c / I_c(0)$ versus T/T_c for $PrBa_2Cu_3O_{7-\delta}$ *SNS edge* junctions [71] with (a) $L=10$ and (b) L=20 *nm*. The solid curves are provided as guides to the eye. Curve (a) is offset in the vertical direction for clarity.

Figure 14. $I_c / I_c(0)$ versus $T/\sim$ for three edge microbridges in which the interlayer is deposited onto a discontinuous film which comprises both base and counterelectrodes. (a) *Ag* [78]. (b) *Ag / Au* alloy [78]. (c) *Au* [51], The solid lines are $I_c / I_c(0) = 1 - T/T_c$. The dotted curves are provided as guides to the eye. Curves (a) and (b) are offset in the vertical direction for clarity.

Figure 15. $I_c / I_c(0)$ versus $T/\sim$. for three Au edge microbridges. (a) High I_cR_n sample [79]. (b) Low I_cR_n sample with parasitic shunt conductance [80]. (c) Same sample after etching to remove shunt path [80]. The solid lines are $I_c / I_c(0) = 1 - T/T_c$. The dotted curves are provided as guides to the eye. Curves (a) and (b) are offset in the vertical direction for clarity.

Figure 16. $I_c / I_c(0)$ versus T/T_c for three Au edge microbridges [81]: (a) Low I_cR_n sample with parasitic shunt conductance, (b) and (c) high I_cR_n samples. The solid lines are $I_c / I_c(0) = 1 - T/T_c$. The dotted curves are provided as guides to the eye. Curves (a) and (b) are offset in the vertical direction for clarity.

Figure 17. $I_c / I_c(0)$ versus T/T_c for a $CaRuO_3$ edge microbridge [82]. The solid line is $I_c / I_c(0) = 1 - T/T_c$. The dotted curve is provided to guide to the eye.

Figure 18. $I_c / I_c(0)$ versus T/T_c for several junctions whose behavior can be termed "quasi-exponential." (a) Ag step edge microbridge [79]. (b) Co-planar Au bridge [83]. (c) $YBa_2CoCu_2O_7$ edge junction [84]. (d) $Bi_2Sr_2CaCu_2O_8$ - $Bi_2Sr_2CuO_y$ - $Bi_2Sr_2CaCu_2O_8$ sandwich junction [85]. (e) $Hg_2Ba_2Ca_2Cu_3O_{10}$ grain boundary junction [86]. The solid curves are $I_c / I_c(0) = (1 - T/T_c)^{2.5}$. Curves (a) - (d) are offset in the vertical direction for clarity.

Figure 19. Dependence of $\delta_i = A, / \Delta_\infty$ on the interface parameter $\gamma = (\mathcal{N}_n\rho_s / \mathcal{N}_s\rho_n)^{1/2}$ for (a) $T = 0.9\,T_c$, (b) $T = 0.5\,T_c$, and (c) $T = 0.1\,T_c$. The dashed curves represent the approximations $\delta_i = (1 - \sqrt{2}\xi_{sd} / b_i)^{1/2}$ (for $\gamma << 1$) and $\delta_i = b_i / \sqrt{2}\xi_{sd}$ (for $\gamma >> 1$), respectively.

Figure 20. Dependence of α, in the relationship $I_c \propto (T_c - T)^\alpha$ on the interface parameter $\gamma = (\mathcal{N}_n\rho_s / \mathcal{N}_s\rho_n)^{1/2}$, obtained from the behavior of δ_i^2 in Eqn. (13), in the region $0.001 < 1 - T/T_c < 0.01$. For rigid boundary conditions, α =1, for soft, a =2.

Figure 21. Dependence of normalized I_cR_n on reduced temperature for $L / \xi_{nd}(T_c)$ =0, 2, 3, 4, 5, 6, 8, 10, and 12 (solid curves) for Likharev's theory of SNS junctions in the dirty limit under rigid boundary conditions [104]. The dashed curves are de Gennes(s predictions, Eqn. (8) [88].

Figure 22. Dependence of normalized I_c on reduced temperature for $L / \xi_{nd}(T_c)$ =0, 1, 2, 3, 4, 5, 6, 8, 10, and 12 (top to bottom) for Likharev's theory of SNS junctions in the dirty limit under rigid boundary conditions [1 04]. The dashed line is the linear dependence $I_c / I_c(0) = 1 - T/T_c$.

Figure 23. Dependence on reduced temperature of the decay length L_o in the expression $J_c = J_{co}\exp(-L/\mathrm{LO})$, normalized to $\xi_{nd}(T_c)$. (a) Likharev's theory [1 04], for $5 \le L/\xi_{nd}(T_c) \le 12$. (b) de Gennes's theory: $Lo = \xi_{nd}(T_c)$.

Figure 24. Dependence on reduced temperature of the prefactor J_{co} in $J_c = J_{co}\exp(-L/L(,)$ normalized to its value at $T = O$, $J_{co}(0) = 0.70\Delta_\infty(0)/(e\rho_n\xi_{nd}(T_c))$. (a) Likharev's theory [1 04], for5SL/~~~(~)<12, (b) de Gennes's theory.

Figure 25. Dependence of $4\pi kTC/\Delta_\infty$ on the interface parameter $\gamma_b = r_c/\rho_n\xi_{nd}(T_c)$ in the limit $T \to T_c$ [96]. The approximations $1-\gamma_b$ and $1/\gamma_b$, appropriate for $\gamma_b << 1$ and $\gamma_b >> 1$ respectively, are also shown.

Figure 26. Dependence of ξ_n on ℓ_n, with both quantities normalized by ξ_{nc}, for 3d metals with $T_{cn} = 0$. Curve (a) is the exact result, Eqn. (29). Curve (b) is the approximation given in Eqn. (30), Curves (c) and (d) represent the asymptotic clean and dirty limits, respectively, both of which represent upper bounds for ξ_n.

Figure 27, Dependence of normalized I_cR_n on reduced temperature for $L/\xi_{nd}(T_c) = 0$, 1, 2, 3, 4, 6, 8, and 10 (top to bottom) for SNS junctions in the clean limit under rigid boundary conditions [1 16].

Figure 28, Dependence of normalized I_c on reduced temperature for $L/\xi_{nd}(T_c) = 0$, 1, 2, 3, 4, 6, 8, and 10 (top to bottom) for *SNS* junctions in the clean limit under rigid boundary conditions [1 16]. The dashed line is the linear dependence $I_c/I_c(0) = 1 - T/T_c$.

Figure 29. Dependence of normalized I_c on reduced temperature for a $Pb-Cu-Pb$ microbridge [125]. The inset shows the temperature dependence of I_cR_n on a logarithmic scale, The solid lines were obtained from Likharev's theory [1 04] using $L/\xi_{nd}(T_c) = 8$.

Figure 30. $I_c/I_c(0)$ versus T/T_c for a *Nb* microbridge [1 33]. The solid line is $I_c/I_c(0) = 1 - T/T_c$. The dashed curve is the theoretical prediction for an ideal clean point contact, Eqn. (4).

Figure 31. Calculated $\xi_n(T)$ for ρ_n values of (a) 1, (b) 3, and (c) 10 Ω -*pm* with $T_{cn} = 50$ K (upper curves), The temperature and resistivity ranges were chosen to span those of interest for substituted- $YBa_2Cu_3O_{7-\delta}$ interlayer devices. For comparison, the lower curves (primed labels) show $\xi_n(T)$ for $T_{cn} = 0$.

Figure 32. Dependence of ξ_n on ℓ_n, with both quantities normalized by ξ_{nc}, for 3d

metals with $T_{cn}=0$. Curve (a) is the exact result, Eqn. (29). Curve (b) is the approximation given in Eqn. (40), which works well for $\ell_n > \xi_{nc}$. Curve (c) represents the dirty limit, Eqn. (7).

Figure 33. Dependence of I_cR_n on L at 4.2 K [151] and fits to the dependence $I_cR_n \propto I_c = I_{co}\exp(-L/L_o)$. (a) Ag bridges ($I_{co}R_n$ =0.112 $mV, L_o=44.1nm$). (b) Ag / AU bridges ($I_{co}R_n=3.72$ mV, $L_o=18.3$ inn).

Figure 34. $I_c / I_c(0)$ versus T_c for four AU edge microbridges [150] with fixed $YBa_2Cu_3O_{7-\delta}$ film thickness of 80 nm and varying step height d_{step}. (a) $d_{step}=80$ nm, I_c (0) $=560$ μA. (b) $d_{step}=110$ nm, $I_c(0)=180$ μA. (C) $d_{step}=110$ nm, $I_c(0)=120$ μA. (d) $d_{step}=140$ $nm, I_c(0)=98$ μA. The solid curves are I_c /1,(0)=1 - T/T_c. The dotted curves are provided as guides to the eye. Curves (a) - (c) are offset in the vertical direction for clarity.

Figure 35. $I_c / I_c(0)$ versus T/T_c for the $CaRuO_3$ edge junction of Fig. 12a along with the predictions of Likharev's theory for (a) $L/\xi_{nd}(T_c)=4$ (the best fit) and (b) $L/\xi_{nd}(T_c)=12$ (the expected value). The solid line is $I_c/I_c(0) = 1- T/T_c$.

Figure 36. $J_c(L)$ for $CaRuO_3$ edge junctions at 4,2 K [66]. Line (a) is $J_c(L)$ calculated from $J_c=J_{co}\exp(-L/L_o)$ with $J_{co}(0) = 0.70\Delta_\infty(0)/(e\rho_n\xi_{nd}(T_c))$ =3.6 $A/\mu m^2$ and $L_o=3.18\xi_{nd}(T_c)$ =2.6 nm. Line (b) is a two-parameter fit to the data using the same exponential form, resulting in $J_{co}(0)=31mA/\mu m^2$ and L_o =5.6 nm.

Figure 37. $J_c(L)$ for $SrRuO_3$ edge junctions at 4.2 K [67]. Line (a) is $J_c(L)$ calculated from $J_c=J_{co}\exp(-L/L,))$, w ith $J,O(0) = 0.70\,\Delta_\infty(0)/(\gamma_b^2 e\rho_n\xi_{nd}(T_c))=5.6\ mA/\mu m^2$ ($\gamma_b^2=$ 1000) and $L_o = 3.18\,\xi_{nd}(T_c)$ =4.2 nm. Line (b) is a two-parameter fit to the data using the same exponential form, resulting in $J_{co}(0) = 1.2\ mA/\mu m^2$ and L_o =8.5 nm.

Figure 38, Comparison of calculated [20] and experimental [75] $I_c(T;L)$ for Ca - substituted $YBa_2Cu_3O_{7-\delta}$ junctions with interlayers (a) 20, (b) 40, and (c) 60 nm thick. Data are indicated by triangles, squares, and circles, respectively. The conventional proximity effect calculations used no arbitrary fitting parameters, with T_c=88 and T_{cn}=50 K.

Figure 39, Comparison of calculated [20] and experimental [74] $I_c(T;L)$ for Co- substituted $YBa_2Cu_3O_{7-\delta}$ junctions with interlayers (a) 15, (b) 30, and (c) 45 nm thick. Data are indicated by triangles, squares, and circles, respectively. The conventional proximity effect calculations used no arbitrary fitting parameters, with T_c =88 and T_{cn}=50 K.

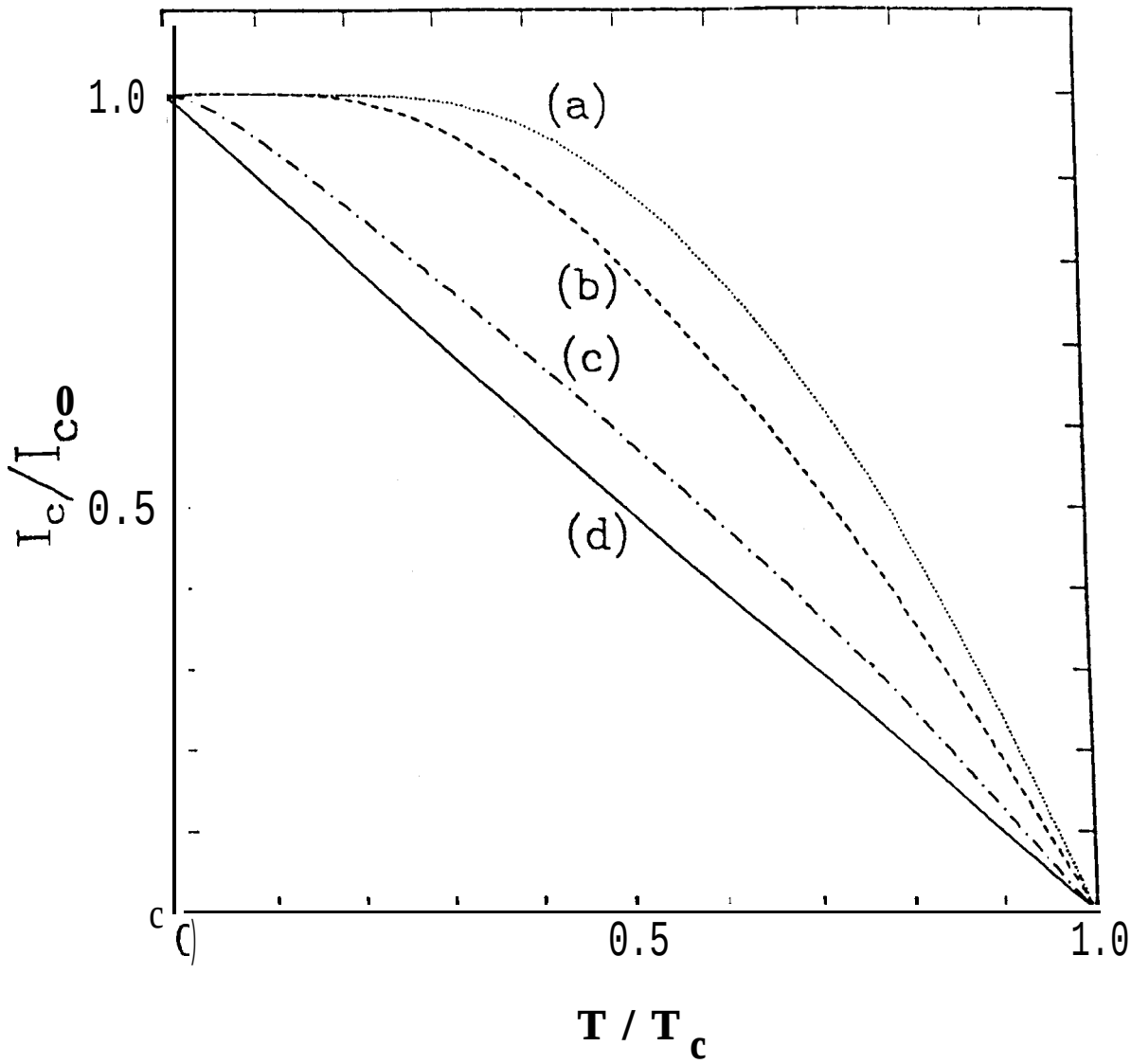
1.0
0.5
0
0
0.5
1.0
(a)
(b)
(c)
(d)
I_c/I_{c0}
T / T_c

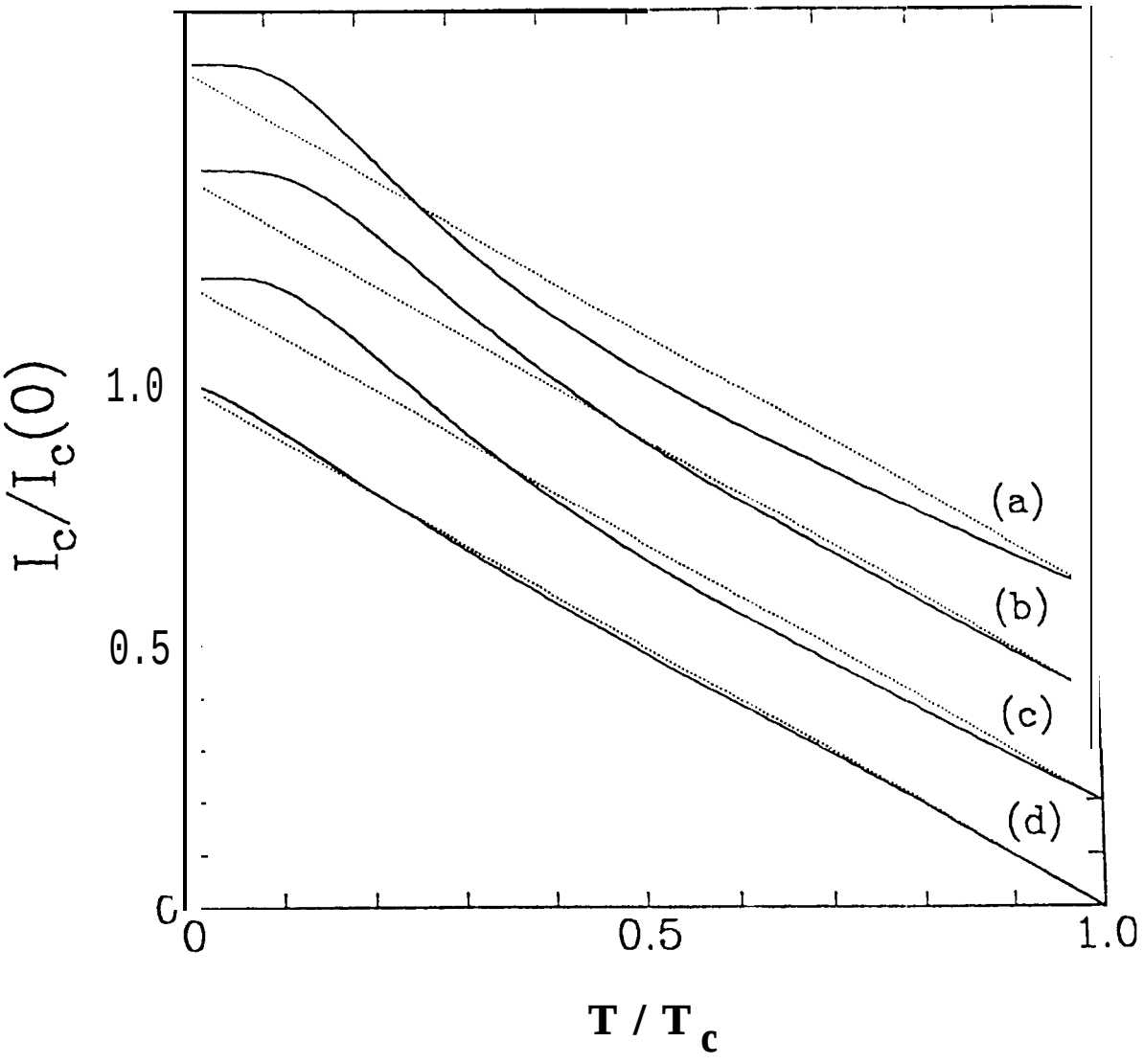
$I_c/I_c(0)$
1.0
0.5
0
0
0.5
1.0
T / T c
(a)
(b)
(c)
(d)

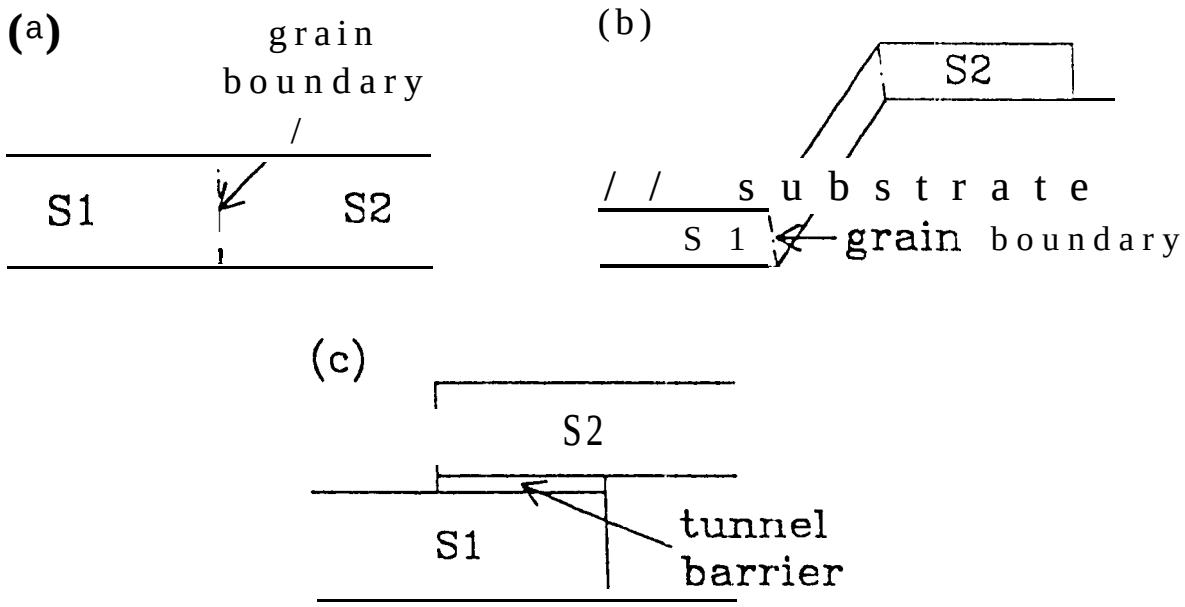
(a)
grain
boundary
S1
S2
(b)
S2
substrate
S 1
grain boundary
(c)
S2
S1
tunnel
barrier

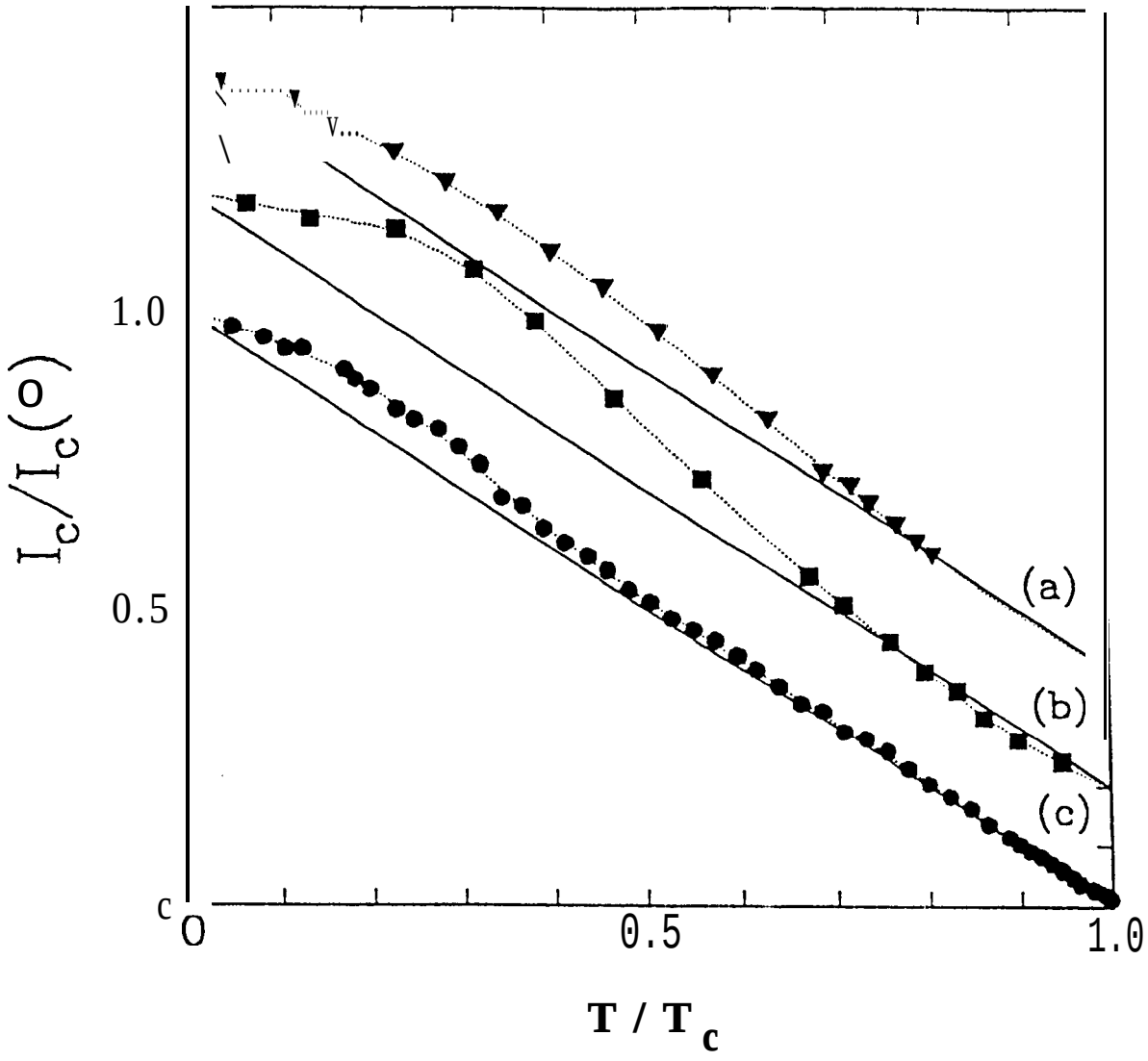
1.0
0.5
0
0.5
1.0
$I_c/I_c(0)$
T / T_c
(a)
(b)
(c)

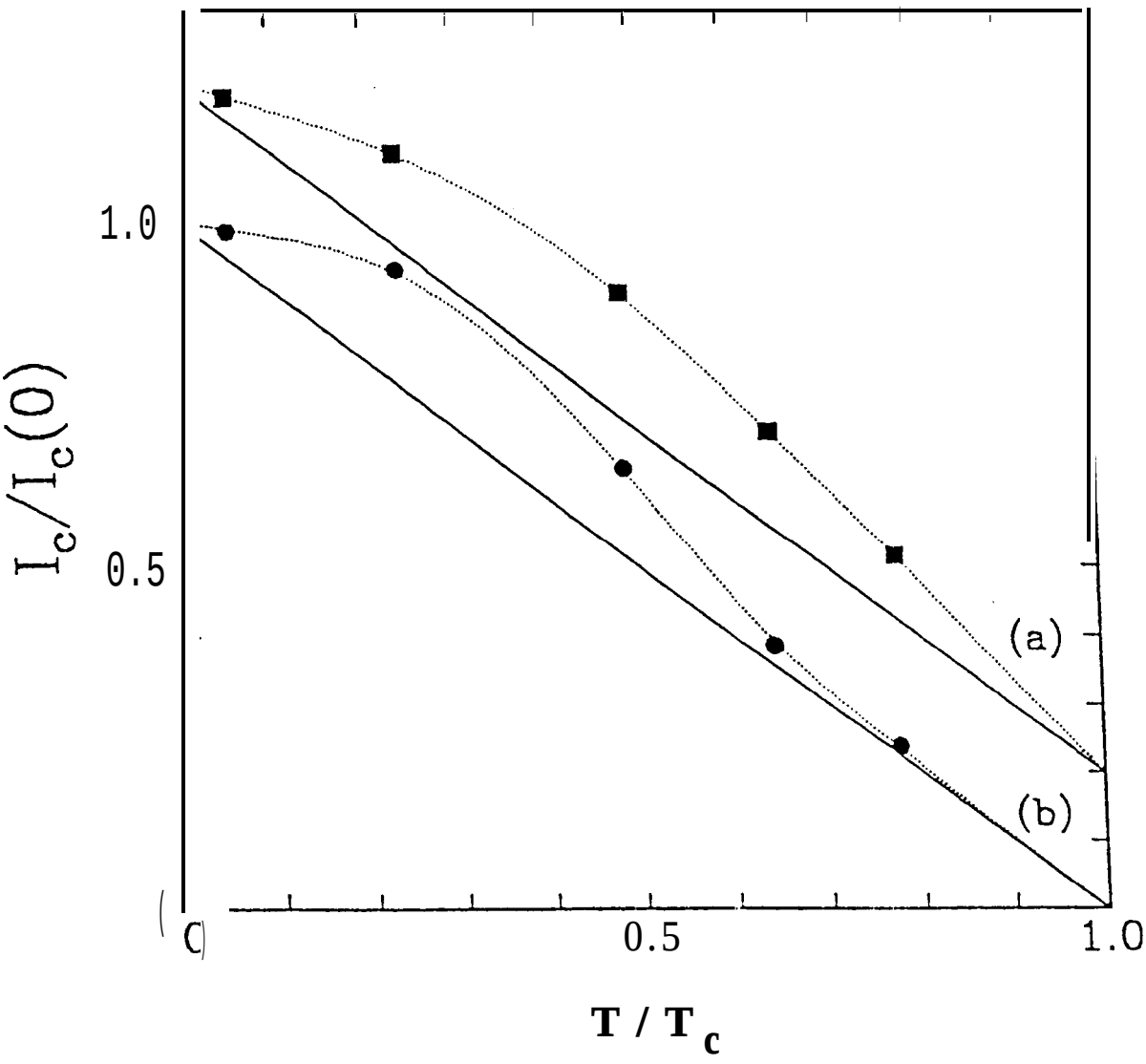
1.0
0.5
$I_c/I_c(0)$
(a)
(b)
0.5
1.0
T / T c

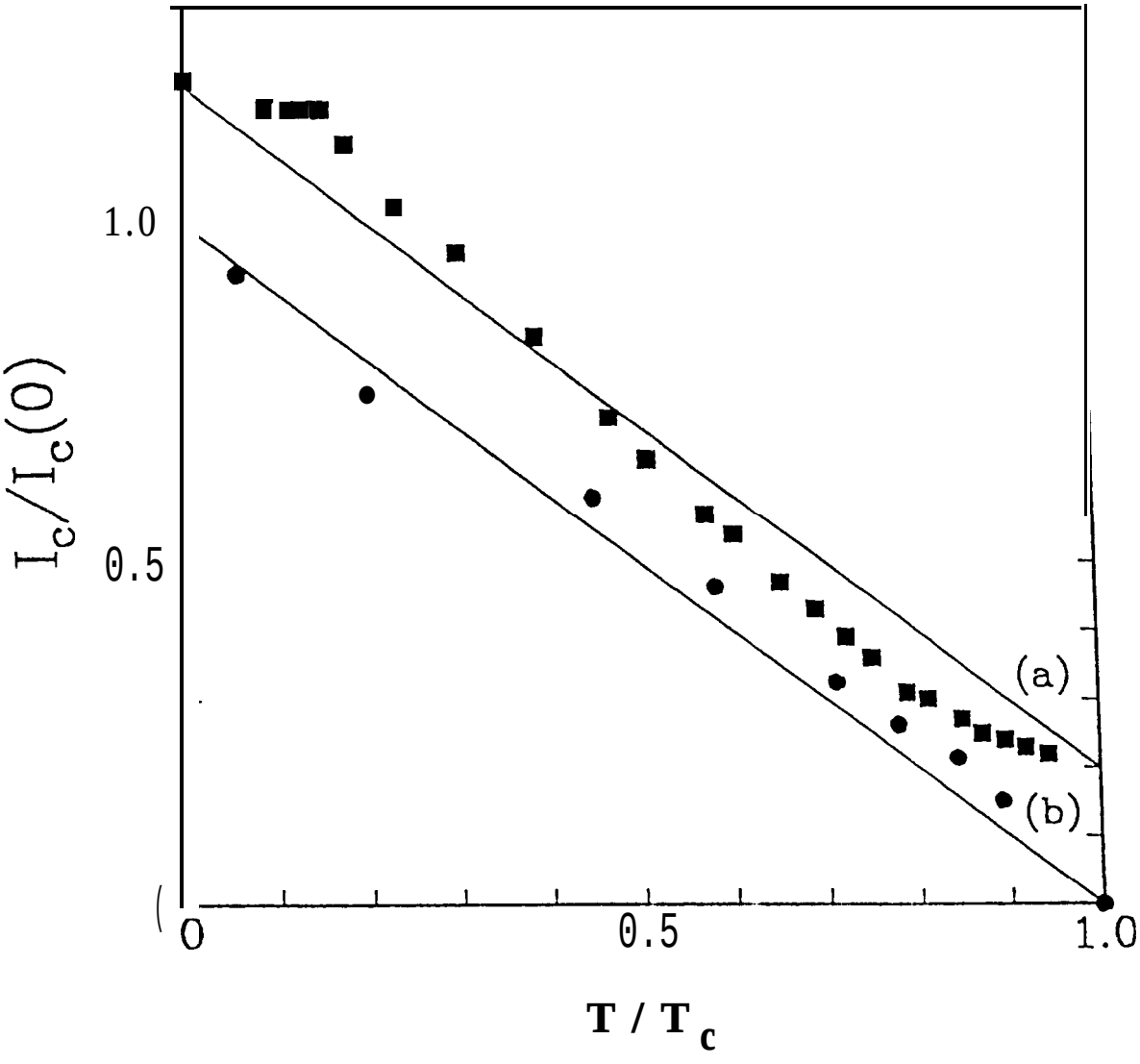
1.0
0.5
$I_c/I_c(0)$
0
0.5
1.0
(a)
(b)
T / T c

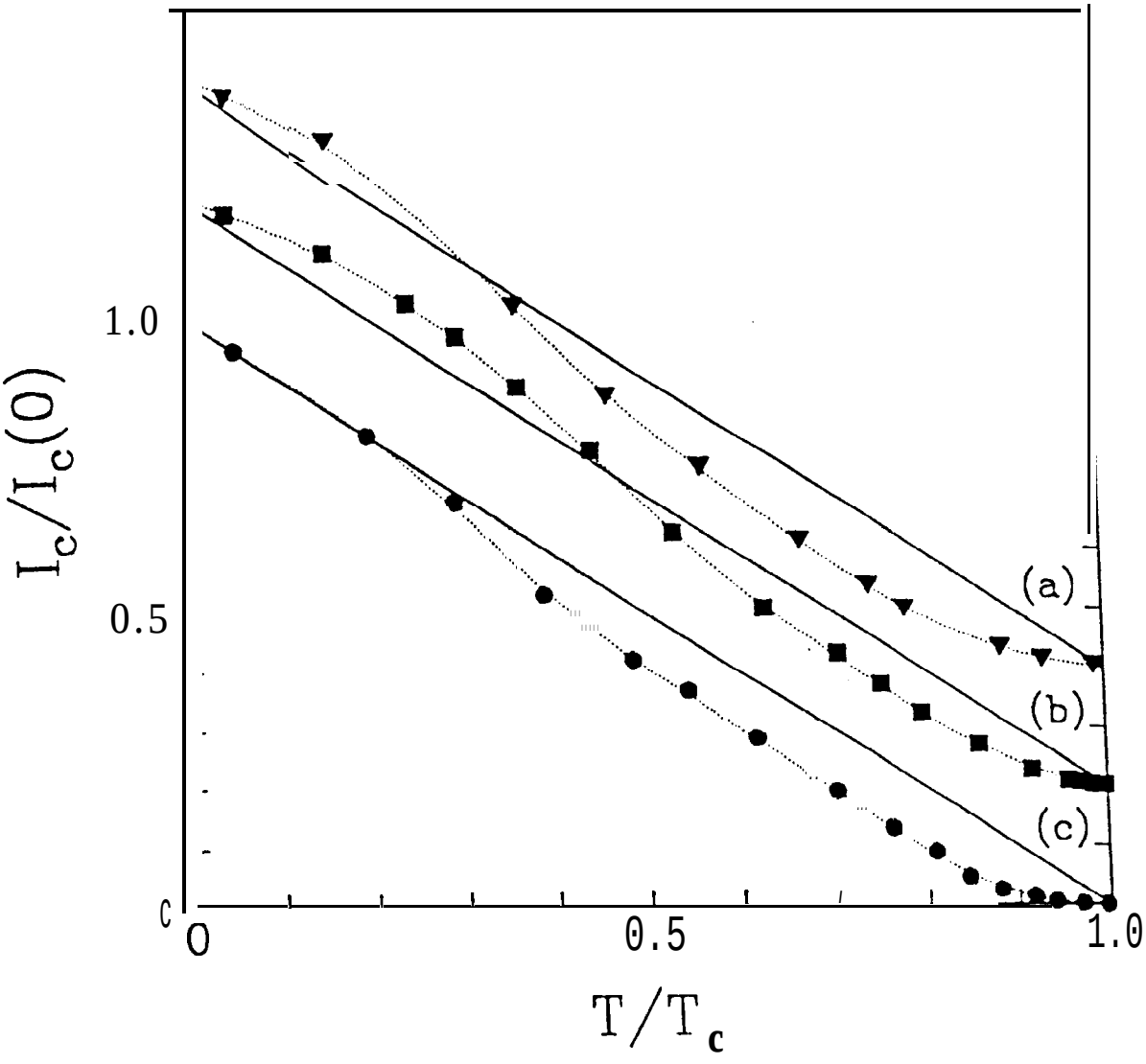

Delin/Kleinsasser

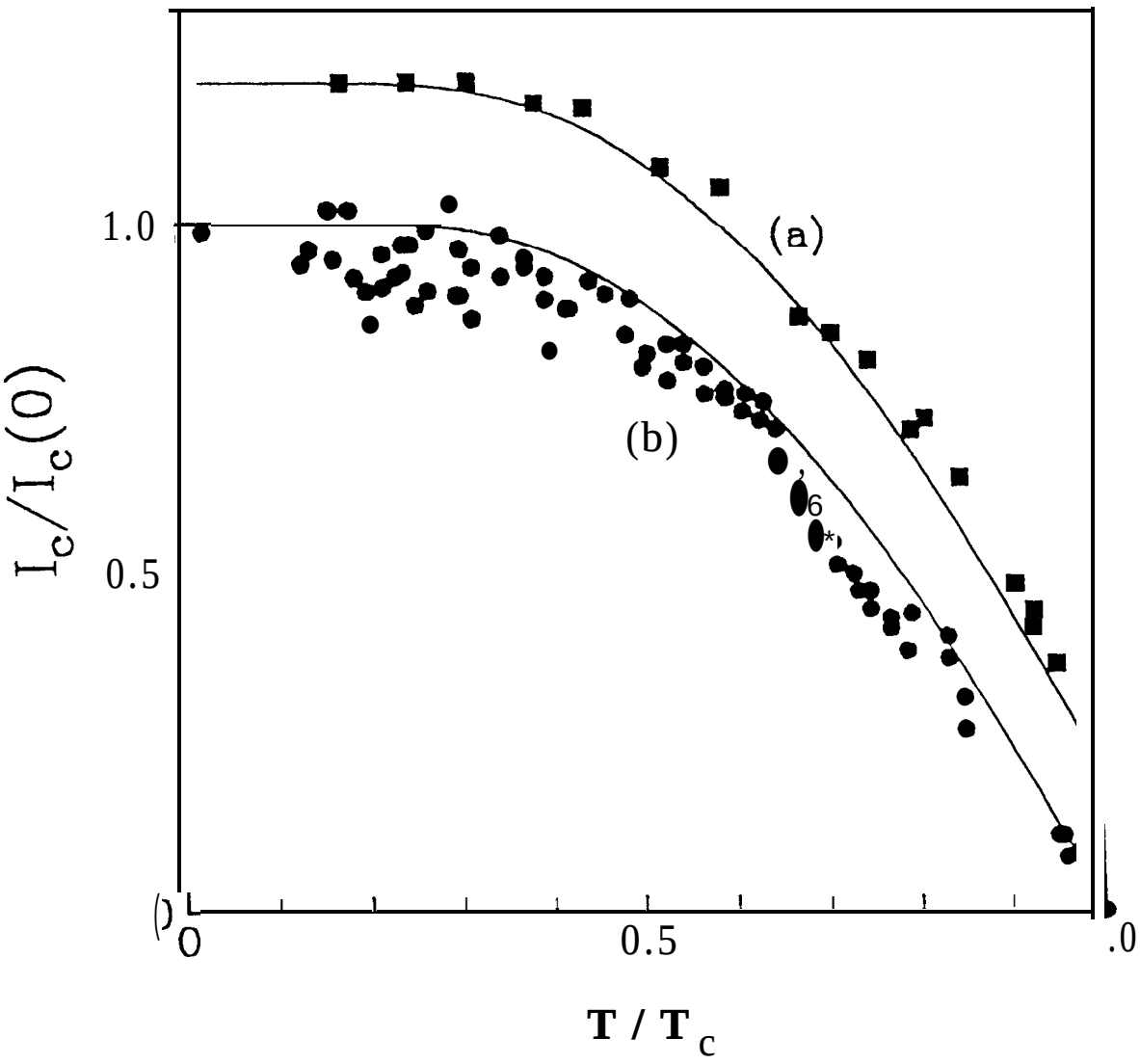
1.0
0.5
0
0.5
1.0
(a)
(b)
$I_c/I_c(0)$
T / T_c

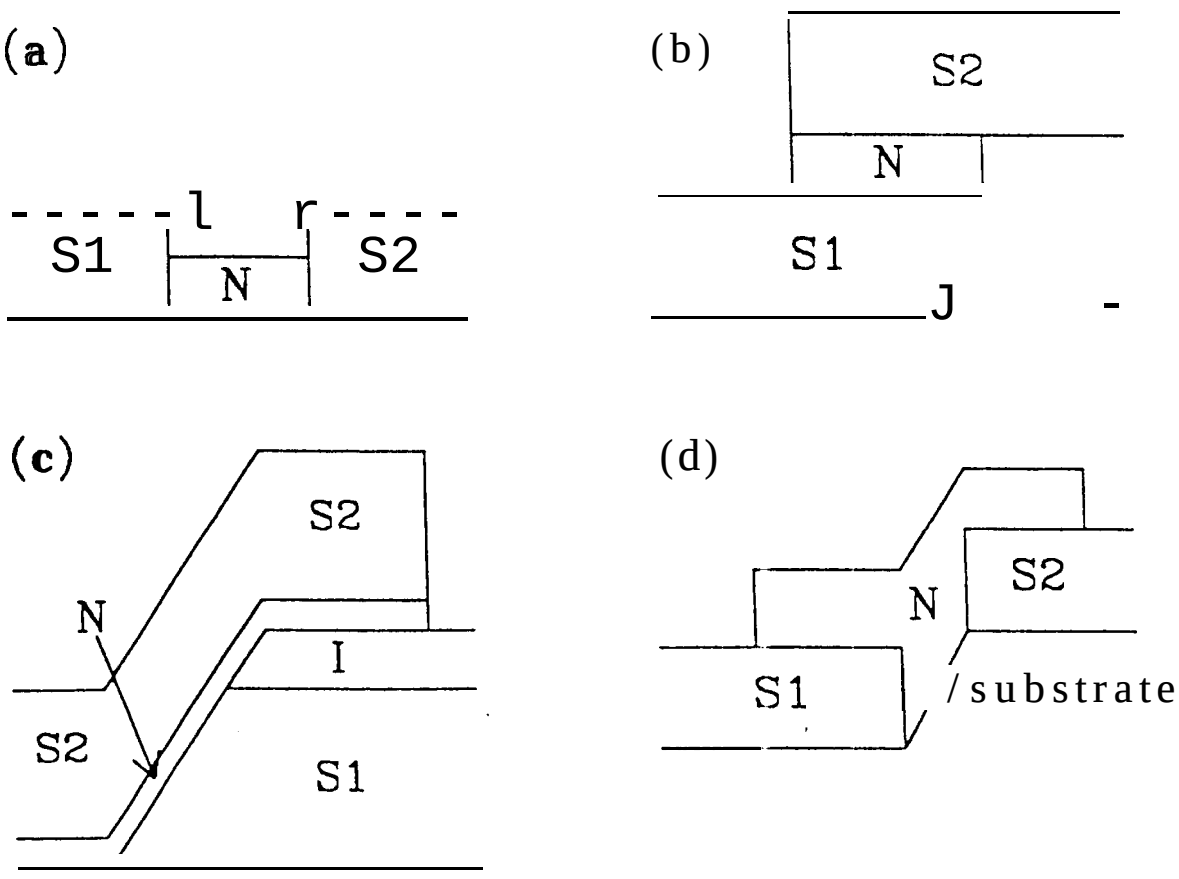
(a)
l
r
S1
N
S2
(b)
S2
N
S1
J
(c)
S2
N
I
S2
S1
(d)
N
S2
S1
/substrate

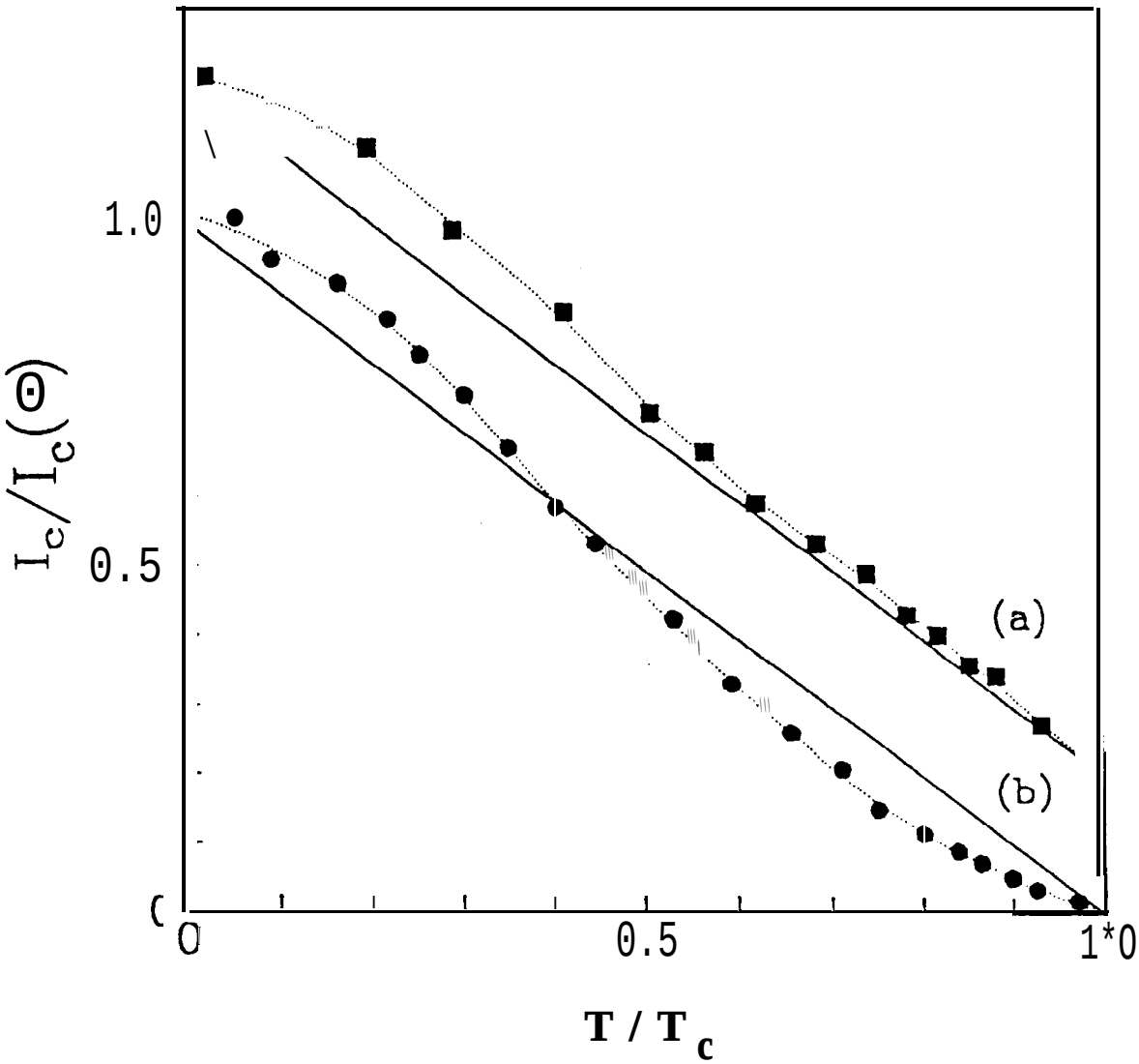
1.0
0.5
0
$I_c/I_c(0)$
(a)
(b)
0
0.5
1*0
T / T c

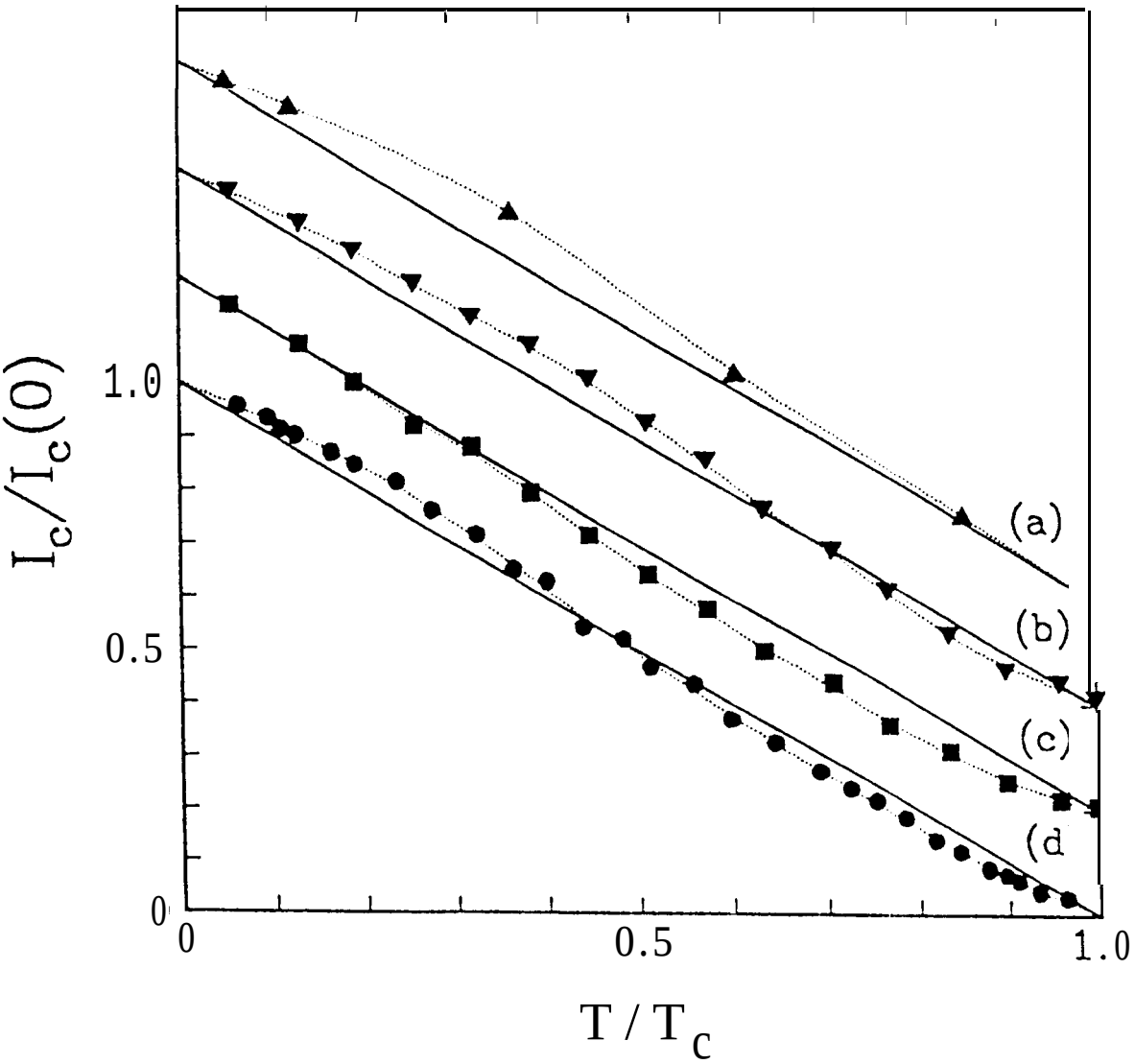
$I_c/I_c(0)$
1.0
0.5
0
0
0.5
1.0
T/T_c
(a)
(b)
(c)
(d

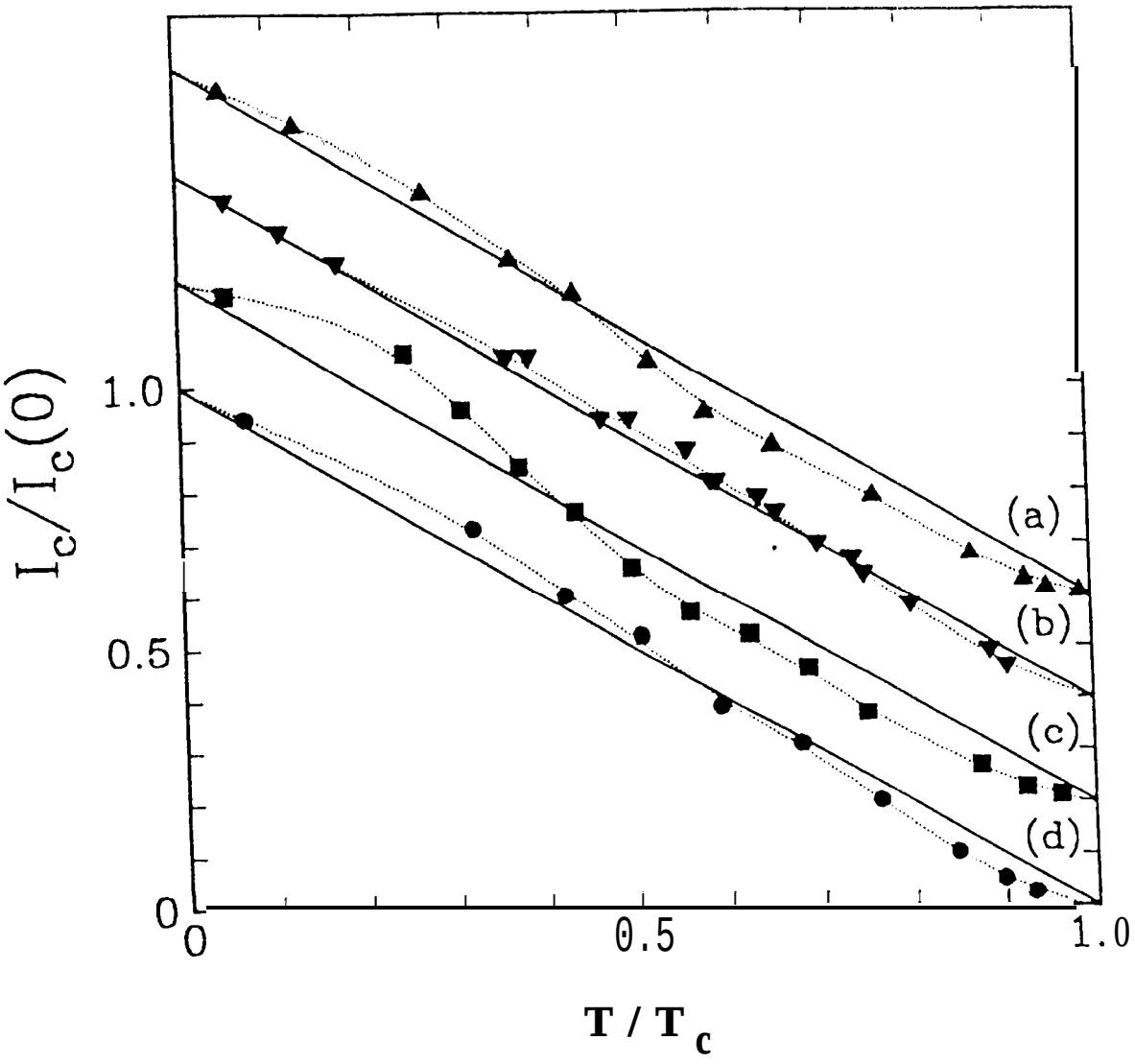
$I_c/I_c(0)$
1.0
0.5
0
0
0.5
1.0
(a)
(b)
(c)
(d)
T / T c

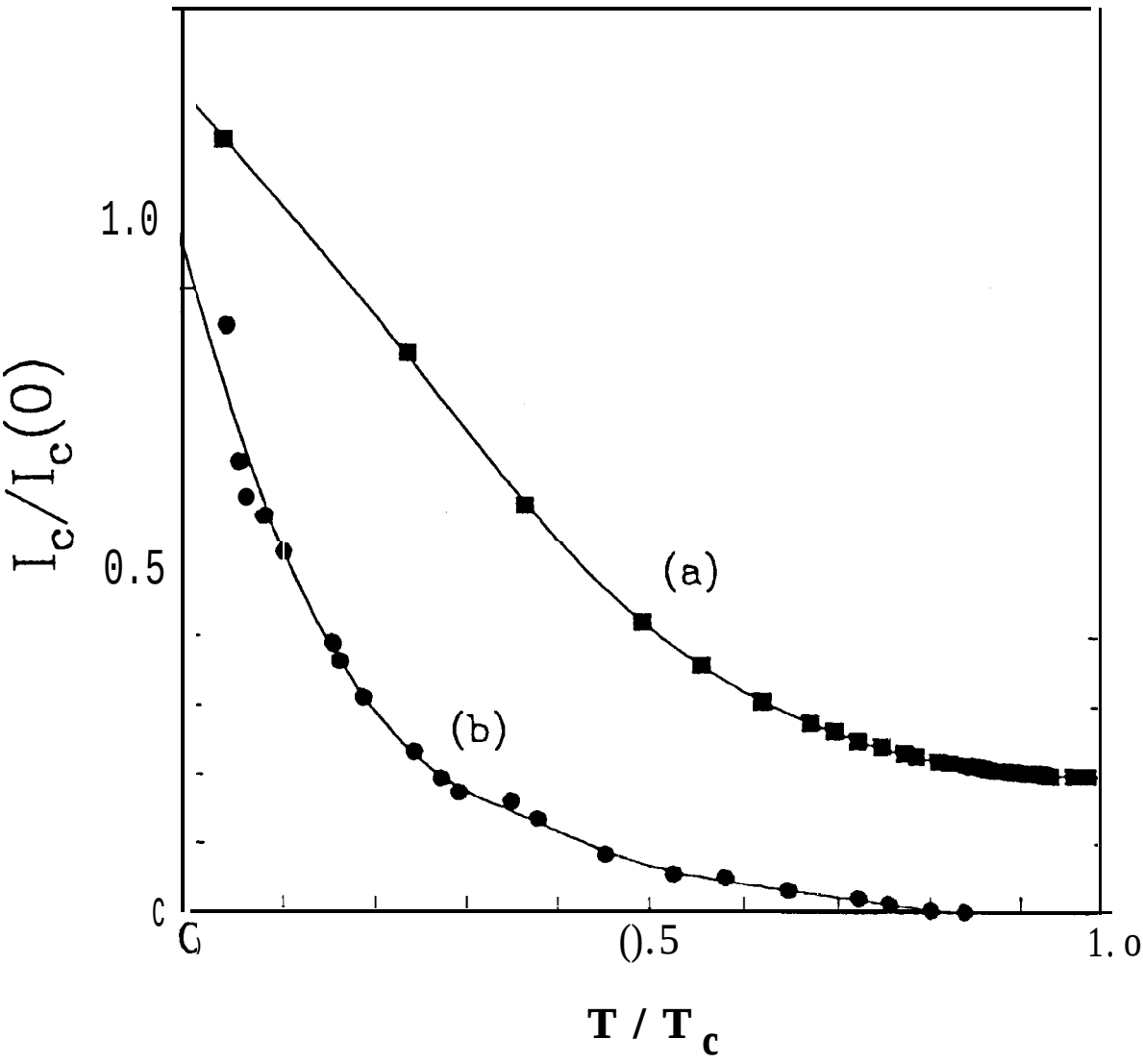
1.0
0.5
0
$I_c/I_c(0)$
(a)
(b)
0
0.5
1.0
T / T c

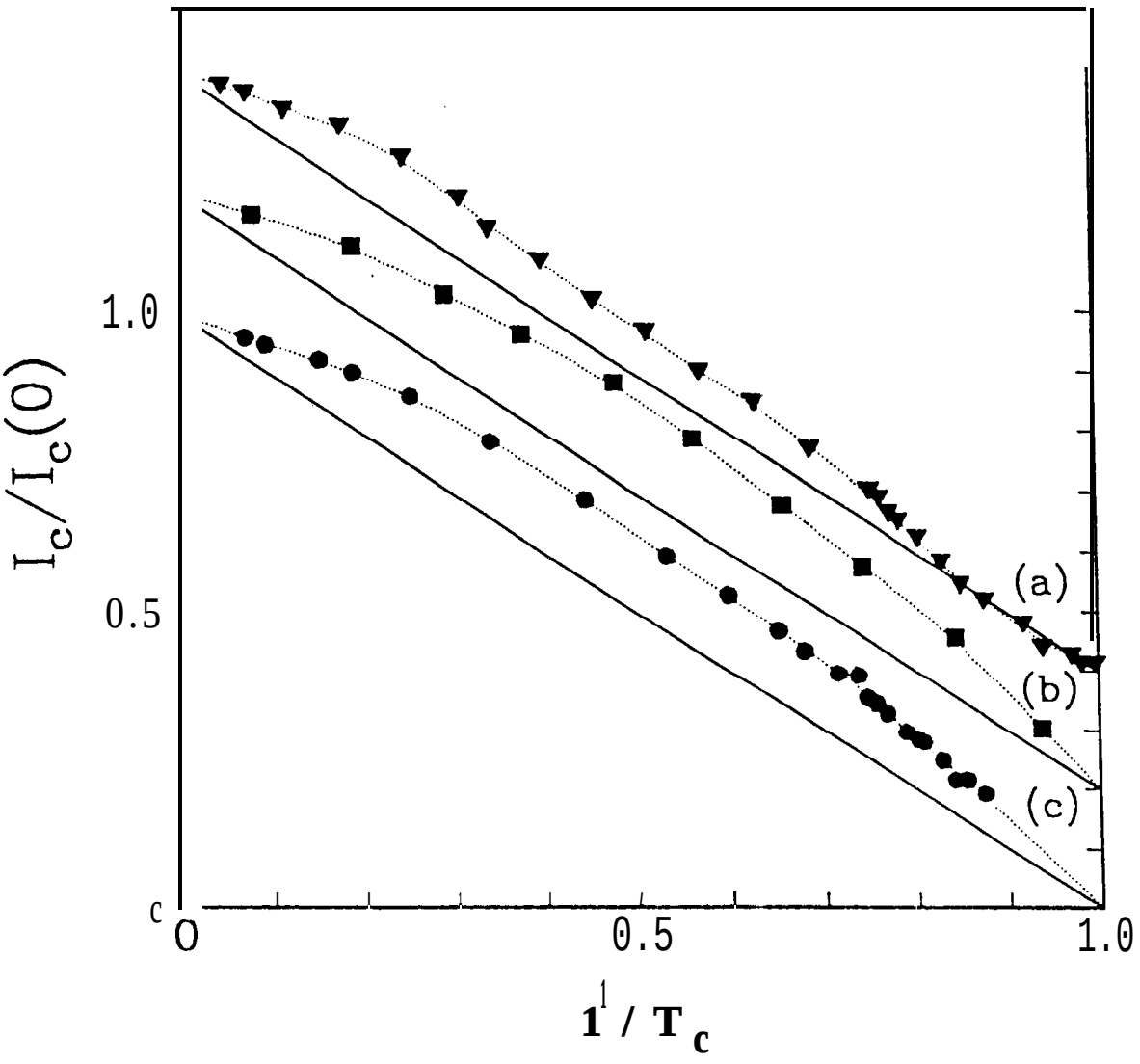
1.0
0.5
0
0.5
1.0
$I_c/I_c(0)$
$1^1 / T_c$
(a)
(b)
(c)

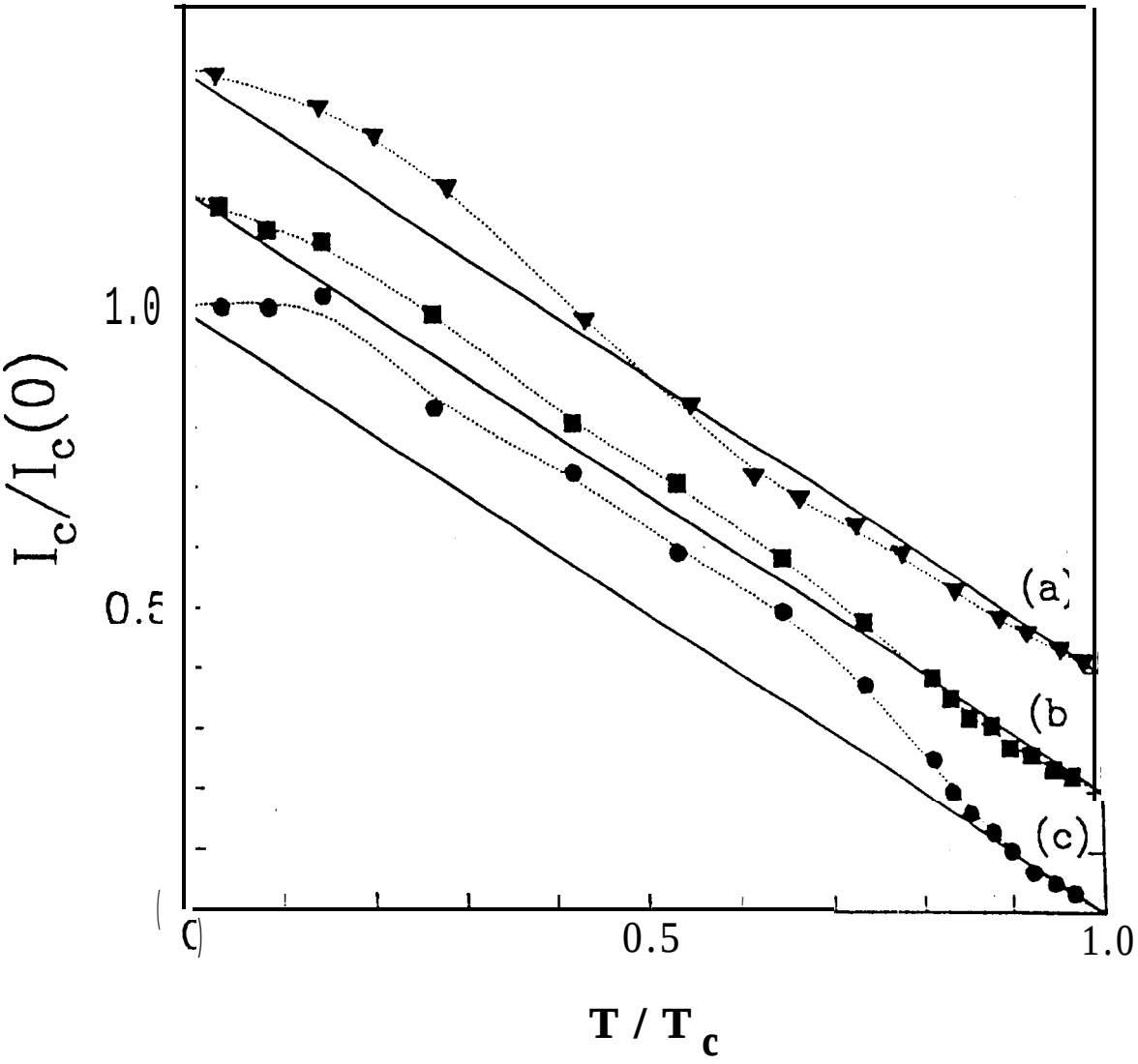

July 18, 1995

Figure 15

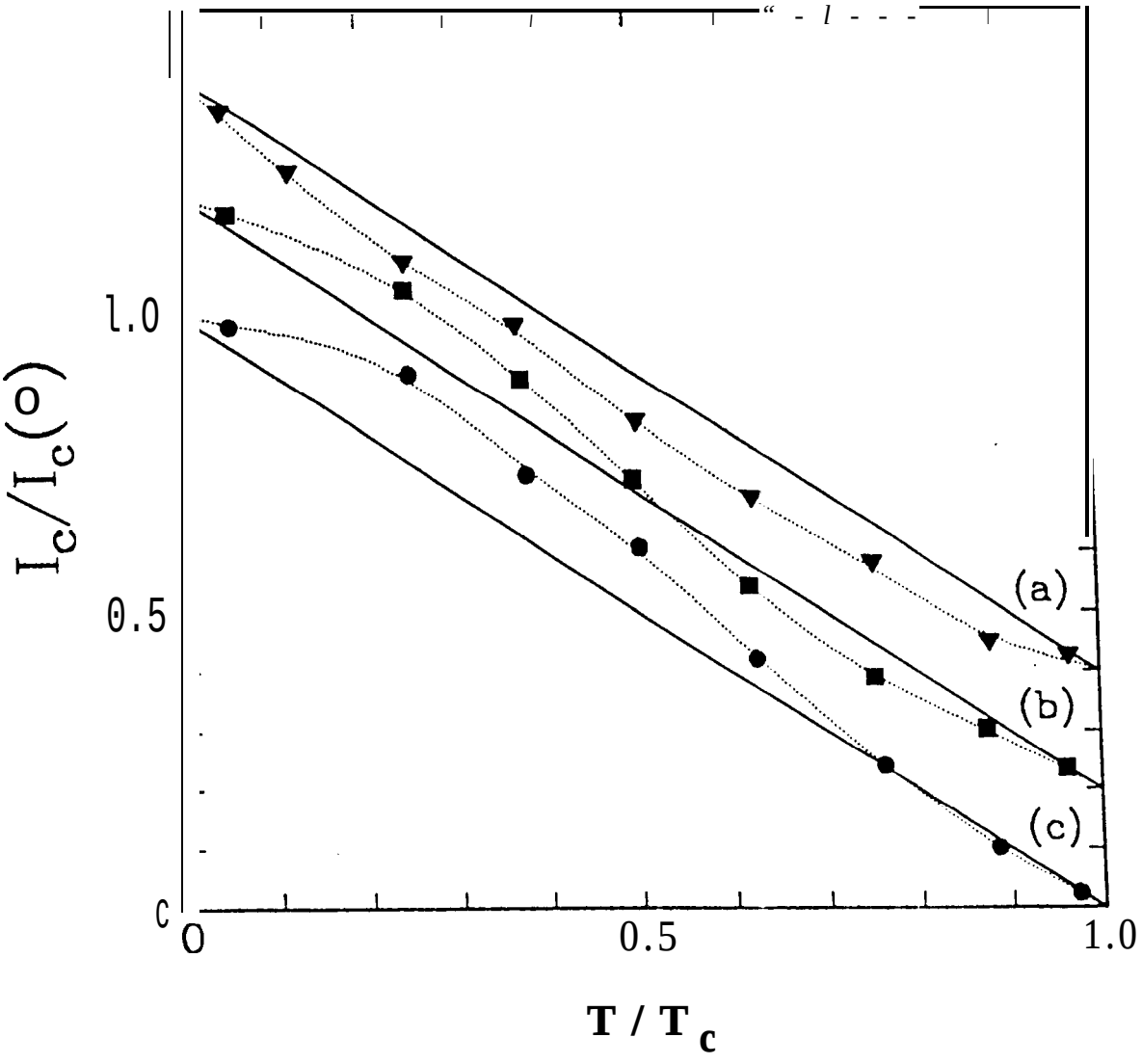
l.0
0.5
0
$I_c/I_c(0)$
0
0.5
1.0
T / T c
(a)
(b)
(c)

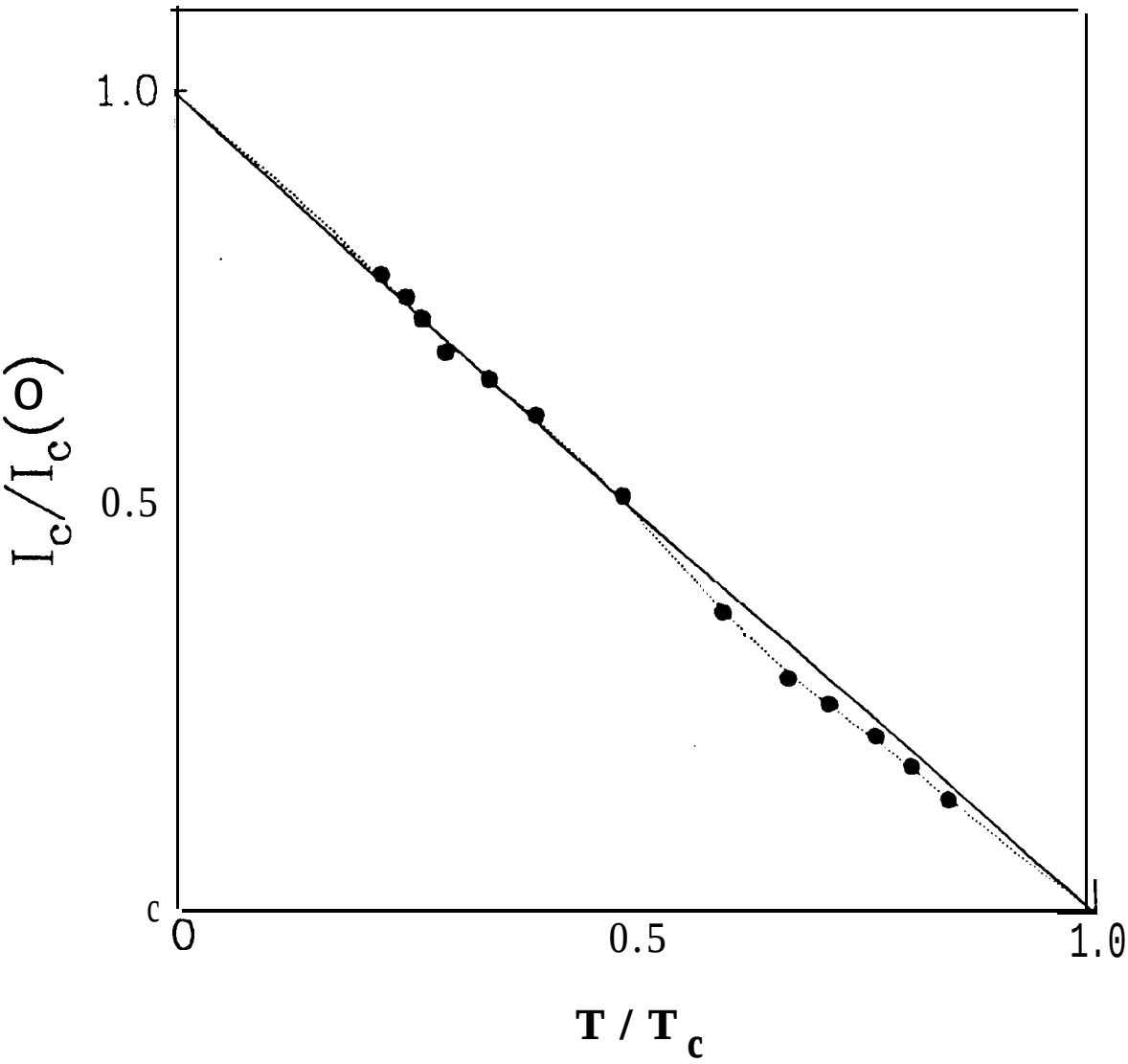
1.0
0.5
0
0.5
1.0
$I_c/I_c(0)$
T / T_c

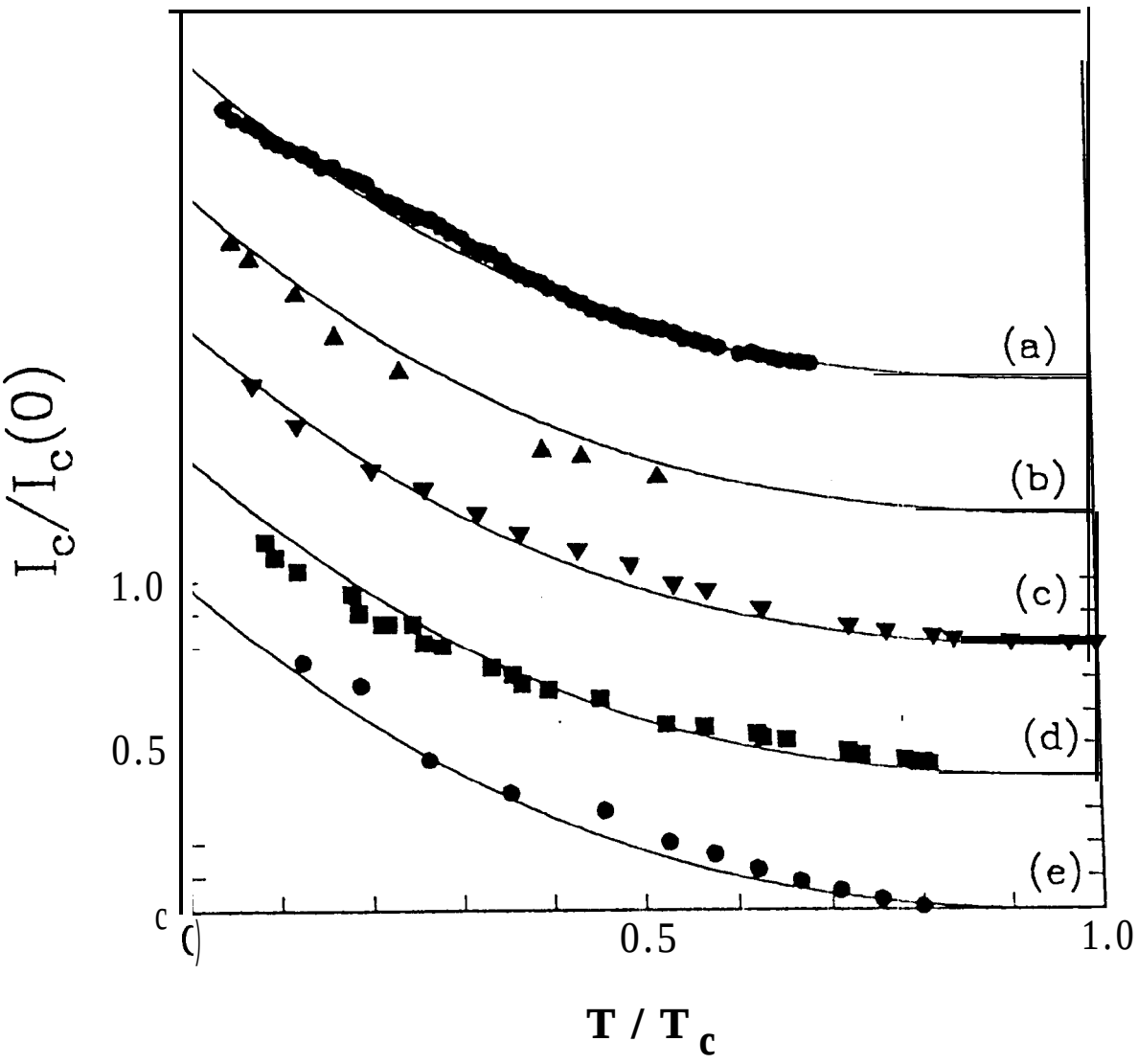
$I_c/I_c(0)$
1.0
0.5
0
0
0.5
1.0
T / T c
(a)
(b)
(c)
(d)
(e)

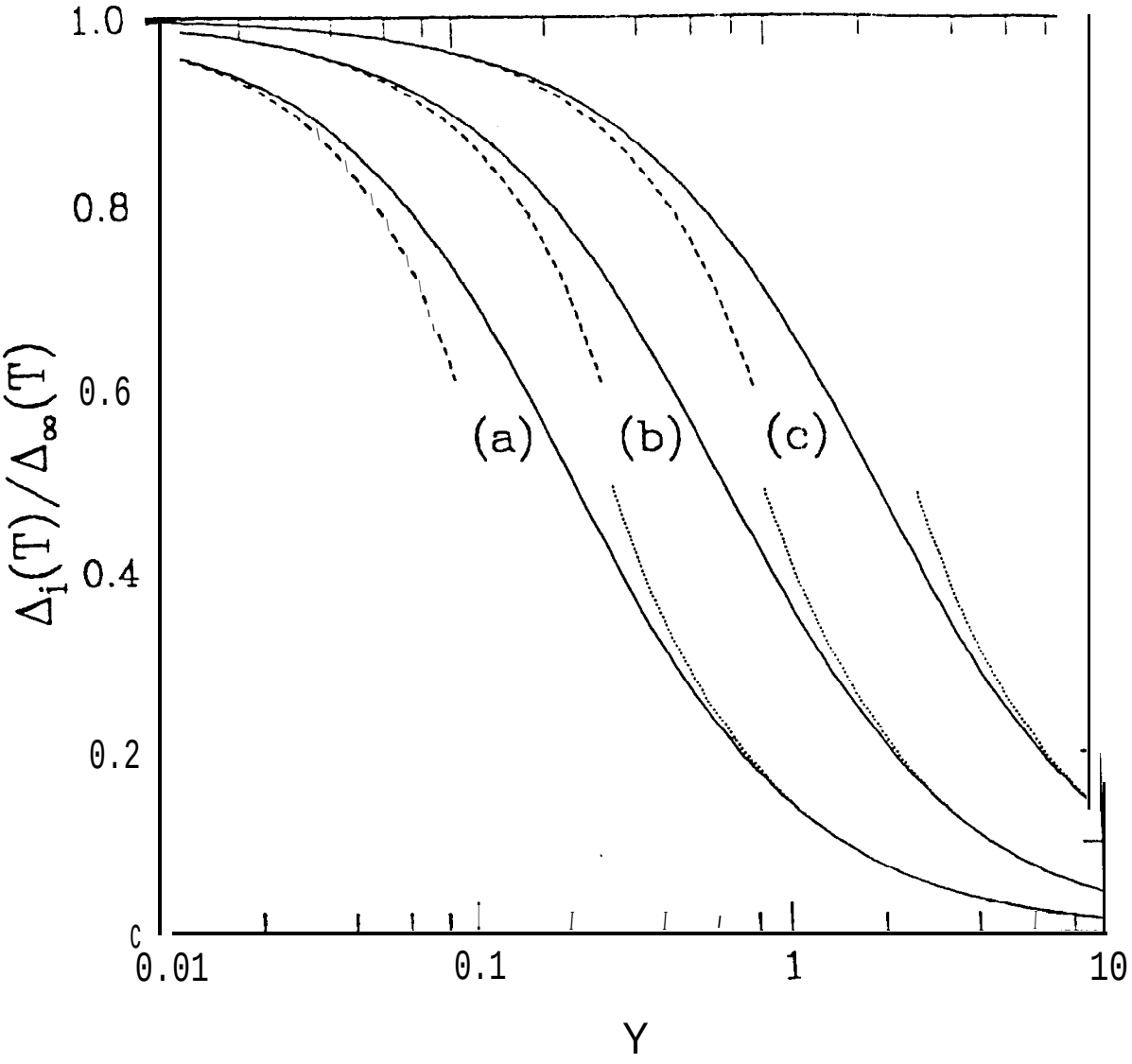
1.0
0.8
0.6
0.4
0.2
0
$\Delta_i(T)/\Delta_\infty(T)$
(a)
(b)
(c)
0.01
0.1
1
10
Y

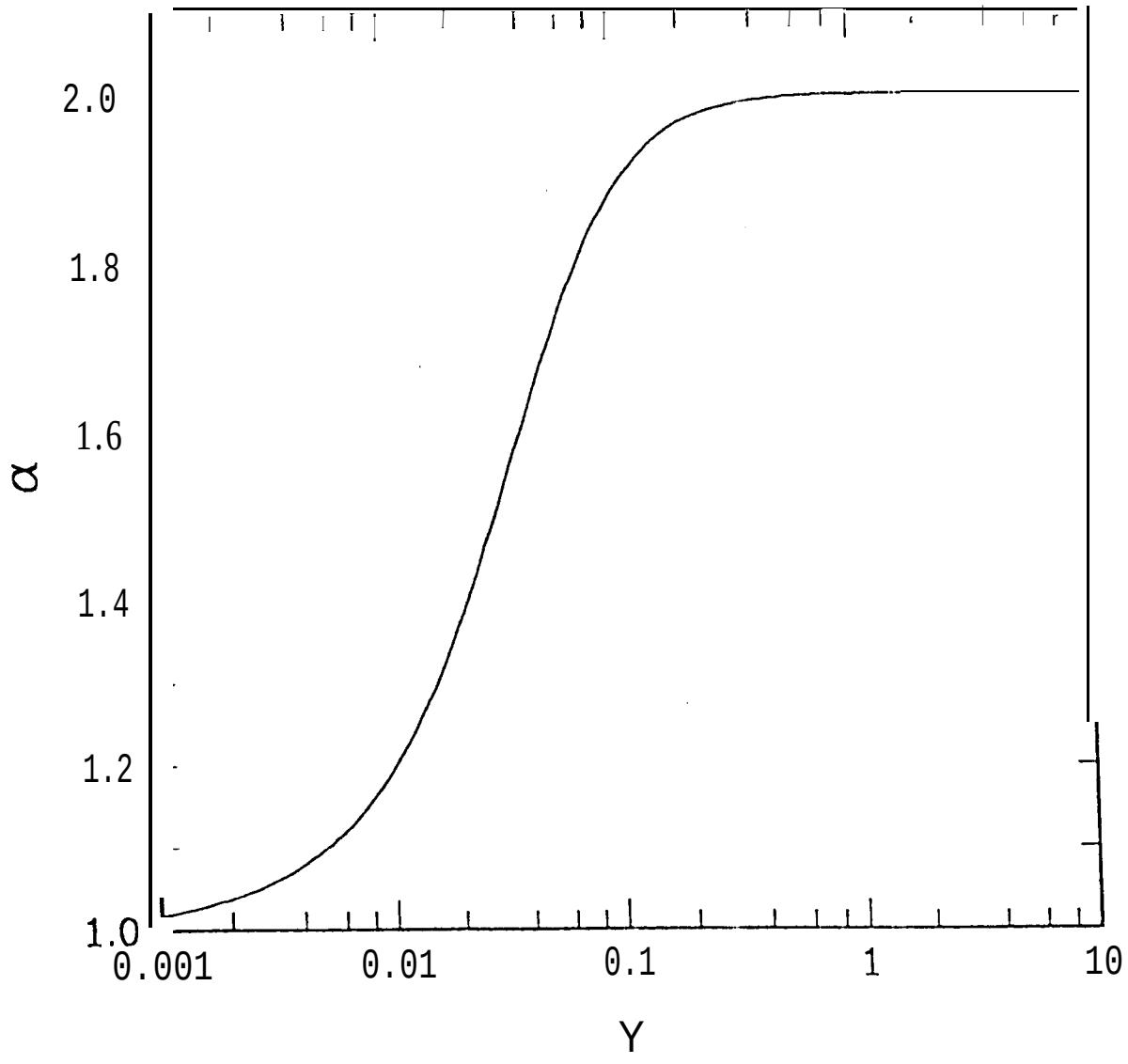
2.0
1.8
1.6
1.4
1.2
1.0
α
0.001
0.01
0.1
1
10
Y

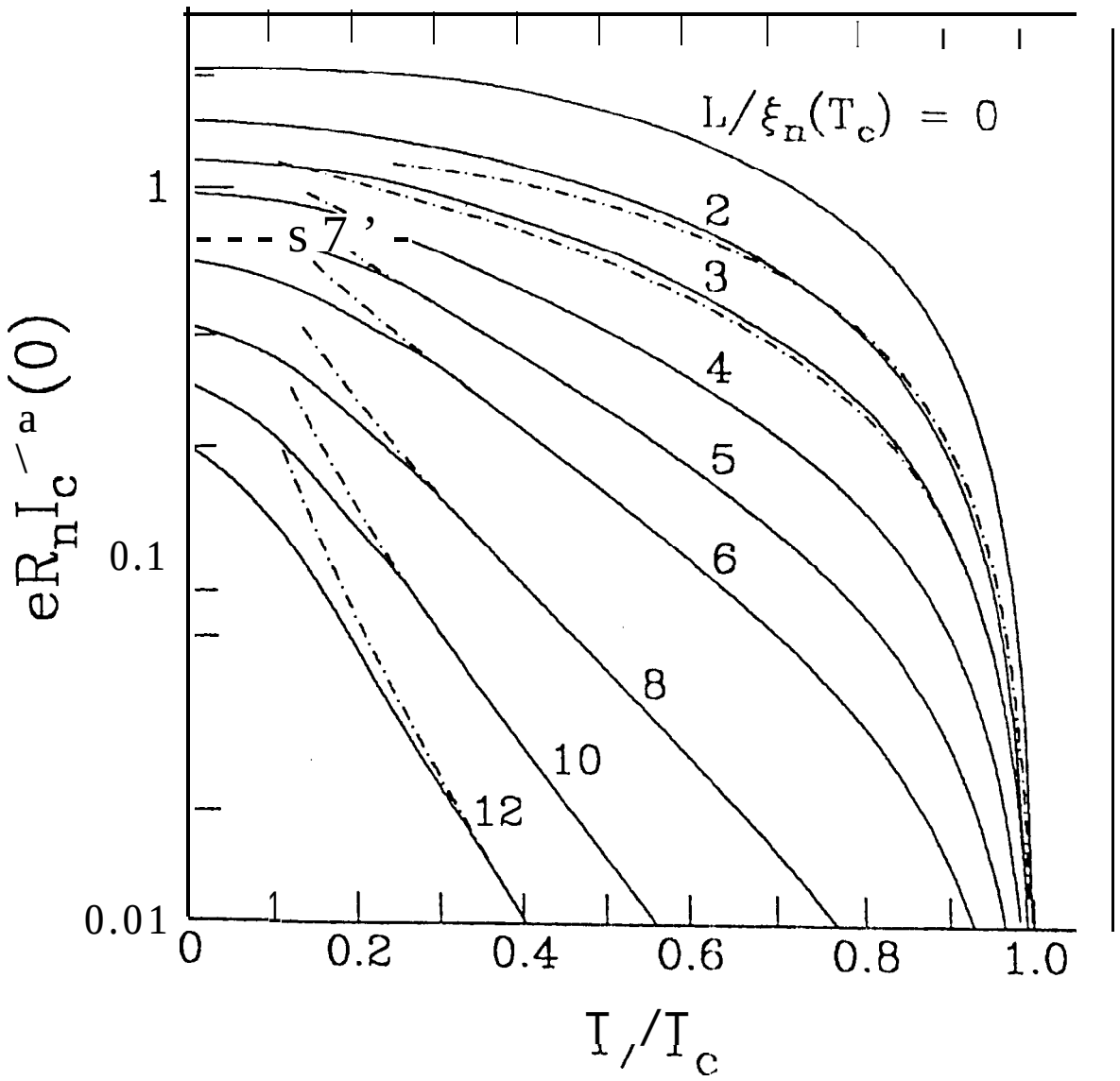
$L/\xi_n(T_c) = 0$
2
3
4
5
6
8
10
12
7
1
0.1
0.01
0
0.2
0.4
0.6
0.8
1.0
$eR_nI_c^{-a}(0)$
T/T_c

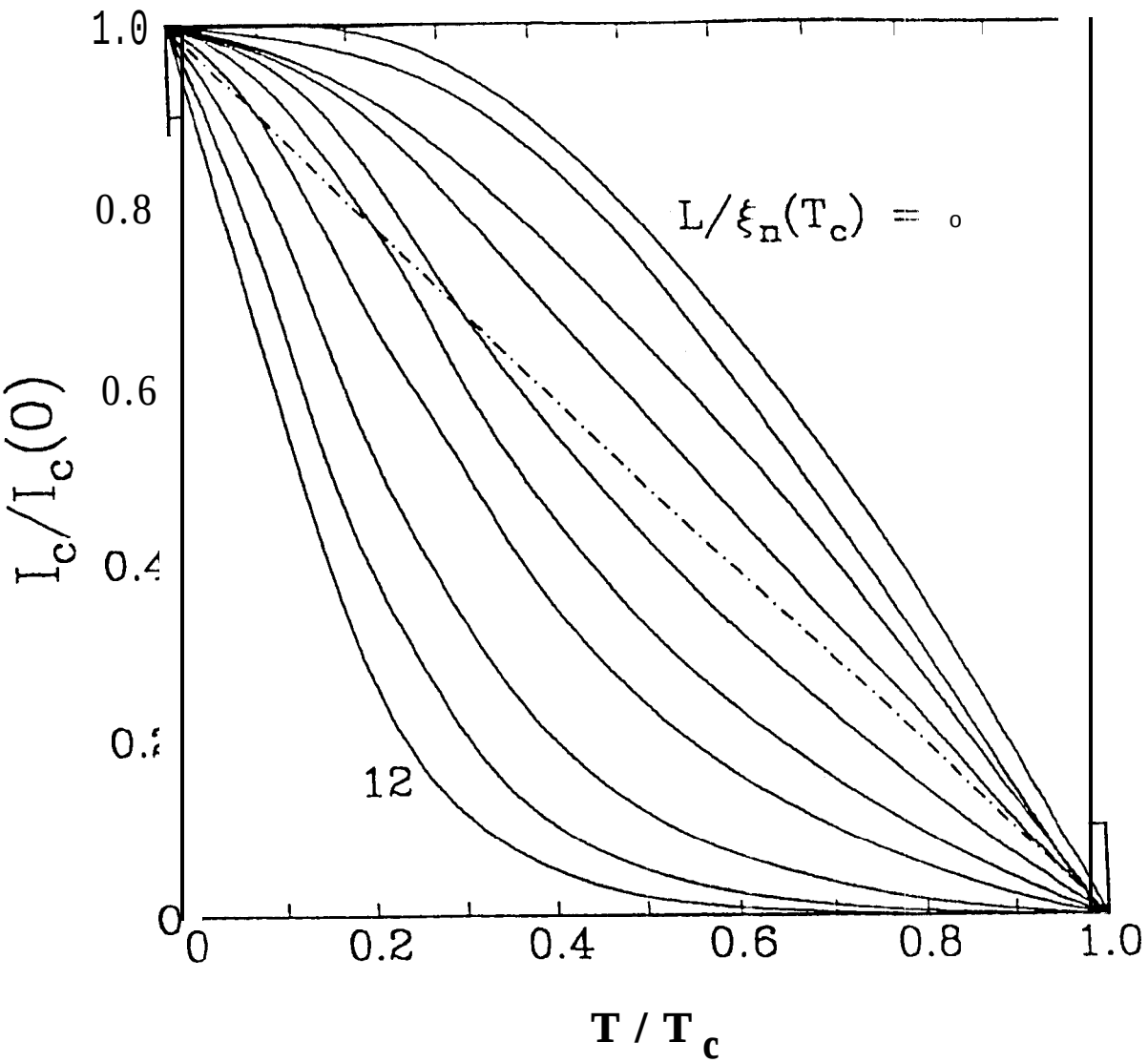
1.0
0.8
0.6
0.4
0.2
0
$I_c/I_c(0)$
$L/\xi_n(T_c) = 0$
12
0
0.2
0.4
0.6
0.8
1.0
T / T c

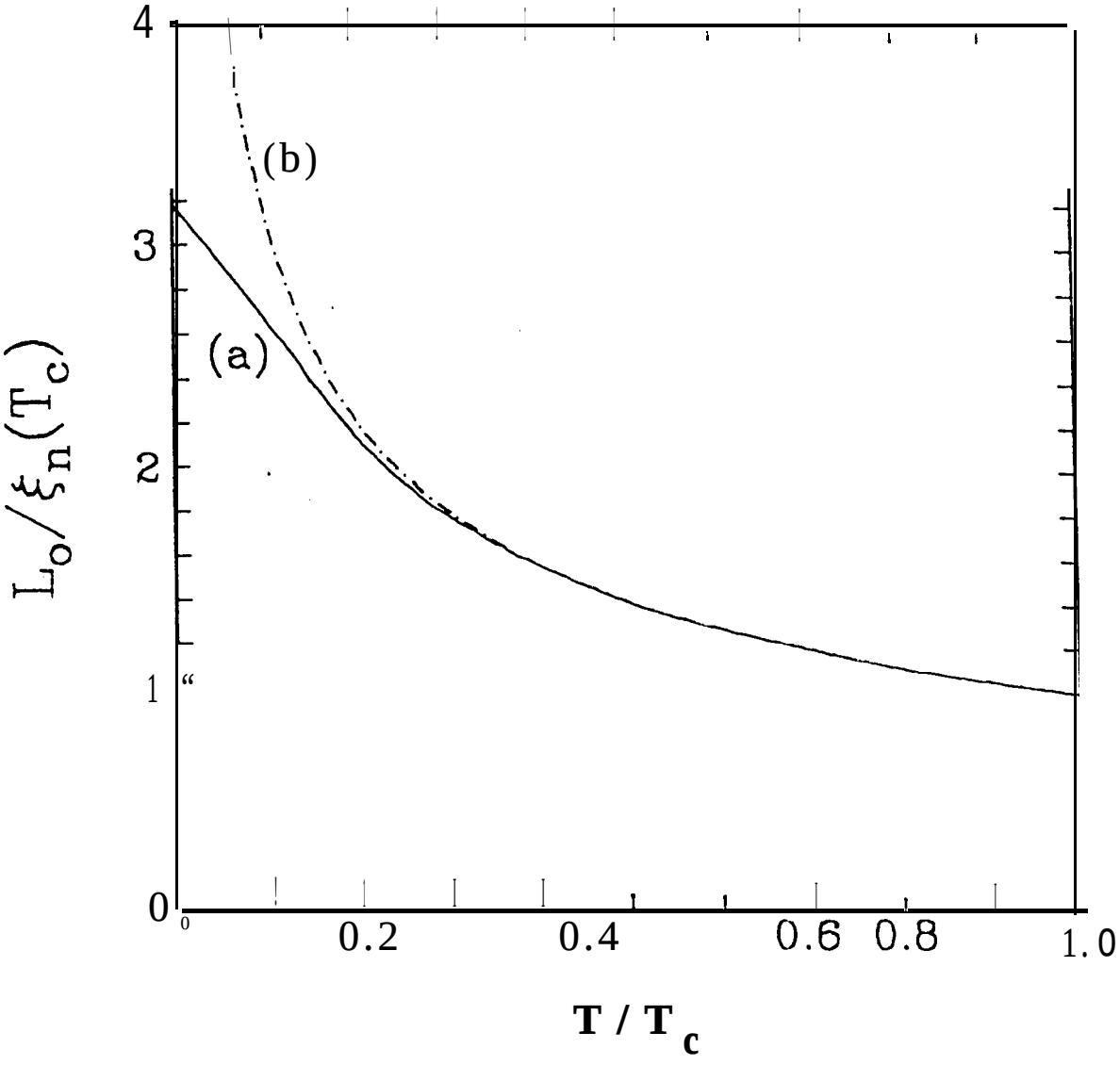

Delin/Kleinsasser July 18, 1995 Figure 23

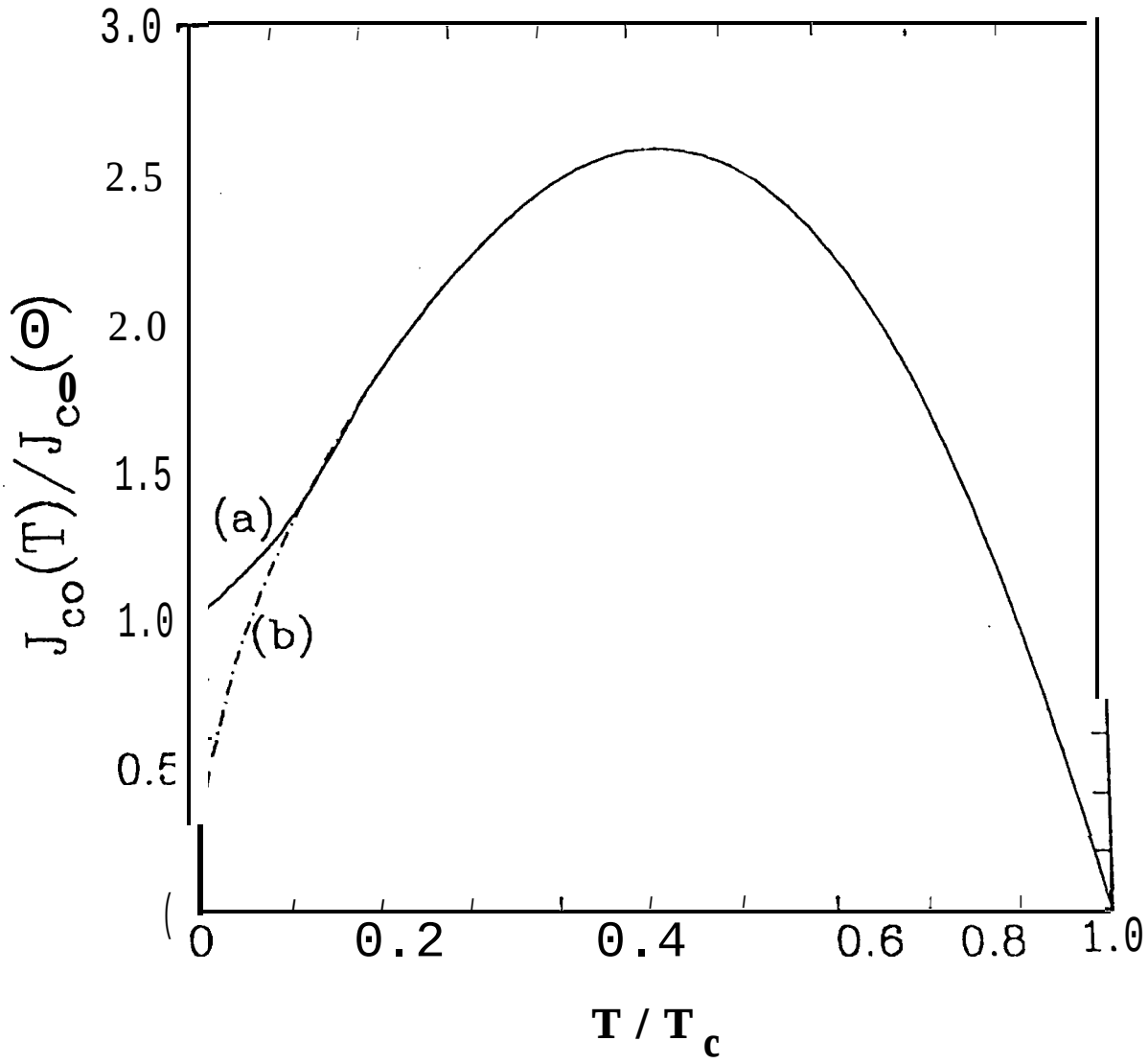
3.0
2.5
2.0
1.5
1.0
0.5
0
0.2
0.4
0.6
0.8
1.0
(a)
(b)
$J_{co}(T)/J_{co}(0)$
T / T c

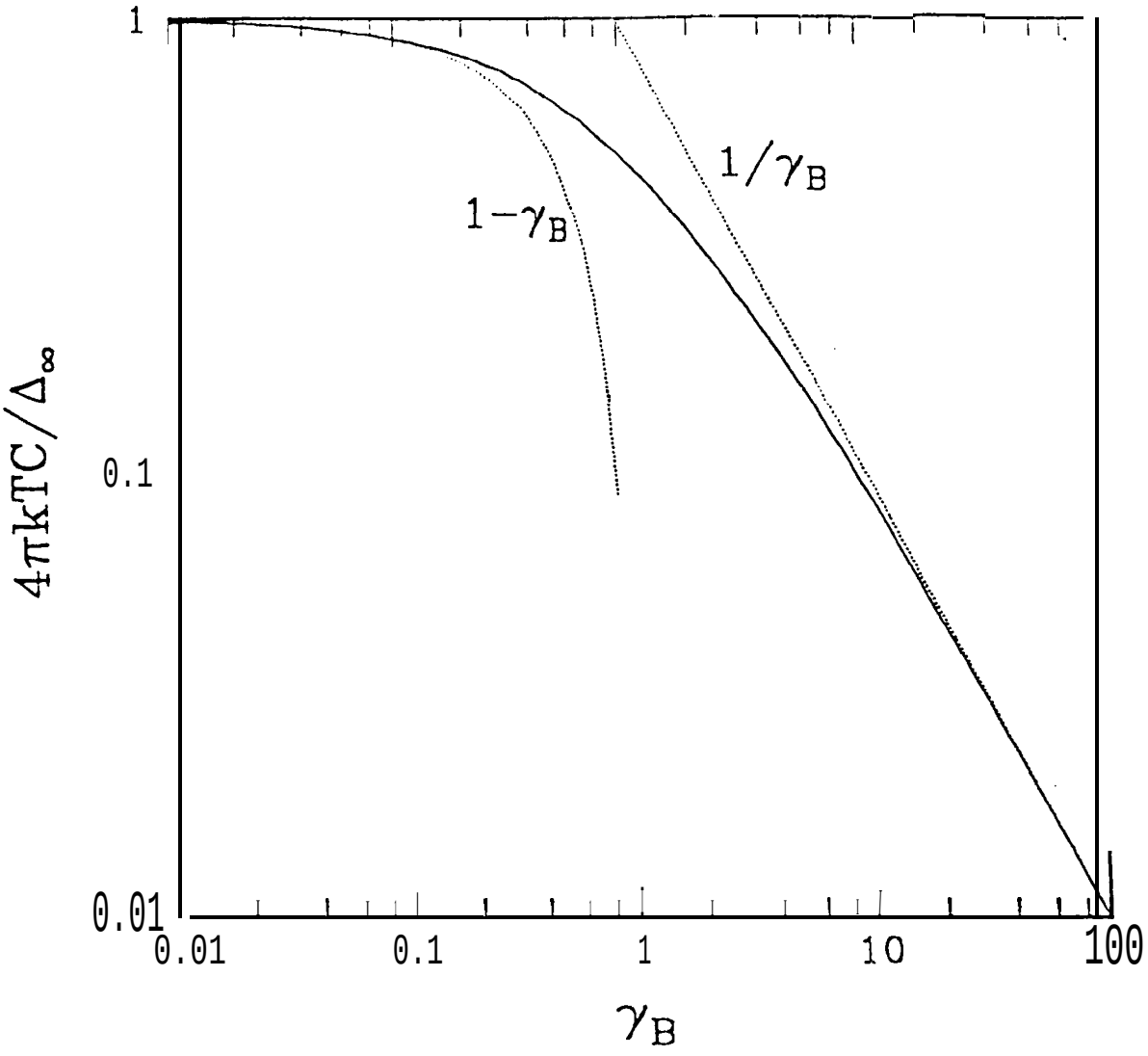
1
0.1
0.01
0.01
0.1
1
10
100
$4\pi kTC/\Delta_\infty$
γ_B
$1/\gamma_B$
$1-\gamma_B$

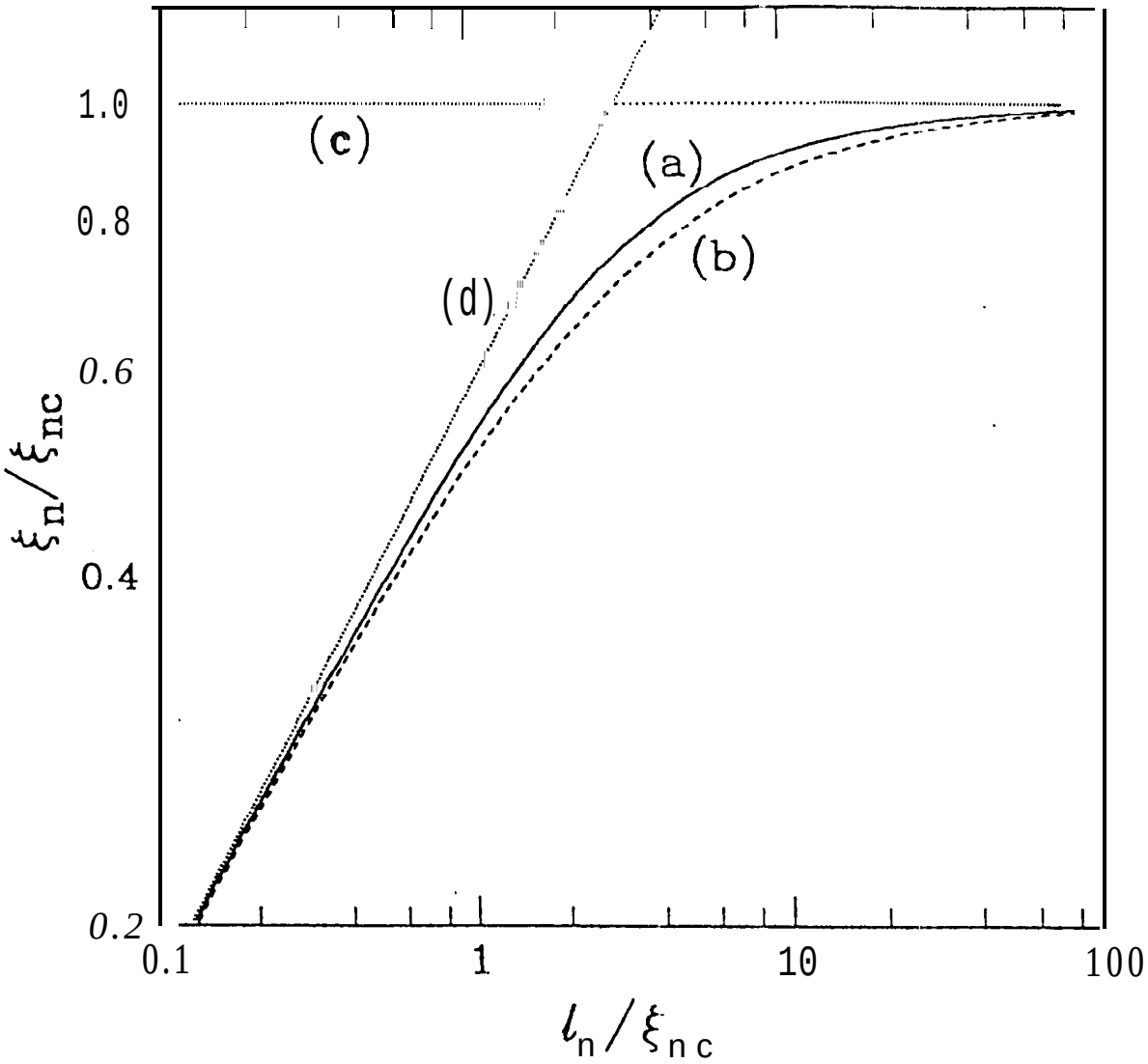
1.0
0.8
0.6
0.4
0.2
ξ_n/ξ_{nc}
(c)
(a)
(b)
(d)
0.1
1
10
100
l_n/ξ_{nc}

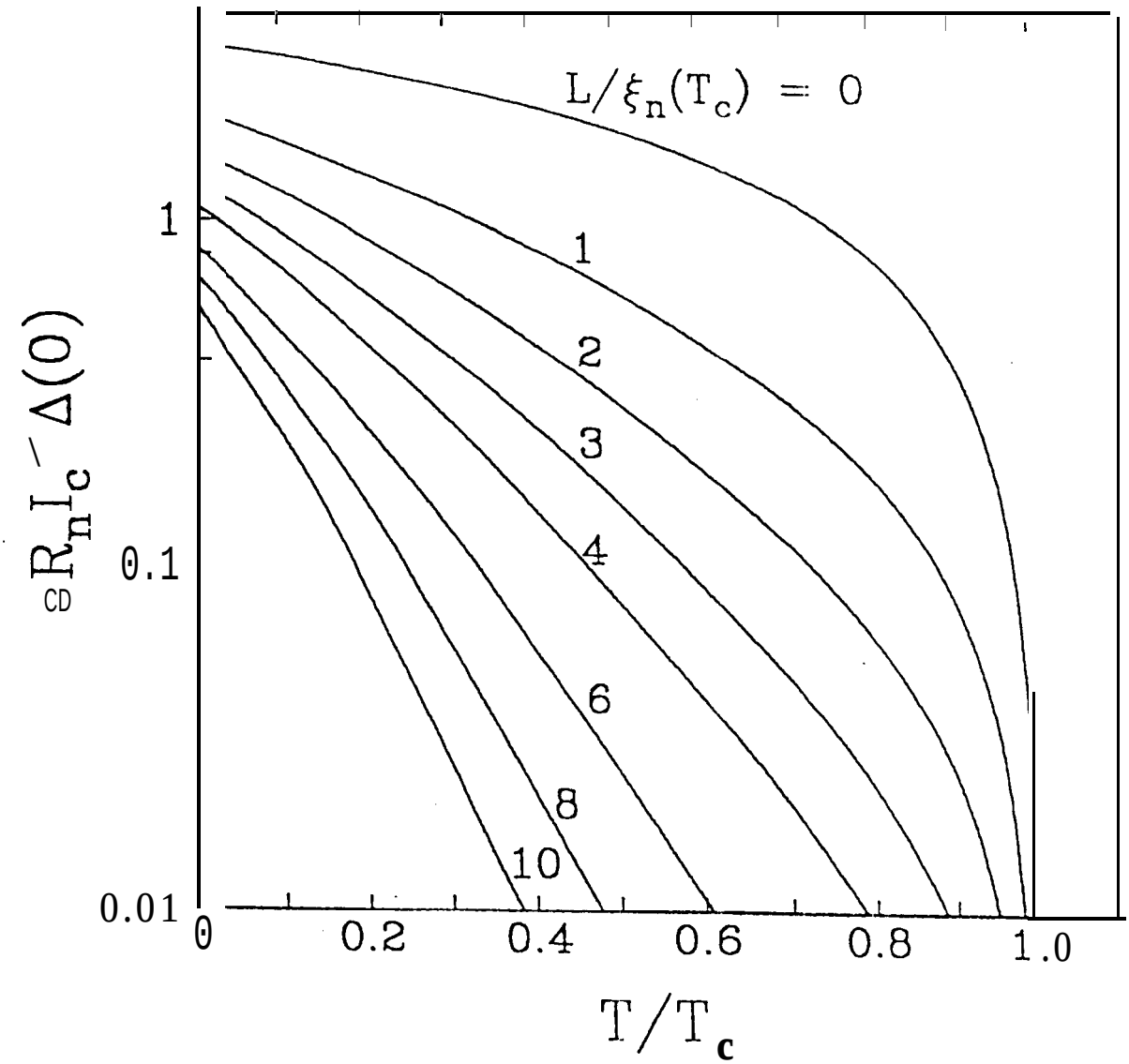
$L/\xi_n(T_c) = 0$
1
2
3
4
6
8
10
1
0.1
0.01
$R_n I_c / \Delta(0)$
CD
0
0.2
0.4
0.6
0.8
1.0
T/T_c

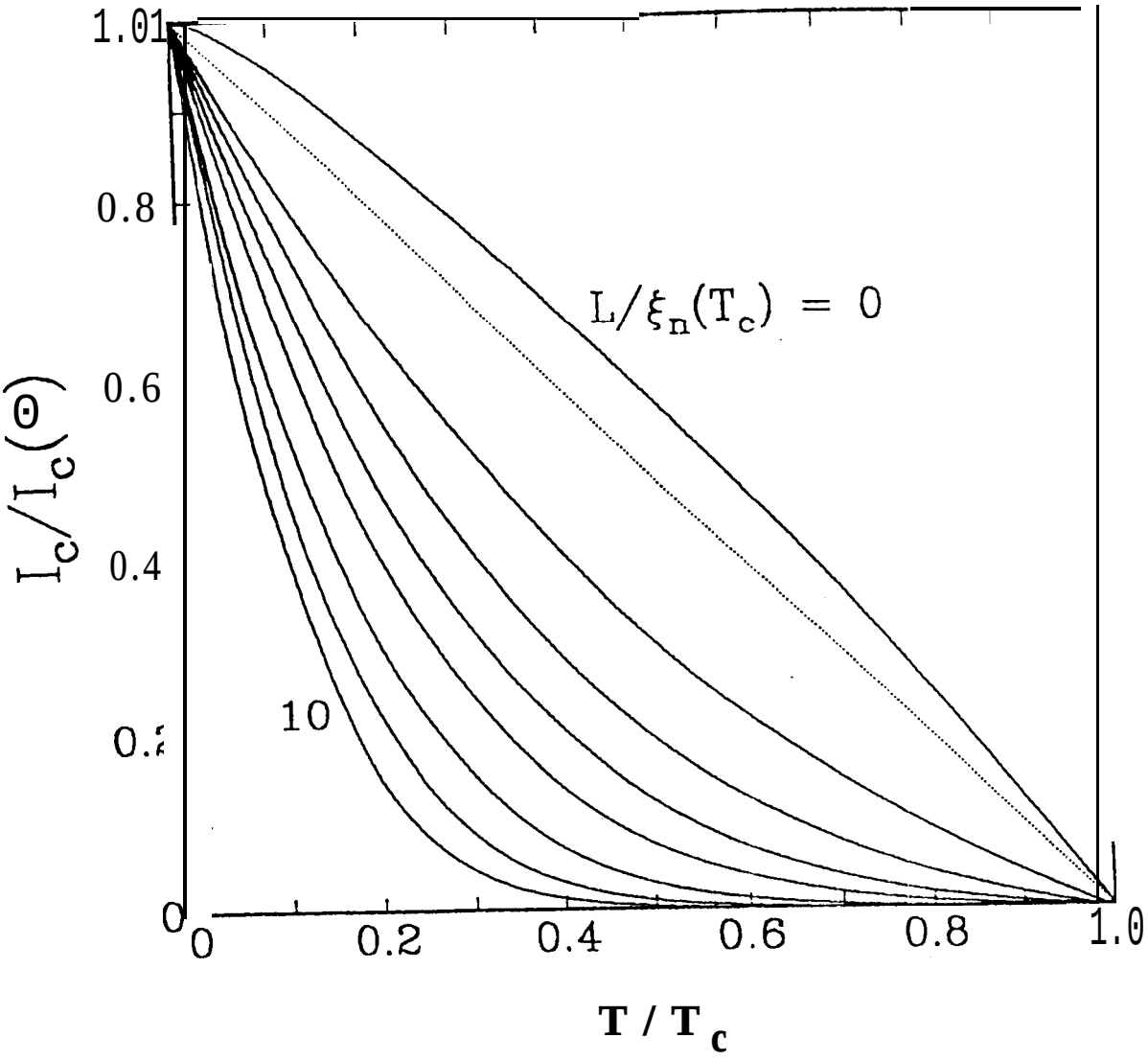
1.01
0.8
0.6
0.4
0.2
0
0
0.2
0.4
0.6
0.8
1.0
$I_c/I_c(0)$
T / T_c
$L/\xi_n(T_c) = 0$
10

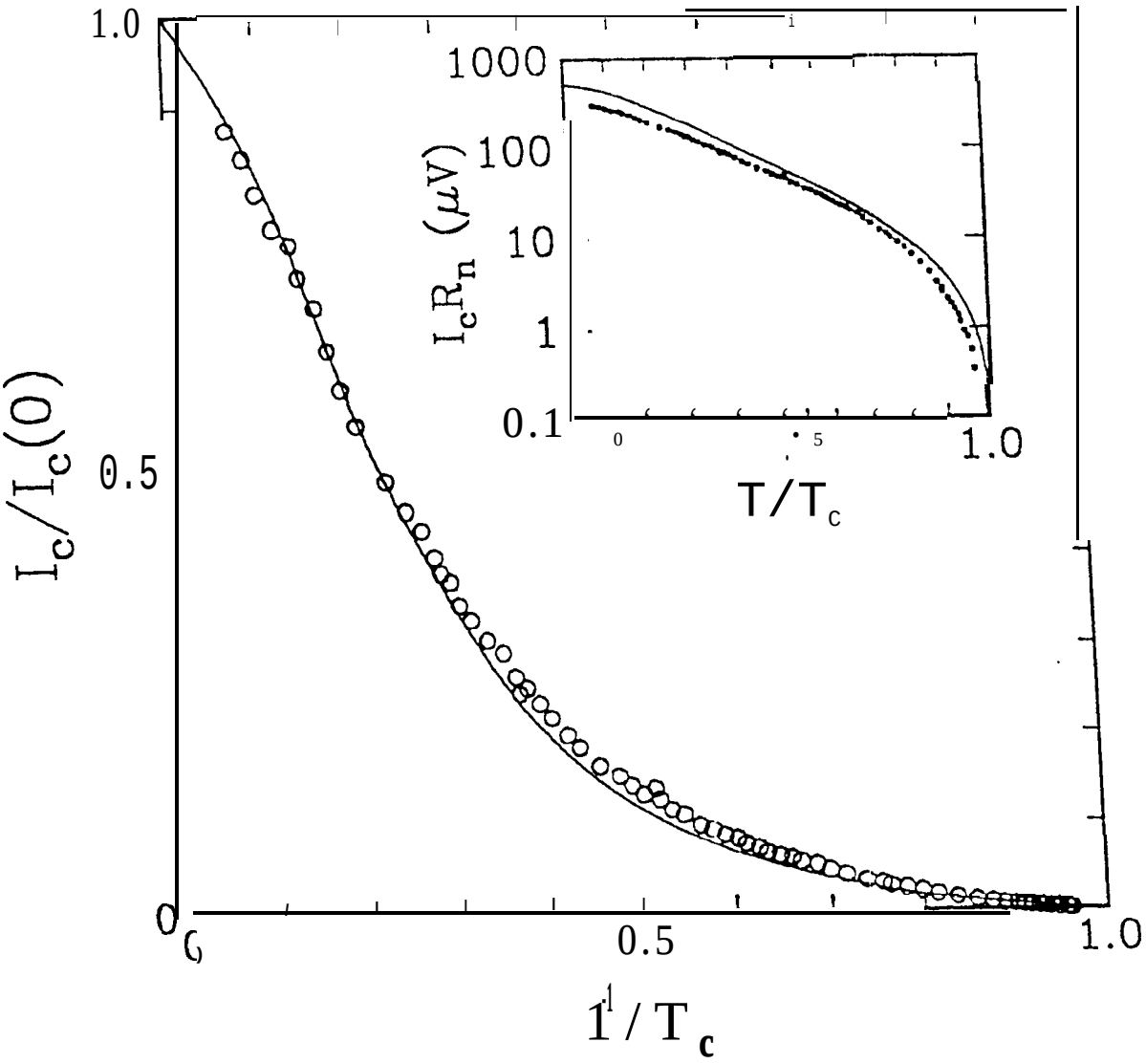
1.0
0.5
0
0
0.5
1.0
$I_c/I_c(0)$
$1/T_c$
1000
100
10
1
0.1
I_cR_n (μV)
0
.5
1.0
T/T_c

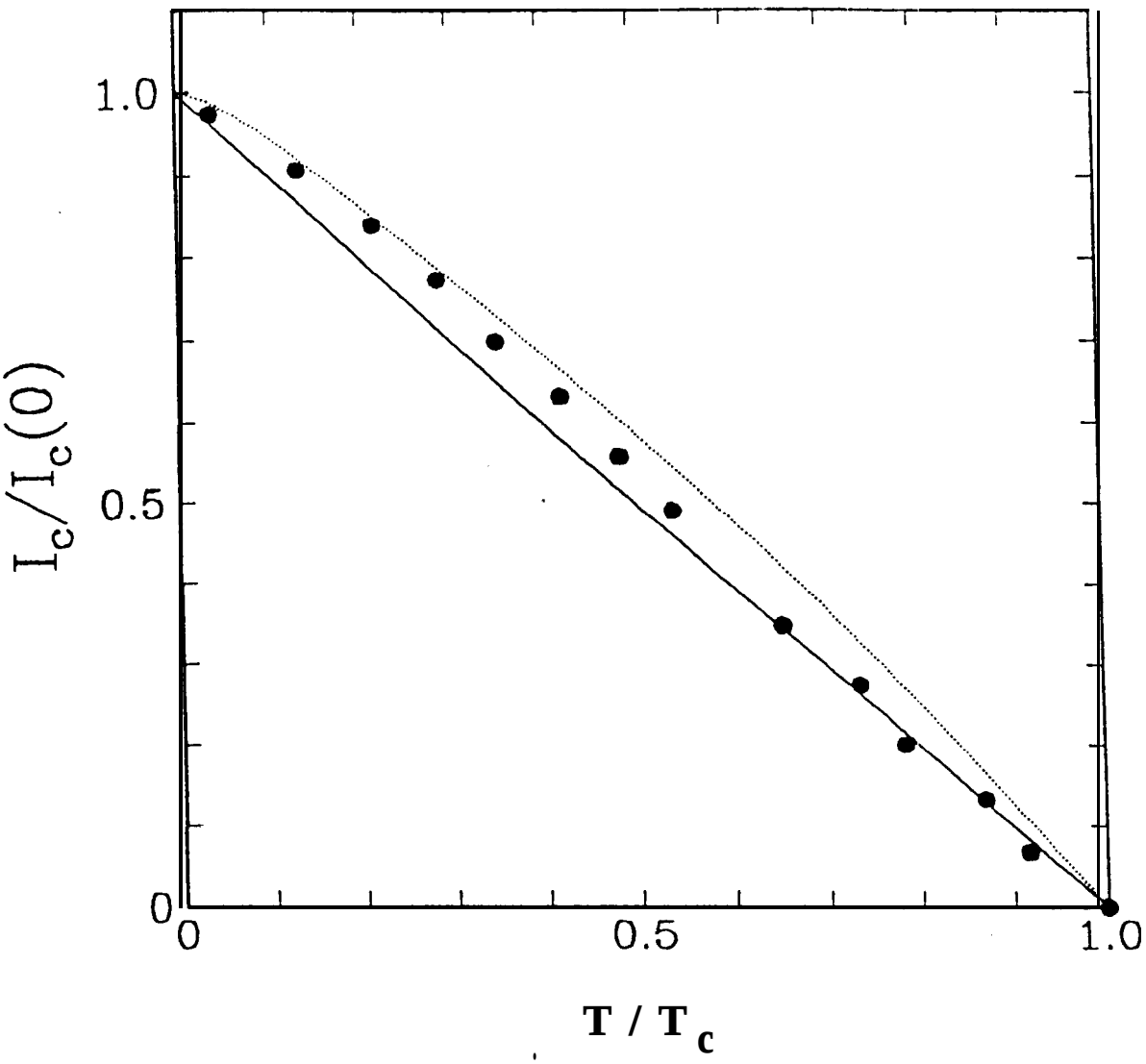
1.0
0.5
0
$I_c/I_c(0)$
0
0.5
1.0
T / T_c

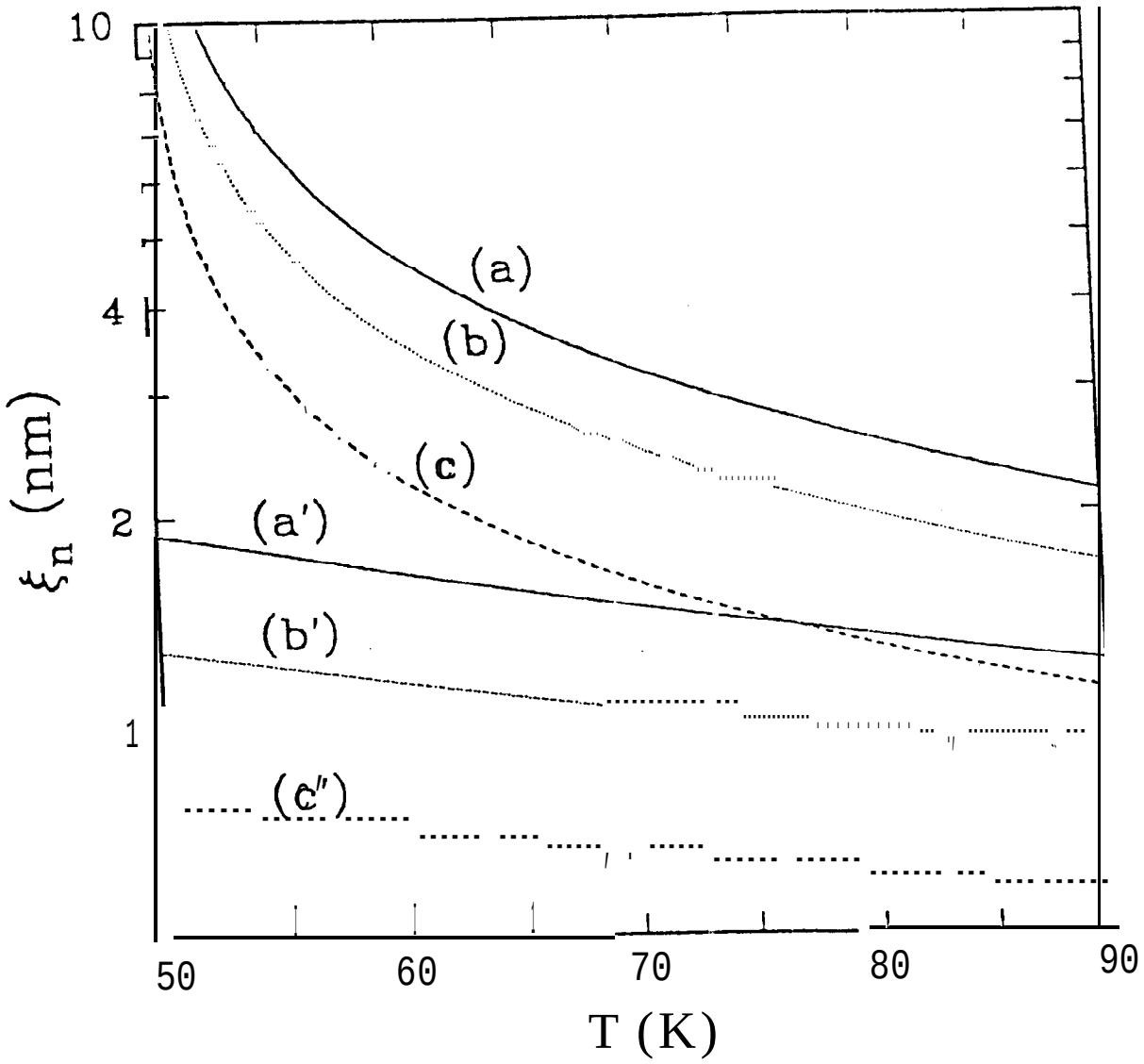

Delin/Kleinsasser

July 18, 1995

Figure 31

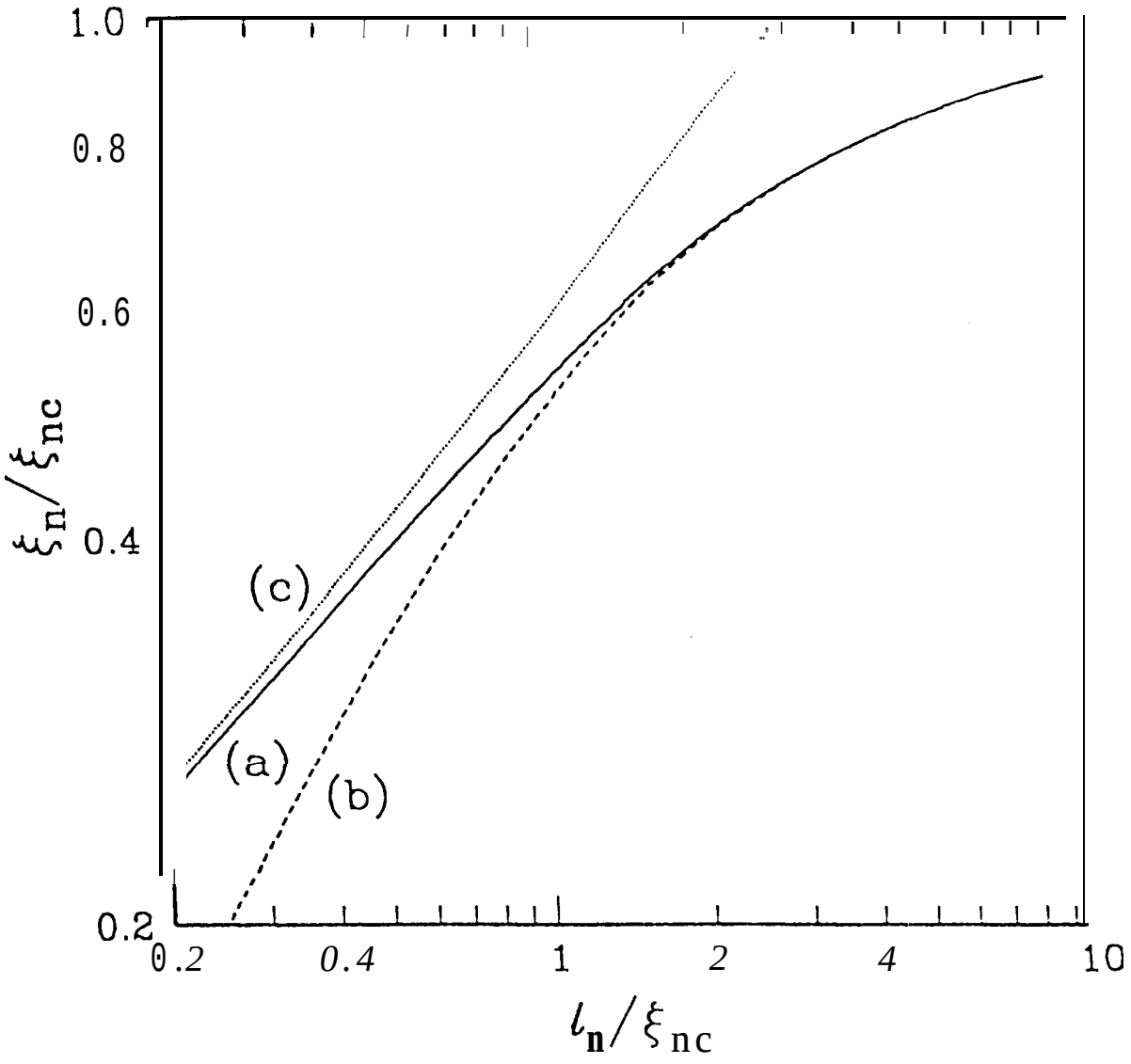
1.0
0.8
0.6
0.4
0.2
ξ_n/ξ_{nc}
(c)
(a)
(b)
0.2
0.4
1
2
4
10
l_n/ξ_{nc}

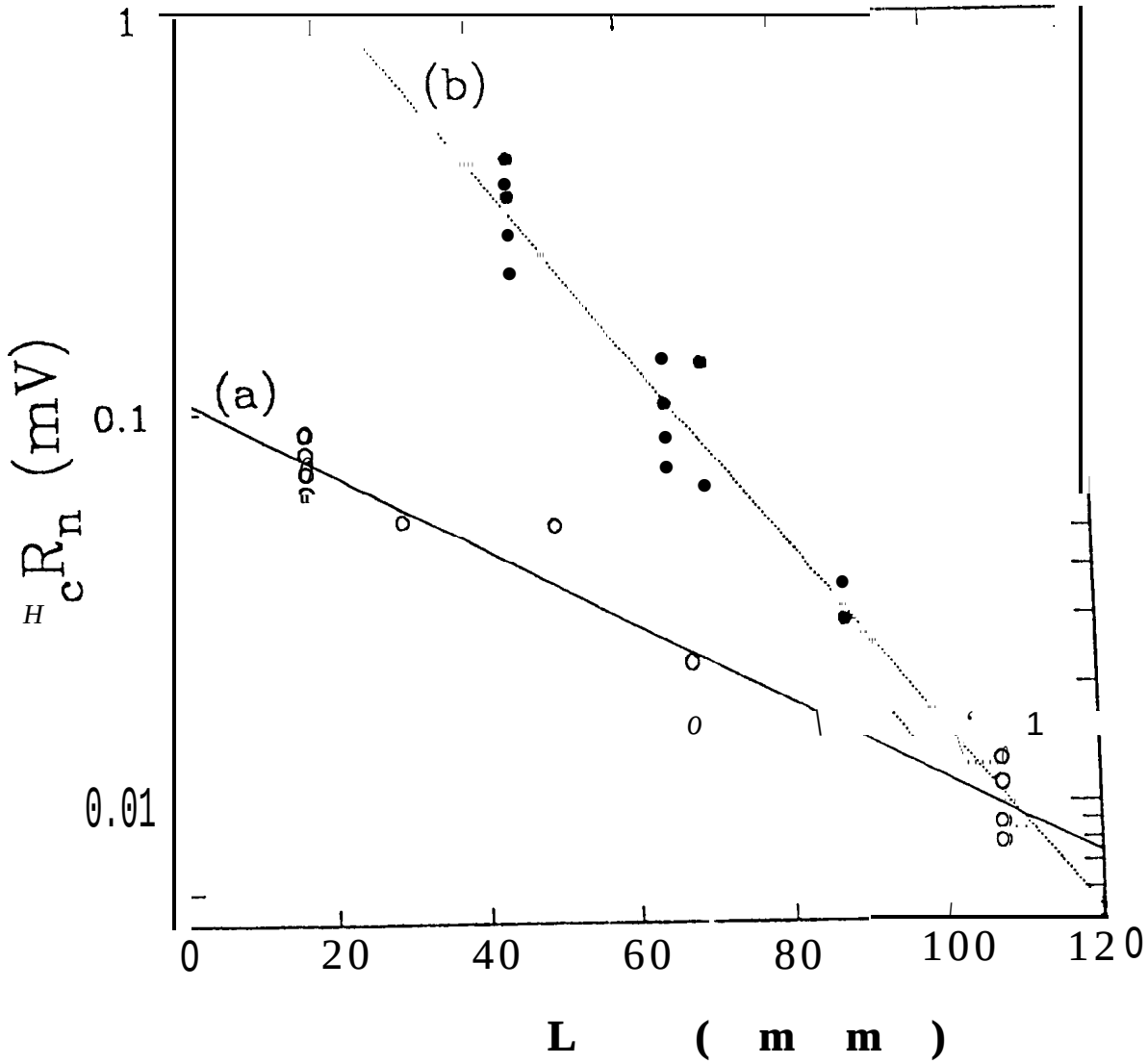
1
0.1
0.01
(b)
(a)
$_{H}^{c}R_{n}$ (mV)
0
20
40
60
80
100
120
L (m m)

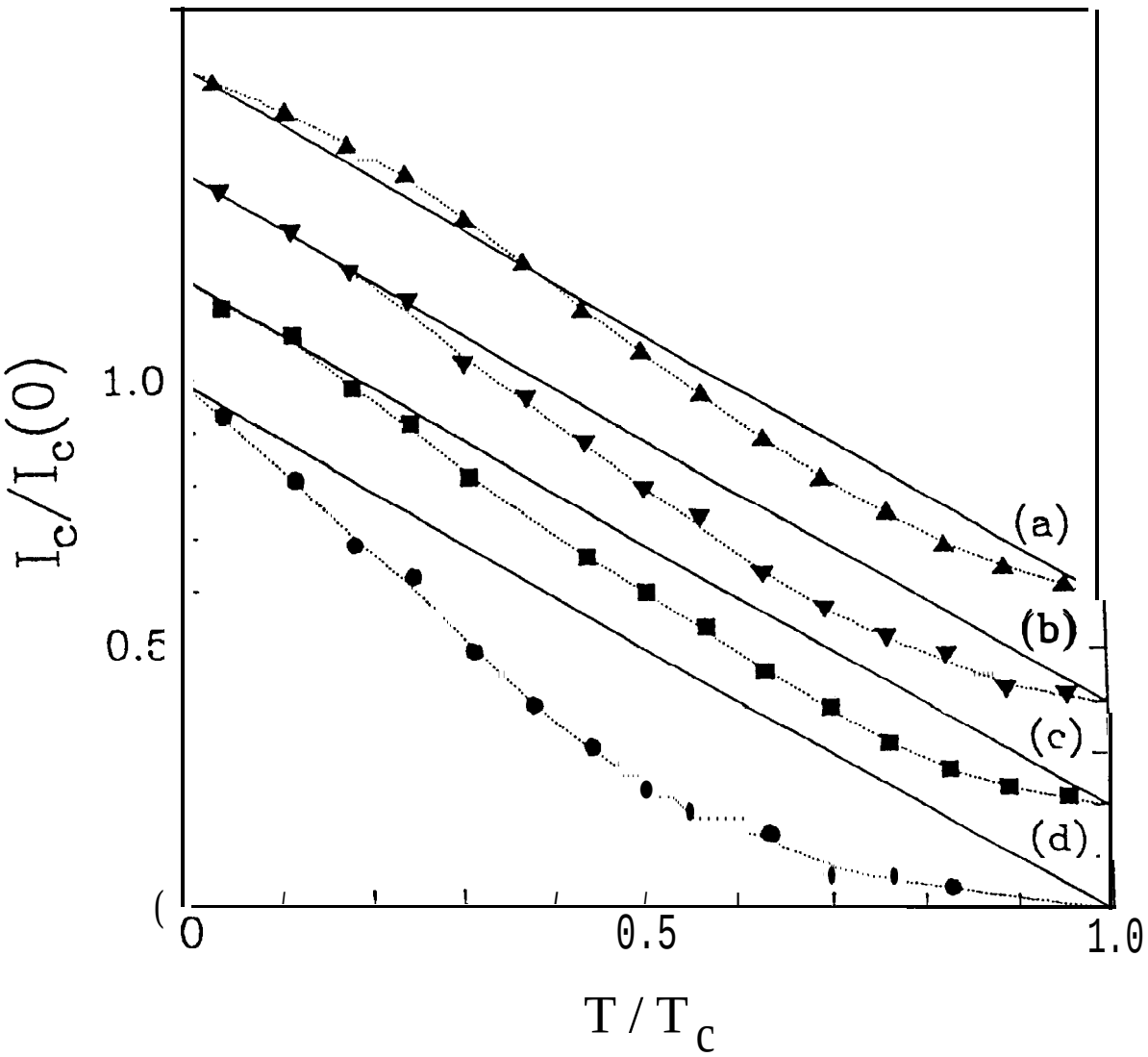
$I_c/I_c(0)$
1.0
0.5
0
0.5
1.0
T/T_c
(a)
(b)
(c)
(d)

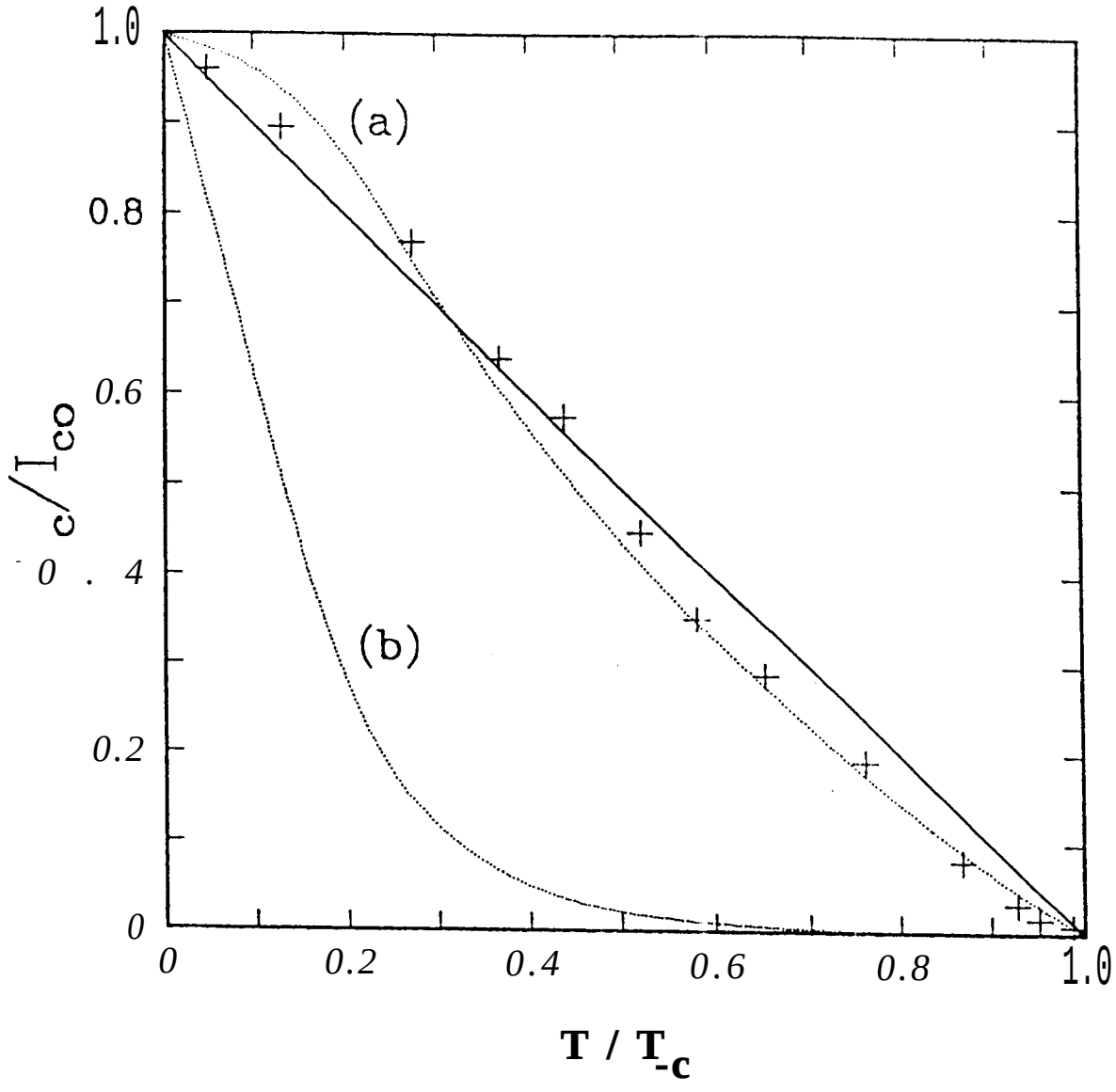
1.0
0.8
0.6
0.4
0.2
0
I_c/I_{co}
(a)
(b)
0
0.2
0.4
0.6
0.8
1.0
T / T_c

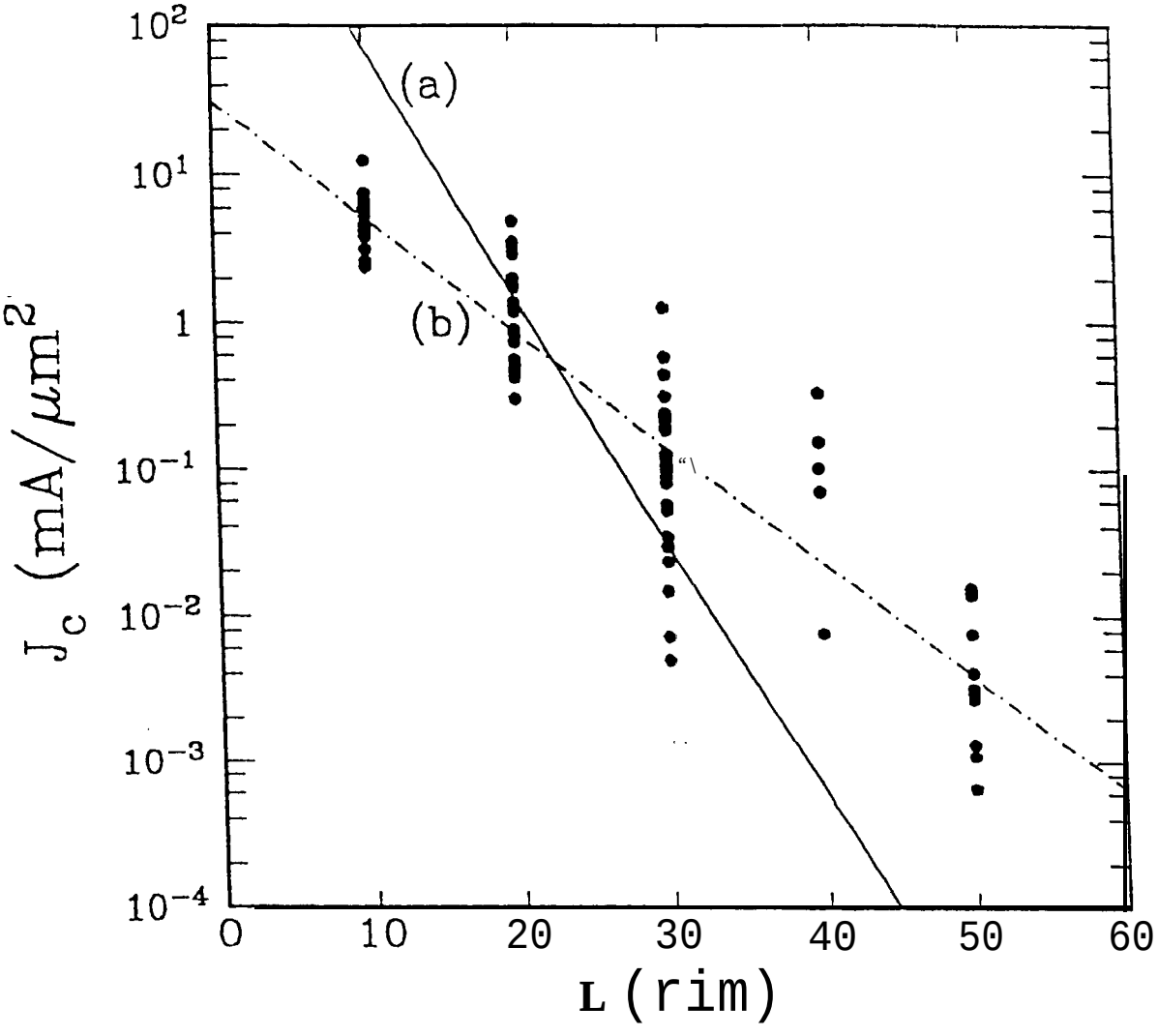
10^2
10^1
1
10^{-1}
10^{-2}
10^{-3}
10^{-4}
J_c (mA/μm^2)
(a)
(b)
0
10
20
30
40
50
60
L (rim)

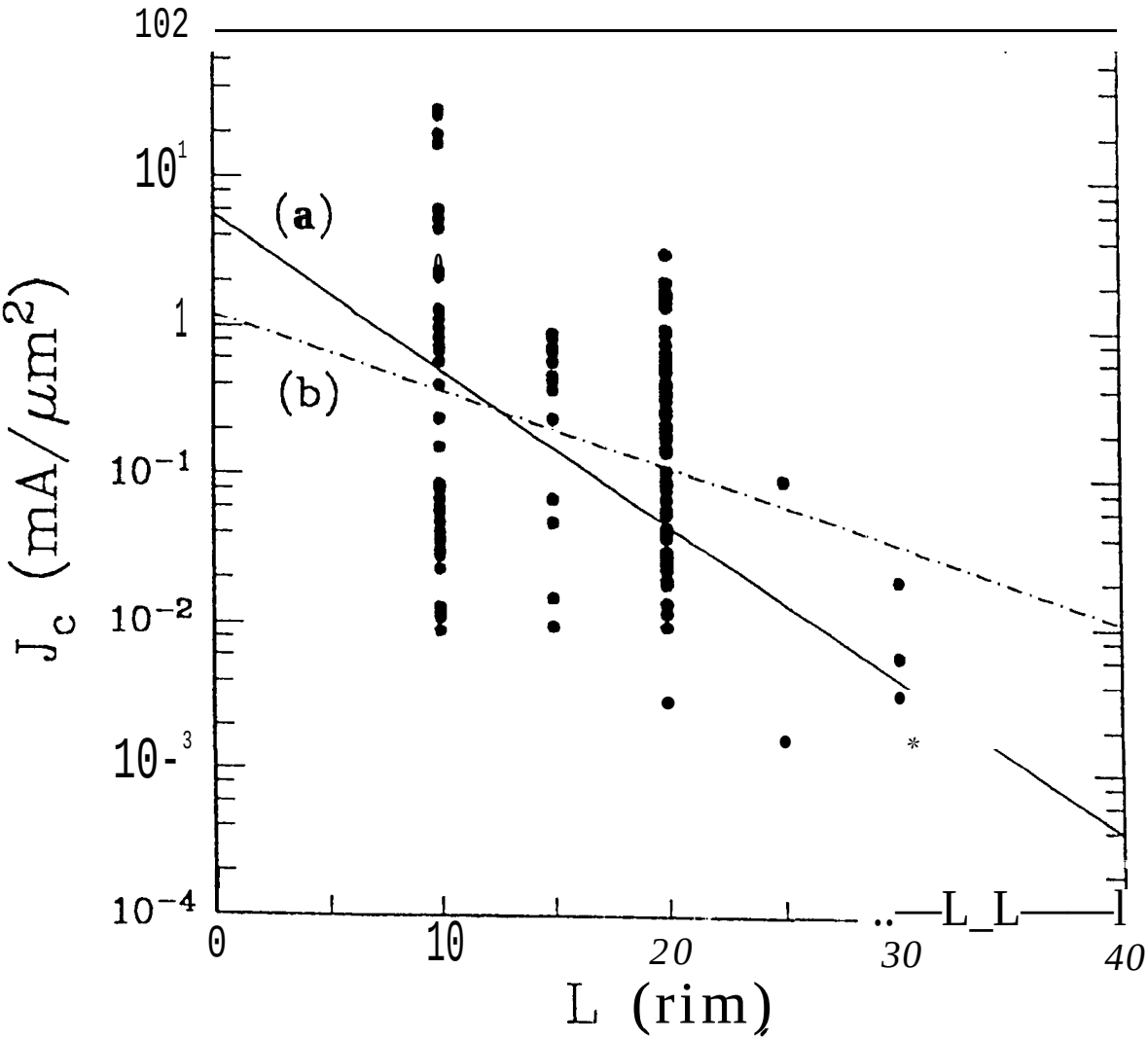
102
10^1
1
10^{-1}
10^{-2}
10^{-3}
10^{-4}
(a)
(b)
J_c (mA/μm^2)
0
10
20
30
40
L (rim)

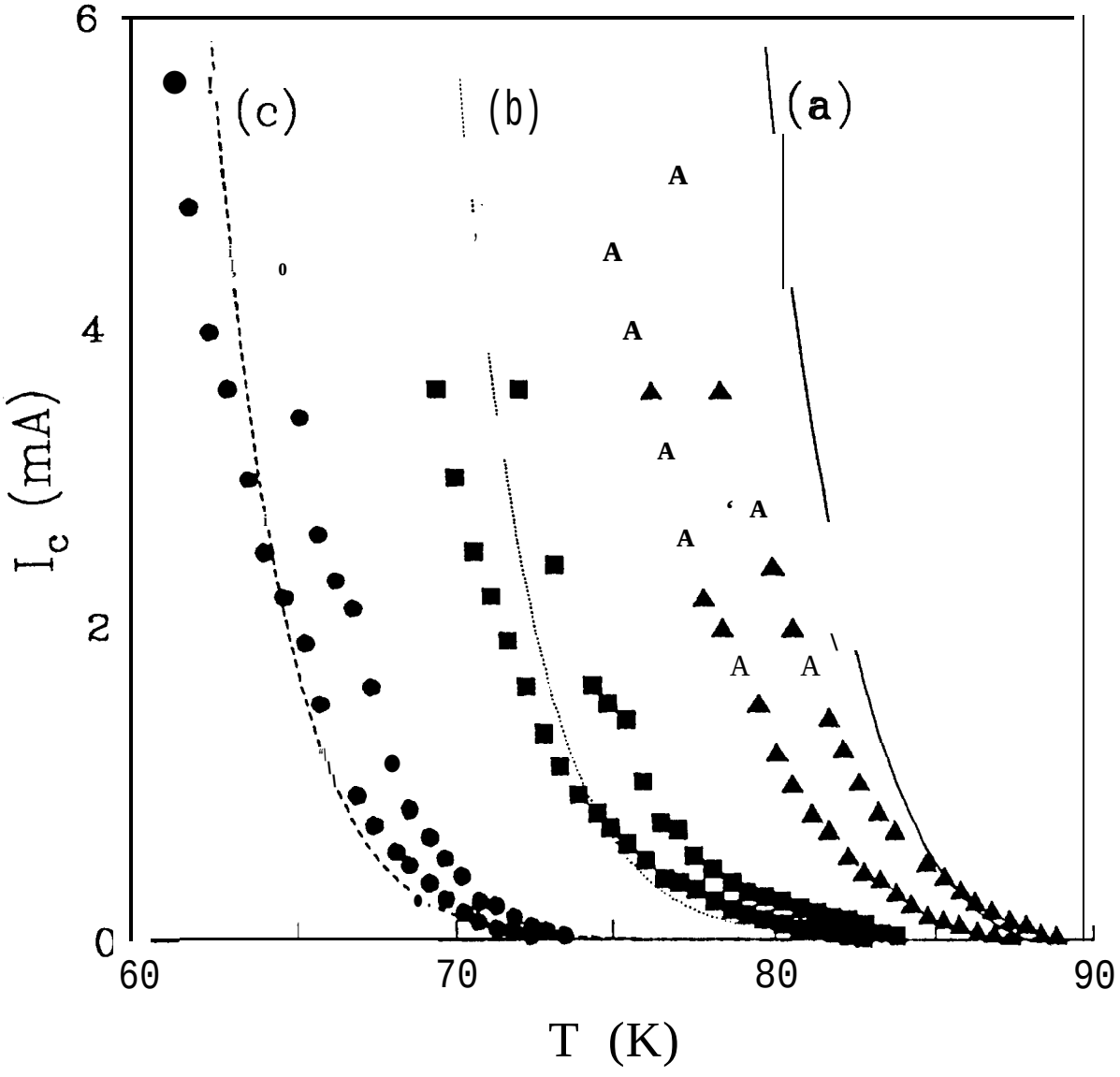
6
4
2
0
I_c (mA)
60
70
80
90
T (K)
(c)
(b)
(a)

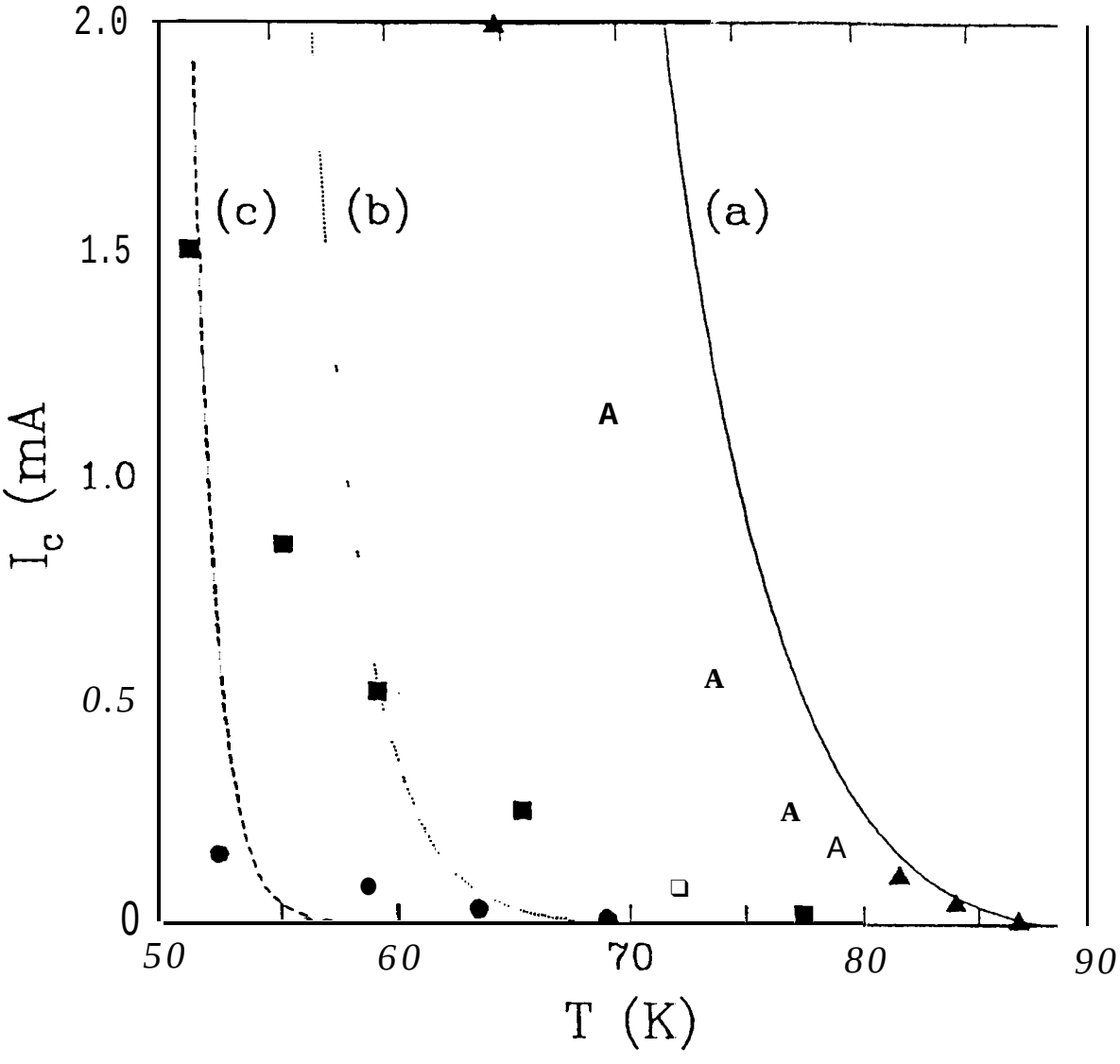
2.0
1.5
1.0
0.5
0
I_c (mA
(c)
(b)
(a)
A
A
A
A
50
60
70
80
90
T (K)